



저작자표시-비영리-변경금지 2.0 대한민국

이용자는 아래의 조건을 따르는 경우에 한하여 자유롭게

- 이 저작물을 복제, 배포, 전송, 전시, 공연 및 방송할 수 있습니다.

다음과 같은 조건을 따라야 합니다:



저작자표시. 귀하는 원저작자를 표시하여야 합니다.



비영리. 귀하는 이 저작물을 영리 목적으로 이용할 수 없습니다.



변경금지. 귀하는 이 저작물을 개작, 변형 또는 가공할 수 없습니다.

- 귀하는, 이 저작물의 재이용이나 배포의 경우, 이 저작물에 적용된 이용허락조건을 명확하게 나타내어야 합니다.
- 저작권자로부터 별도의 허가를 받으면 이러한 조건들은 적용되지 않습니다.

저작권법에 따른 이용자의 권리는 위의 내용에 의하여 영향을 받지 않습니다.

이것은 [이용허락규약\(Legal Code\)](#)을 이해하기 쉽게 요약한 것입니다.

[Disclaimer](#)

Doctoral Thesis

# C–H Functionalization of Substituted Aromatic Compounds Using Transition-Metal Catalysts

Hyun Ji Yang

Department of Energy and Chemical Engineering  
(Chemical Engineering)

Graduate School of UNIST

2017



# C–H Functionalization of Substituted Aromatic Compounds Using Transition-Metal Catalysts

Hyun Ji Yang

Department of Energy and Chemical Engineering  
(Chemical Engineering)

Graduate School of UNIST

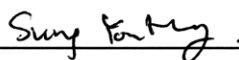
# C–H Functionalization of Substituted Aromatic Compounds Using Transition-Metal Catalysts

A thesis/dissertation  
submitted to the Graduate School of UNIST  
in partial fulfillment of the  
requirements for the degree of  
Doctor of Philosophy

Hyun Ji Yang

06/02/2017 of submission

Approved by



---

Advisor

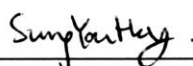
Prof. Sung You Hong

# C–H Functionalization of Substituted Aromatic Compounds Using Transition-Metal Catalysts

Hyun Ji Yang

This certifies that the thesis/dissertation of Hyun Ji Yang is  
approved.

06/02/2017 of submission



\_\_\_\_\_  
Advisor: Prof. Sung You Hong



\_\_\_\_\_  
Prof. Ja Hun Kwak: Thesis Committee Member #1



\_\_\_\_\_  
Prof. Kwangjin An: Thesis Committee Member #2



\_\_\_\_\_  
Prof. Changduk Yang: Thesis Committee Member #3



\_\_\_\_\_  
Prof. Chang Young Lee: Thesis Committee Member #4

*Devoted to my loved family, especially my parents*

## Abstract

Development of C–C formation methods has been a key research topic in synthetic organic chemistry fields. Recently, there have been extensive reports on C–H functionalization, a methodology to generate C–C bonds by activating C–H bond, while other C–N or C–O bond formations have been allowed. Traditional metal-catalyzed cross-coupling reaction has been one of the most useful synthetic methods for the formation of C–C bonds, a theme of the 2010 Nobel prize in chemistry. Yet, there is an inconvenience requiring laborious procedures to prepare organic halides or organometallic reagents. On the other hand, C–H activation can avoid these steps and it has influenced the broad field of chemical synthesis of small molecules, pharmaceuticals, fine chemicals, biomolecules, and organic-based materials. In this thesis, we have designed and performed both homogeneous and heterogeneous C–H functionalizations. Reaction optimization and substrate scope tests have been carried out to reveal the synthetic utilities.

In the first chapter, we have established the first *meta*-selective C–H bond arylation of anilides using copper-exchanged zeolites. The Cu-zeolites have showed high catalytic activities on the low copper concentration (0.5 mol%). And we have demonstrated that Cu-zeolites are chemically stable and robust as recyclable catalysts. In the second chapter, we demonstrated a microwave-assisted *meta*-selective direct (hetero)arylation of pivanilides to accelerate copper catalysis. The ligand-free Cu<sup>II</sup>-β system has showed improved catalytic stability over consecutive runs. In addition, homogeneous Cu(OTf)<sub>2</sub> and heterogeneous Cu<sup>II</sup>-β zeolite catalysts have been systematically compared to reveal their catalytic characteristics. In the last chapter, the main focus of the thesis, we have designed a straightforward synthetic route to access tailored triphenylenes as graphene segments. We have achieved mono- and bis-annulation of pivanilides in a one-step. Moreover, the method has been extended to the application of field-effect transistor sensor for alcohol vapor detection.

*Keywords: C–H functionalization, direct arylation, zeolite, microwave heating, triphenylene.*





## Table of Contents

<i>Abstract</i> .....	i
<i>Table of Contents</i> .....	iii
<i>List of Figures</i> .....	vi
<i>List of Tables</i> .....	ix
<i>List of Schemes</i> .....	x
<i>Abbreviation</i> .....	xi
<b>Chapter I. Introduction</b> .....	1
1. Transition-Metal Catalyzed C–C Bond Formation .....	1
1.1. Cross-Coupling Reactions .....	1
1.1.1. The History of Cross-Coupling Reactions .....	2
1.1.2. Mechanism of Cross-Coupling Reactions .....	3
1.1.3. Recent Advances in Cross-Coupling Reactions .....	4
1.2. C–H Activation and Functionalization .....	5
1.2.1. History of C–H Activation and Functionalization .....	6
1.2.2. Mechanism of C–H Activation and Functionalization .....	7
1.2.3. Key Examples of C–H Activation and Functionalization .....	8
2. Heterogeneous Catalysts .....	9
2.1. Heterogeneous Catalytic Reactions .....	10
2.2. Metal-Exchanged Zeolites as Heterogeneous Catalysts .....	10
2.2.1. Types of Zeolites .....	10
2.2.2. Zeolite Frameworks .....	11
2.2.2.1. Geometry and Structures .....	11
2.2.2.2. Zeolite Framework Structures .....	12
2.2.3. Ion-Exchange and Adsorption Properties of Zeolites .....	12
2.2.4. Single-Site Catalysis by (Metal-Exchanged) Zeolites .....	13
3. Microwave Reactions .....	15
3.1. Physical Background .....	15
3.2. Microwave-Assisted Organic Synthesis .....	16
4. References .....	17

<b>Chapter II. C–H Bond Arylation of Anilides inside Copper-Exchanged Zeolites</b> .....	20
1. Introduction .....	20
2. Results and Discussion .....	22
3. Conclusions .....	29
4. Experimental .....	30
4.1. General Procedures and Materials .....	30
4.2. Preparation and Characterizations of Copper-Zeolites .....	30
4.3. Protocol for the Direct Arylation .....	30
4.4. Zeolite Cluster Models .....	31
4.5. Kinetic Experiments .....	31
4.6. Computational Methods .....	32
4.6.1. Grand Canonical Monte Carlo (GCMC) Simulation .....	32
4.6.2. Results of GCMC Simulation .....	32
4.6.3. Pore- and Molecular Size Comparison .....	34
4.6.4. DFT Calculation .....	34
4.7. Textural Properties of Zeolites .....	37
5. References .....	37
<b>Chapter III. Efficient Copper Catalysts for C–H Bond Arylation under Microwave Heating: Direct Access to Multi-Substituted Pivanilides</b> .....	40
1. Introduction .....	40
2. Results and Discussion .....	41
3. Conclusions .....	46
4. Experimental .....	47
4.1. General .....	47
4.2. Preparation of the Catalysts and General Protocol for Direct Arylation .....	47
4.3. General Procedure for Synthesis of Pivanilide Substrates .....	47
4.4. Recycling Test .....	48
4.5. Synthesis of Pivanilide Substrates .....	48
4.6. Synthesis and Analytical Data for Iodonium Salts .....	49
4.7. Synthesis and Analytical Data for Pivanilides by Microwave Reactor .....	50
5. References .....	53

<b>Chapter IV. An Annulative Synthetic Strategy for Building Triphenylene Frameworks by Multiple C–H Bond Activations</b> .....	55
1. Introduction .....	55
2. Results and Discussion .....	57
3. Conclusions .....	62
4. Experimental .....	63
4.1. General Methods .....	63
4.2. Synthesis of Arene Substrates .....	63
4.2.1. General Procedure for the Preparation of Pivanilide Substrates .....	63
4.2.2. General Procedure for the Preparation of 2-Pyrrolidinone Substrates .....	64
4.2.3. General Procedure for the Preparation of <i>N</i> -Isopropylbenzamide Substrates .....	64
4.3. Synthesis of Cyclic Diaryliodonium Salts .....	65
4.4. Substituted Triphenylenes and Phenanthro[9,10- <i>b</i> ]Triphenylenes .....	66
4.5. <i>Ortho</i> -Arylation under the Standard Conditions .....	72
4.6. Radical Route in Pd-Catalyzed Reaction: Control Reaction .....	73
4.7. Additional Annulative $\pi$ -Extension Reactions .....	73
4.8. Fabrication of Alcohol FET Sensors .....	75
4.8.1. CVD Synthesis and Transfer of Graphene .....	75
4.8.2. Fabrication of Field-Effect Transistors .....	75
4.8.3. Electrical Characterizations .....	76
4.9. The Photophysical Properties of Compounds <b>4</b> .....	77
5. References .....	78
<b>Chapter V. Acknowledgement (English version)</b> .....	80
<b>Acknowledgement (Korean version)</b> .....	81

## List of Figures

**Figure 1.1.** General reaction scheme and an example of cross-coupling reaction.

**Figure 1.2.** Simplified history of cross-coupling reactions.

**Figure 1.3.** General scheme and an example for C–H functionalization.

**Figure 1.4.** Schematic representation of the progress of a heterogeneous catalytic reactions.

**Figure 1.5.** Structural units of zeolite A, sodalite and faujasite.

**Figure 1.6.** Some common zeolites frameworks (a) zeolite A (3D, 4.2 Å), (b) zeolite Y (3D, 7.4 Å), (c) zeolite L (1D, 7.1 Å), (d) ZSM-5 (silicalite) (2D, 5.3 × 5.6 Å, 5.1 × 5.5 Å). D stands for the dimensions of channel system.

**Figure 1.7.** Schematic presentation of ion-exchange process in the mixture of ammonium chloride solution and sodium-zeolites.

**Figure 1.8.** Adsorption of a small molecule (acetone) inside a zeolite Y pore (window 7.4 Å, cage 13.2 Å).

**Figure 1.9.** (a) brief scheme of single-atom catalysis, (b) a HAADF-STEM image of a Pt/ZnO nanobelt model catalyst presenting different Pt atoms, (c) various metallic clusters positioned onto the ZnO surface.

**Figure 1.10.** Electric (*E*) and magnetic (*H*) field components in microwaves. (web source: [http://www.srh.noaa.gov/jetstream/remote/remote\\_intro.html](http://www.srh.noaa.gov/jetstream/remote/remote_intro.html))

**Figure 1.11.** Schematic representation of heating mechanism (red color stands for higher temperature while blue color indicates lower temperature).

**Figure 2.1.** Conversion vs. reaction time plot on the same Cu<sup>II</sup> concentration (0.5 mol%).

**Figure 2.2.** Kinetic studies of direct arylation using copper catalysts (0.5 mol%). (a) A plot of  $\ln([1]_t/[1]_0)$  vs. time (b) a plot of  $\ln k$  vs.  $1/T$ .

**Figure 2.3.** A plot of  $\ln k$  vs.  $\ln [Cu(OTf)_2]$ .

**Figure 2.4.** Copper-aryl intermediate structures well-fitted inside zeolite frameworks. (a) Cu-Y 78T cluster model, and (b) Cu-beta 55T cluster model. Solid lines represent zeolite framework and ball-and-sticks are used to present the copper-aryl complexes. Oxygen: red, nitrogen: blue, carbon: grey, hydrogen: white, copper: reddish orange, silicon: yellow, and aluminum: pink. (For interpretation of the references to color in this figure legend, the reader is referred to the web version of this article.)

**Figure 2.5.** HRTEM images Cu-beta (2.94 wt%). (a,b) fresh sample, and (c,d) sample after the reaction.

**Figure 2.6.** Bright-field (BF) TEM images (left) and EDS elemental distribution of Al (middle) and Cu (right) of Cu-beta (2.94 wt%). (a) fresh sample and (b) the sample after the direct reaction.

**Figure 2.7.** Kinetic plots for Cu-Y, Cu-beta, and copper triflate at different temperatures.

**Figure 2.8.** Adsorption isotherms of **1** in Cu-Y (10.34 wt%), Cu- $\beta$  (2.94 wt%), and Cu-MOR (5.14 wt%) at (a) 298 K and (b) 343 K. The modeled zeolites are shown with black dots, which represent probable sites of the adsorbate molecule **1** after the GCMC simulation at the fugacity, 1000 kPa.

**Figure 2.9.** Adsorption isotherms of product **2**.

**Figure 2.10.** (a) Zeolite structures (Y: left, beta: right). Cyan colored parts of CPK models represent bottle neck in Y and cross section of beta. Arrow indicates the diffusion path of **2** inside zeolites, (b) the most stable conformer of product **2**, (c) the bent and torsional conformer of product **2**.

**Figure 2.11.** (a) and (b) Cu-Y models with initial positions of  $Cu^{II}$  ion at sites (i) and (ii), respectively. (c) and (d) Cu-beta models with initial positions of  $Cu^{II}$  ion at sites (i) and (ii), respectively.

**Figure 2.12.** Schematic representation of simulation processes.

**Figure 2.13.** Reaction coordinate diagram.

**Figure 3.1.** Outline of microwave-assisted direct arylation via copper catalysis.

**Figure 3.2.** Recyclability test using Cu<sup>II</sup>- $\beta$  in the presence and absence of DTBP.

**Figure 4.1.** Proposed 2-fold C–H arylation mechanism.

**Figure 4.2.** (a) Interaction of **3aa** with the graphene surface, (b) Transfer characteristics ( $V_D=0.1$  V), (c) Real-time response, (d) Sensor sensitivities.

**Figure 4.3.** (a) Optical microscope image of the graphene channel FETs. The width of the channel is 5  $\mu\text{m}$ , and the length of the channel is 70  $\mu\text{m}$ . Scale bar, 50  $\mu\text{m}$ , (b) Output ( $I_D$ - $V_D$ ) characteristics of the graphene FETs before and after **3aa** coating ( $V_G = 0$  V).

**Figure 4.4.** Real-time response of the graphene sensor to ethanol vapor without **3aa**-functionalization at a fixed concentration (1,000 ppm) ( $V_G = 0$  V).

**Figure 4.5.** UV/Vis absorption spectra (solid lines, normalized data) and fluorescence emission spectra (dashed line, normalized data) obtained for compounds **4**.

## List of Tables

**Table 2.1.** Direct arylation of pivanilide **1** with copper catalysts.

**Table 2.2.** Catalyst reusability study in a 0.5 g scale.

**Table 2.3.** ICP analysis results of the Cu-exchanged zeolite samples.

**Table 2.4.** ICP analysis results of the reaction solution after reaction using Cu-beta (2.94 wt%).

**Table 2.5.** Rate constant ( $k$ ) for Cu<sup>II</sup>- $\beta$ , Cu<sup>II</sup>-Y, and Cu(OTf)<sub>2</sub> zeolites.

**Table 2.6.** Textural properties of zeolites.

**Table 3.1.** Optimization of the homogeneous direct arylation process.

**Table 3.2.** Optimization of the heterogeneous direct arylation process.

**Table 3.3.** Substrate scope of the direct arylation reaction.

**Table 3.4.** Scope of the (hetero)aryl group transfer.

**Table 4.1.** Optimization of 2-fold C–H arylation.

**Table 4.2.** Reaction scope.

**Table 4.3.** Miscellaneous reaction scope.

**Table 4.4.** The photophysical properties of compounds **4**.



## List of Schemes

**Scheme 1.1.** (a) the Grignard-based Kharasch coupling, (b) the Heck reaction, (c) the Sonogashira reaction, (d) the Negishi reaction, (e) the Suzuki–Miyaura reaction, (f) the Buchwald coupling, (g) Hartwig coupling.

**Scheme 1.2.** General mechanism of cross-coupling reactions.

**Scheme 1.3.** (a) Cu-catalyzed cross-coupling of boronic esters with aryl iodides, (b) decarbonylative cross-coupling via Ni catalysis. (c) Ru-catalyzed cross-coupling of maleimides with alkenes.

**Scheme 1.4.** (a) the Fujiwara and Moritani reaction, (b) *ortho*-methylation of anilide, (c) application of pyridine-based DG, (d) *meta*-selective Cu-catalyzed arylation, (e) utilization of a ligand.

**Scheme 1.5.** Comparison of conventional cross-coupling with C–H activation.

**Scheme 1.6.** (a) Rh-catalyzed direct C–H vinylation of styrene derivatives, (b) regioselective oxidative trifluoromethylation of imidazoheterocycles, (c) amine-directed *meta*-selective C–H arylation using Pd/norbornene catalytic system.

**Scheme 1.7.** (a) Microwave-assisted Sonogashira cross-coupling reaction (Ar = (hetero)aryl; R = (hetero)aryl or alkyl), (b) synthesis of  $\beta$ - and  $\gamma$ -Hydroxy sulfides using diaryliodonium salts, (c,d) synthesis of *N*-heterocycle compounds (R<sub>1</sub> = Ar and ArCO; R<sub>2</sub> = H, Cl, Et).

**Scheme 2.1.** Outline of the current direct arylation inside copper-exchanged zeolites.

**Scheme 4.1.** Synthesis of triphenylene frameworks.

**Scheme 4.2.** Synthesis of phenanthro[9,10-*b*]triphenylene **4** frameworks.

## Abbreviation

---

<b>ATR</b>	Attenuated Total Reflectance
<b>BHT</b>	Butylated Hydroxytoluene
<b>COMPASS</b>	Condensed-Phase Optimized Molecular Potentials for Atomistic Simulation Studies
<b>COSMO</b>	Conductor-Like Screening Model
<b>CVD</b>	Chemical Vapor Deposition
<b>DBU</b>	1,8-Diazabicyclo(5.4.0)undec-7-ene
<b>DCE</b>	1,2-Dichloroethane
<b>DCM</b>	Dichloromethane
<b>DFT</b>	Density Functional Theory
<b>DGs</b>	Directing Groups
<b>DMF</b>	<i>N,N</i> -Dimethylformamide
<b>DMSO</b>	Dimethyl Sulfoxide
<b>DNP</b>	Double Numerical Plus Polarization
<b>DTBP</b>	2,6-Di- <i>tert</i> -butylpyridine
<b>EDS</b>	Energy Dispersive X-Ray Spectroscopy
<b>ESI</b>	Electrospray Ionization
<b>FET</b>	Field-Effect Transistor
<b>FTC</b>	Framework Type Codes
<b>FT-IR</b>	Fourier Transform Infrared Spectroscopy
<b>GC</b>	Gas Chromatography
<b>GCMC</b>	Grand Canonical Monte Carlo
<b>HAADF-STEM</b>	High Angle Annular Dark Field Scanning Transmission Electron Microscopy
<b>HRMS</b>	High Resolution Mass Spectra
<b>HRTEM</b>	High Resolution Transition Electron Microscope
<b>ICP-OES</b>	Inductively Coupled Plasma Optical Emission Spectroscopy
<b>IZA-SC</b>	Structure Commission of the International Zeolite Association

---

---

<b><i>m</i>-CPBA</b>	<i>m</i> -Chloroperbenzoic Acid
<b>MOR</b>	Mordenite
<b>MS</b>	Mass Spectrometry
<b>MW</b>	Microwave
<b>NBE</b>	Norbornene
<b>NMR</b>	Nuclear Magnetic Resonance
<b>ODCB</b>	1,2-Dichlorobenzene
<b>PAHs</b>	Polycyclic Aromatic Hydrocarbons
<b>PBE</b>	Perdew-Burke-Ernzerhof
<b>PMMA</b>	Poly(methyl methacrylate)
<b>RIE</b>	Reactive Ion Etching
<b>RT</b>	Room Temperature
<b>TBHP</b>	<i>tert</i> -Butyl hydroperoxide
<b>TEM</b>	Transmission Electron Microscopy
<b>TEMPO</b>	2,2,6,6-tetramethyl-1-piperidinyloxy
<b>TFA</b>	Trifluoroacetic Acid
<b>TLC</b>	Thin Layer Chromatography
<b>UV/VIS</b>	Ultraviolet Visible Spectroscopy
<b>ZSM-5</b>	Zeolite Socony Mobil-5

---

## Chapter I

### Introduction

#### 1. Transition-Metal Catalyzed C–C Bond Formation

The development of C–C bond formation chemistry is highly essential for the functionalization and preparation of the backbones of organic molecules.<sup>1</sup> The mechanistic understanding is essential to develop novel and concise synthetic protocols. Particularly in chapters, I focus on the molecular transformations based on transition-metal catalyzed cross-coupling reactions and C–H activations by presenting the history, mechanism, and applications both on homogenous and heterogeneous catalysis.

#### 1.1. Cross-Coupling Reactions

Transition-metal catalyzed cross-coupling reactions have been widely utilized as efficient and practical synthetic tools.<sup>2</sup> It is useful for the synthesis of various C–C bonds to afford biaryl or heteroaryl moieties. As shown in Figure 1.1, there are various named reactions depending on the organometallic compounds. In 2010, Richard F. Heck, Ei-ichi Negishi and Akira Suzuki shared the Nobel Prize in chemistry for their contributions to C–C coupling developments and/or mechanistic studies.<sup>3</sup>

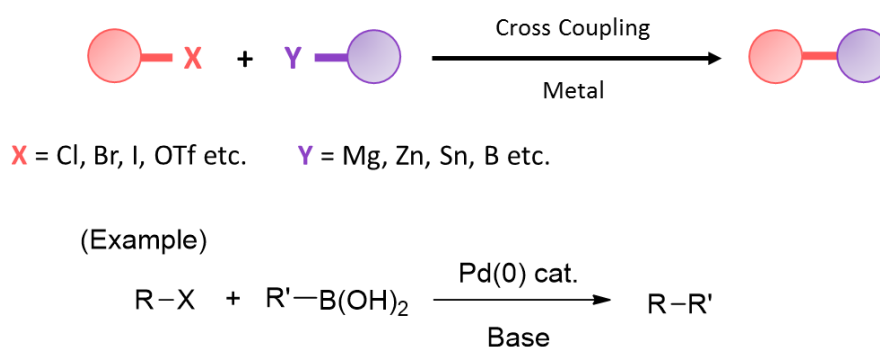


**Figure 1.1.** General reaction scheme and an example of cross-coupling reaction.

Palladium-catalyzed cross-coupling reactions has been one of the most important synthetic methods by providing revolutionized routes with a high practicality for the construction of carbon–carbon (C–C), carbon–nitrogen (C–N), carbon–oxygen (C–O) and carbon–heteroatom (C–X) bonds. These transformations have been widely utilized in both industry and academia.<sup>4</sup> Pd-catalyzed cross-coupling has been rapidly developed as revealed by the increasing number of publications/patents in this area. Since the successful C–C bond formation chemistry, synthetic chemists have been also making an endeavor to discover new C–N or C–X cross-coupling reactions.

### 1.1.1. The History of Cross-Coupling Reactions

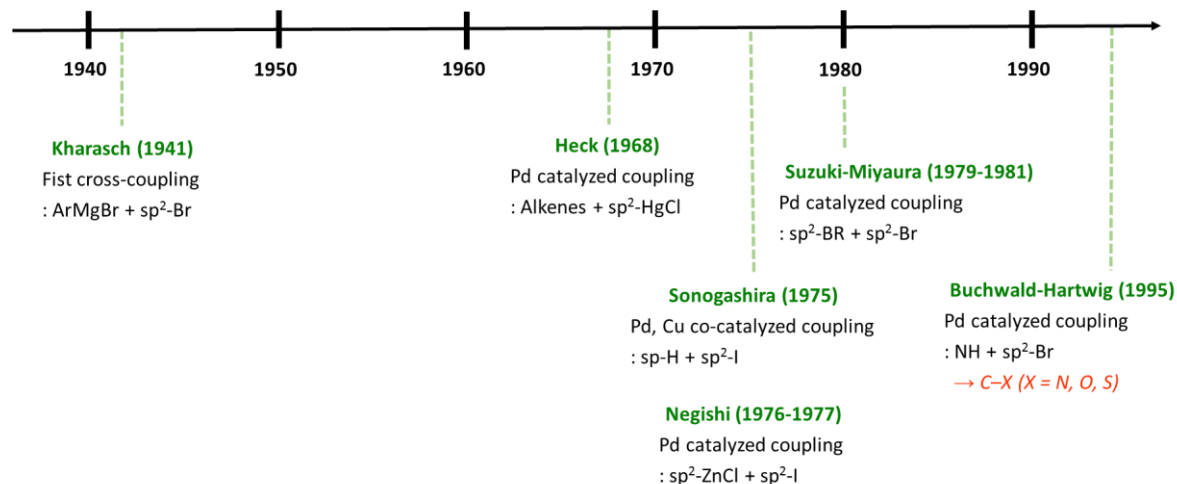
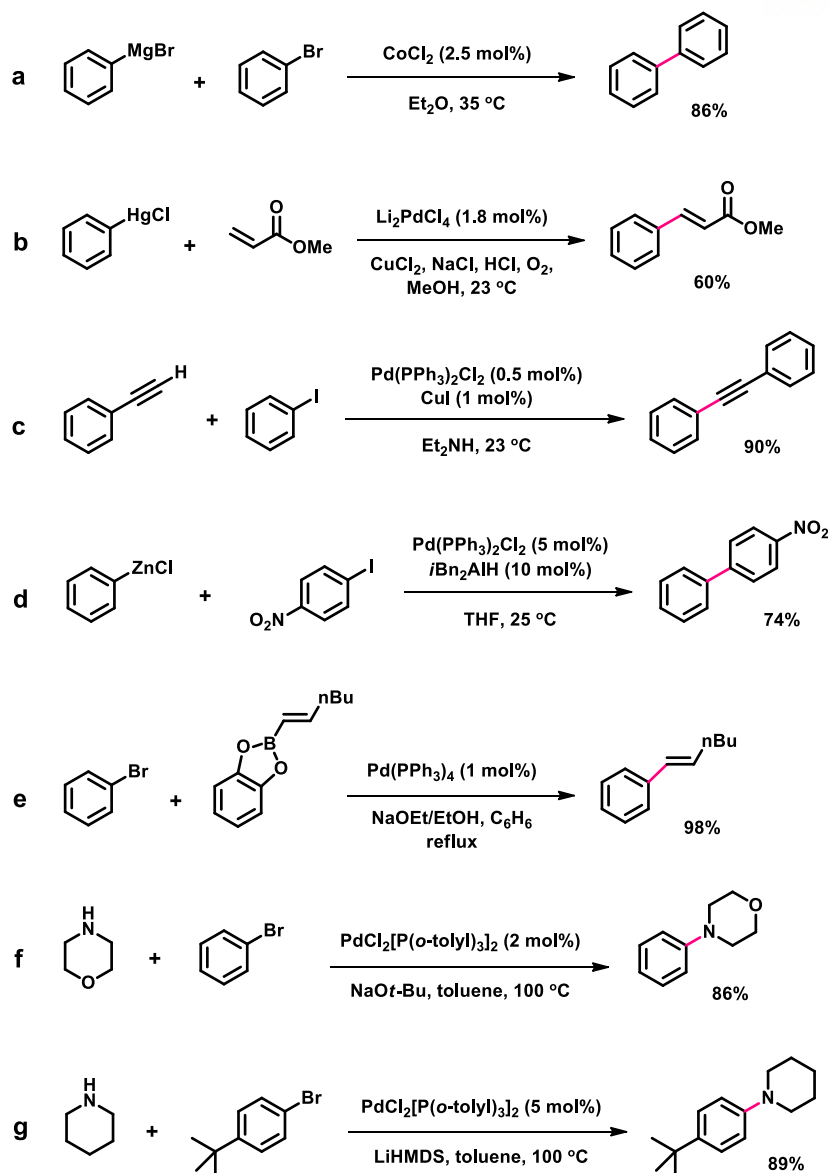


**Figure 1.2.** Simplified history of cross-coupling reactions.

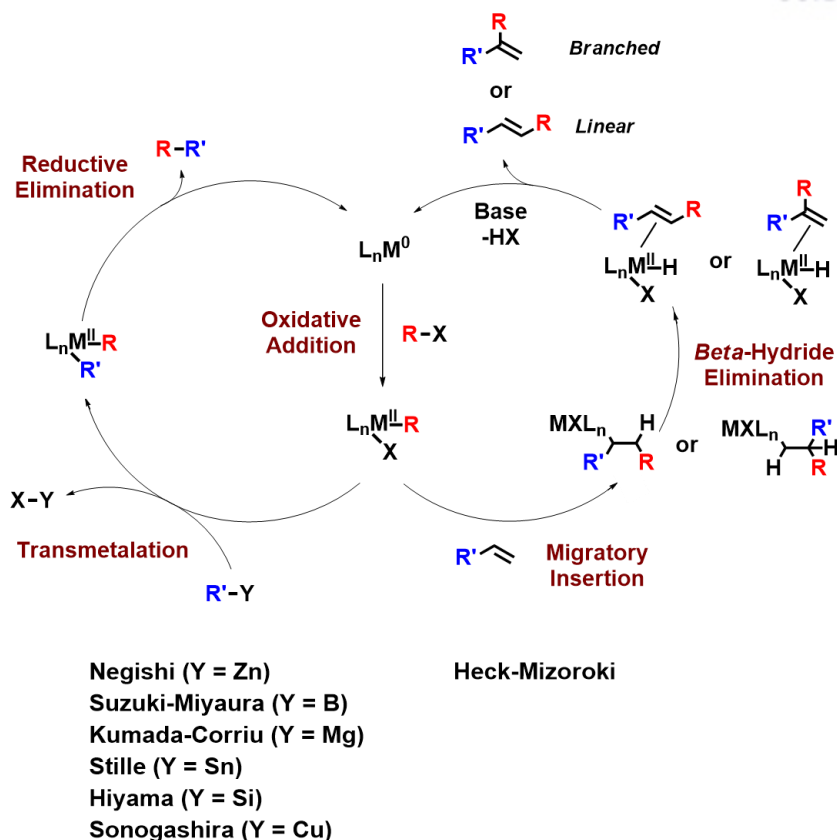
This chapter covers the most prominent milestone examples of cross-coupling reactions presented as the named reactions (Figure 1.2). The first transition-metal catalyzed sp<sup>2</sup>-sp<sup>2</sup> coupling reaction was reported by Kharasch in 1941 based on the Grignard reagent and cobalt catalyst (see Scheme 1.1a).<sup>5</sup> This work was further extended to vinyl bromide by replacing aryl bromide. Approximately three decades later, Pd-catalyzed cross-coupling area began to arise. Heck investigated the arylation of alkenes by using an organomercury reagent in 1968 (Scheme 1.1b).<sup>6</sup> In 1975, the Sonogashira coupling was established under substantially milder reaction conditions using copper co-catalyst to afford copper acetylide intermediate, and this reaction requires only catalytic amount of transition metals (Scheme 1.1c).<sup>7</sup> Negishi reported Ni- or Pd-catalyzed cross-coupling reactions for the first time by utilizing organoaluminium as coupling reagent, followed by the use of aryl zinc reagents in 1976. (Scheme 1.1d).<sup>8</sup> Suzuki and Miyaura reported palladium-catalyzed cross-coupling between alkenylboranes and aryl halides in 1979 (Scheme 1.1e).<sup>9</sup> This cross-coupling reaction has been exceedingly progressed and its mechanism has been studied in detail. With these aids, previously challenging C-C bond formations have been already feasible with the aids of various organometallic reagents. Remarkably, Buchwald and Hartwig independently have discovered the C-N bond formation chemistry using free amines and aryl halides under Pd-catalysis in 1995 (Scheme 1.1f and g).<sup>10,11</sup> This methodology has been also applied to prepare C-O and C-S bonds.



**Scheme 1.1.** (a) the Grignard-based Kharasch coupling, (b) the Heck reaction, (c) the Sonogashira reaction, (d) the Negishi reaction, (e) the Suzuki–Miyaura reaction, (f) the Buchwald coupling, (g) Hartwig coupling.

### 1.1.2. Mechanism of Cross-Coupling Reactions

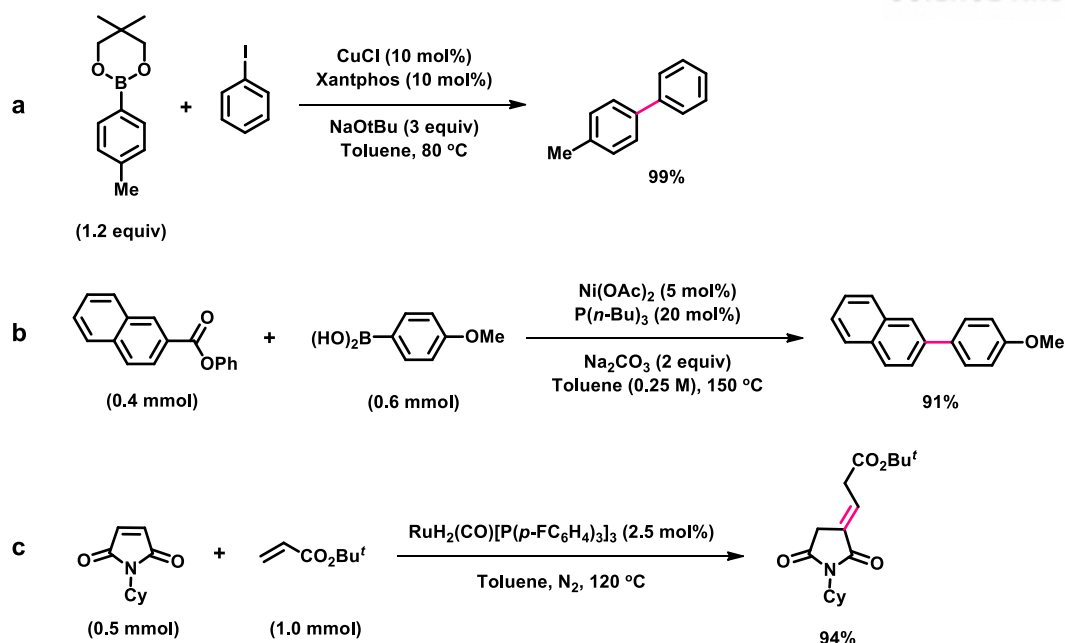
The elementary steps of cross-coupling reaction are generally categorized into three stages, (i) oxidative addition, (ii) transmetalation, and then (iii) reductive elimination in regular sequence. The reaction mechanism starts with the oxidative addition of metal into an organic halide. Consequently, the second reaction partner coordinates metal center with eliminating the functional groups in transmetalation. The final step is the reductive elimination of the two-coupling species while regenerating the catalyst. Notably, the Heck–Mizoroki reaction undergoes through carbometallation and beta-hydride eliminations.<sup>12</sup>



**Scheme 1.2.** General mechanism of cross-coupling reactions. Adapted from reference [4].

### 1.1.3. Recent Advances in Cross-Coupling Reactions

The Brown group developed a copper-catalyzed Suzuki–Miyaura reaction through unique carboboration step. This simple one-pot reaction allows a broad substrate scope and improved orthogonal reactivity compared to palladium-catalyzed processes (Scheme 1.3a).<sup>13</sup> And the Itami group reported the Ni-catalyzed decarbonylative cross-coupling reaction between an organoboron and an ester. They also presented crucial mechanistic features using comprehensive theoretical calculations. This reaction has various scopes including successful aliphatic cross-coupling along with the gram-scale utility (Scheme 1.3b).<sup>14</sup> In addition, the Miura group demonstrated the Ru-catalyzed direct coupling reactions. *N*-substituted maleimides readily undergo intermolecular cross-coupling with electron deficient alkenes. This C–C coupling is simple and provides wide range of alkylidene-succinimide derivatives (Scheme 1.3c).<sup>15</sup>



**Scheme 1.3.** (a) Cu-catalyzed cross-coupling of boronic esters with aryl iodides, (b) decarbonylative cross-coupling via Ni catalysis, (c) Ru-catalyzed cross-coupling of maleimides with alkenes.

## 1.2. C–H Activation and Functionalization

C–H bond functionalization or C–H activation is a powerful way to directly transform C–H bond into other functional groups including C–C, C–N, and C–O bonds.<sup>16</sup> The key step is the agnostic interaction, where a transition metal get involved in the bond cleavage process. The C–H bond is coordinated to a metal while generating an organometallic complex, which leads to M–C intermediate. This first step of making the intermediate is known as C–H bond activation or C–H activation. Subsequently, additional steps are occurred to produce the functionalized product (C–H functionalization). This activation is frequently assisted by directing groups (DGs) including amides, imine, ester, and carboxylate groups.<sup>17</sup>

Although cross-coupling reactions have been one of the most widely used synthetic methods to generate C–C bonds, they require pre-functionalization steps to prepare organic halides or triflates compounds, and organometallic compounds. On the other hand, the C–H activation can avoid these laborious steps. Therefore, transition-metal-catalyzed C–H activation or functionalization chemistry offers step- or atom-economical routes.<sup>18</sup> Unique construction of C–C bonds starting from readily available substrates opens new possibilities to develop concise and unexpected synthetic methods. Moreover, it can be further applied for the efficient modification of complex molecules, originally prepared through multistep syntheses.<sup>19–22</sup>



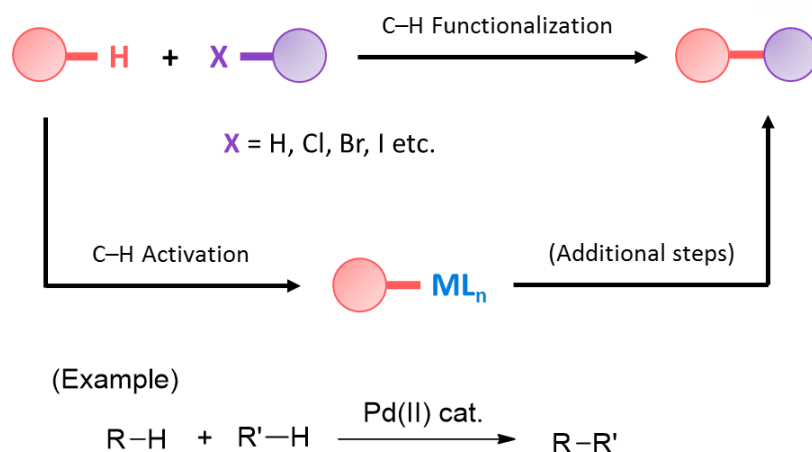
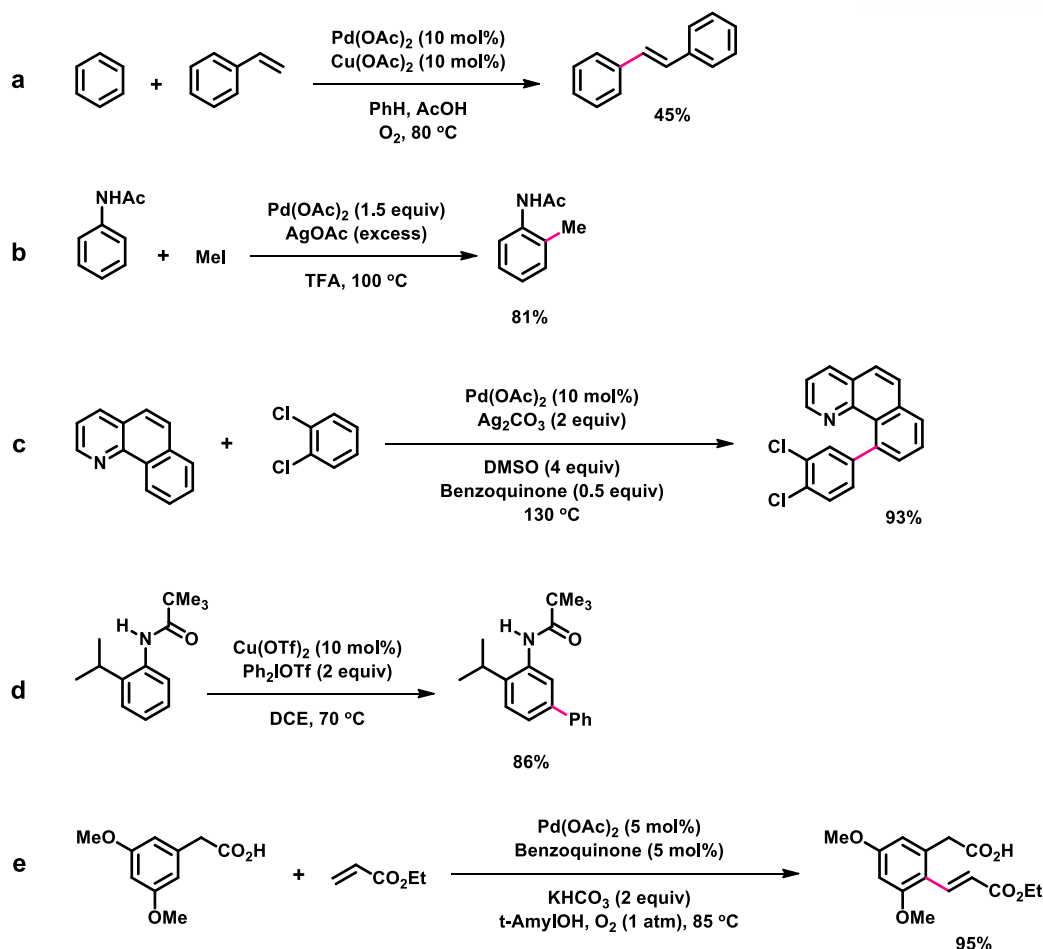


**Figure 1.3.** General scheme and an example for C–H functionalization.

### 1.2.1. History of C–H Activation and Functionalization

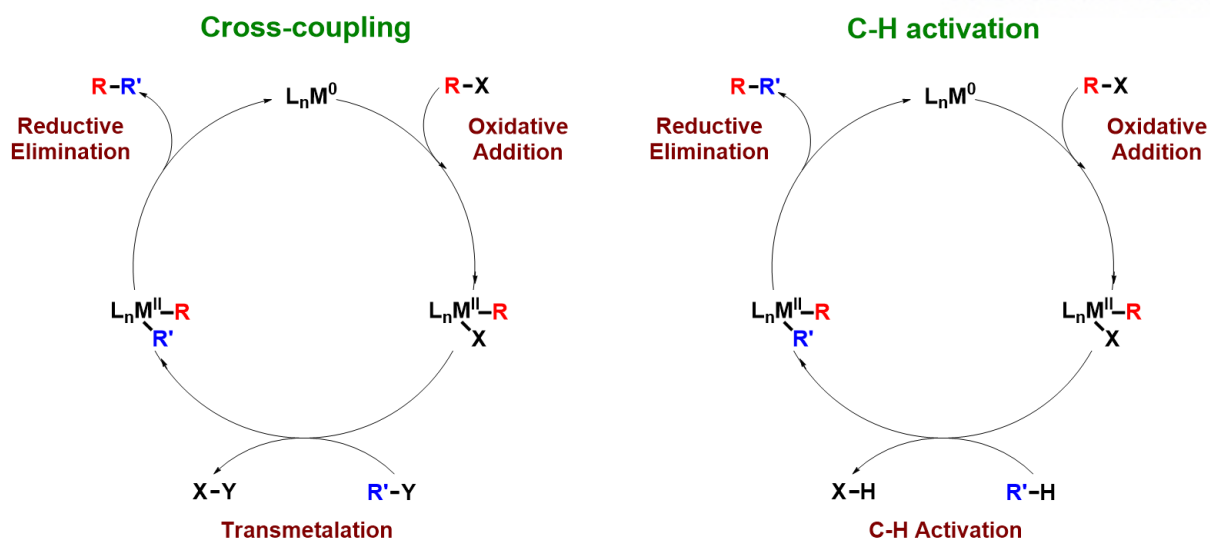
Fujiwara and Moritani reported the Pd-catalyzed dehydrogenative reaction between benzene and styrene in 1969. This seminal work has similarity to cross-coupling reaction, yet without presence of organic halides or organometallic compounds. This reaction set the milestone for the direct coupling between arenes and alkenes (Scheme 1.4a).<sup>23</sup> Tremont and Rhaman demonstrated the first *ortho*-methylation of anilide in 1984. They presented that the reactivity of cyclopalladated intermediate with MeI through Pd<sup>II</sup>/Pd<sup>IV</sup> platform (Scheme 1.4b).<sup>24</sup> In 2007, the Sanford group introduced the oxidative cross-coupling of fused-cyclic arenes with a pyridine moiety as an efficient DG. This work showed a highly chemoselective arylation of benzo[*h*]quinolone under Pd-catalyzed conditions, which was promoted by involving benzoquinone as an oxidant (Scheme 1.4c).<sup>25</sup> Electron-donating groups of arenes typically direct the electrophile to *ortho*- or *para*-position through electrophilic aromatic substitution (S<sub>E</sub>Ar). Thereby, the direct formation of *meta*-substituted anilide products have been intrinsically prohibited. In 2009, the Gaunt group reported the Cu-catalyzed *meta*-selective arylations on anilide derivatives with diaryliodonium salts. Remarkably, this method features broad substrate scope and mild reaction conditions. (Scheme 1.4d).<sup>26</sup> Furthermore, Yu group reported a prominent Pd-catalyzed C–H olefination with controlled positional selectivity and reactivity with the aid of a ligand. This reaction has excellent substrate scope in good yields and enables efficient synthesis of some pharmaceutical drug scaffolds and natural product cores (Scheme 1.4e).<sup>27</sup>



**Scheme 1.4.** (a) the Fujiwara and Moritani reaction, (b) *ortho*-methylation of anilide, (c) application of pyridine-based DG, (d) *meta*-selective Cu-catalyzed arylation, (e) utilization of a ligand.

### 1.2.2 Mechanism of C–H Activation and Functionalization

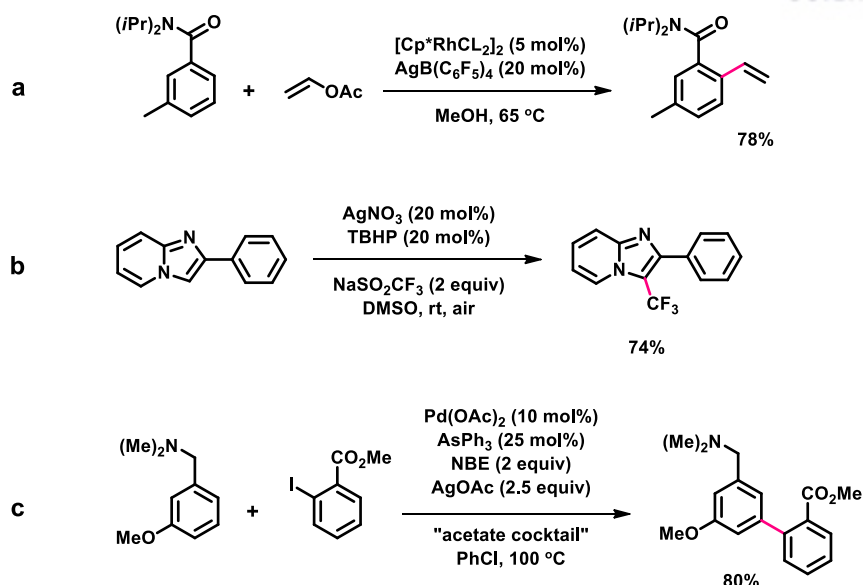
This chapter compares the reaction mechanisms between cross-coupling reaction and C–H activation. As shown in Scheme 1.5, cross-coupling reaction employs organic halides and organometallic compounds. Thus the catalytic cycle require transmetalation and extra procedures to prepare substrates. Instead, C–H activation avoids transmetalation step, and there is no need for preparing pre-functionalization steps.



**Scheme 1.5.** Comparison of conventional cross-coupling with C–H activation. Adapted from reference [18].

### 1.2.3 Key Examples of C–H Activation and Functionalization

Otley and Ellman reported the Rh-catalyzed C–H vinylation of anilides through the release of OAc group. The styrene derivative is formed from an anilide having amide as directing group (Scheme 1.6a).<sup>28</sup> And Hajra and co-workers reported Ag-catalyzed trifluoromethylation of imidazopyridines by employing the Langlois reagent. Mild reaction conditions, regioselectivity, and wide range of substrates scope are the main feature of this work (Scheme 1.6b).<sup>29</sup> Dong group demonstrated a highly *meta*-selective C–H arylation using Pd/norbornene catalytic system (the Catellani type conditions). This method used tertiary amine as a directing group and AsPh<sub>3</sub> as a ligand. The transformation is carried out under this unique “acetate cocktail” conditions (Scheme 1.6c).<sup>30</sup> Heteroarenes are also tolerated under the reaction conditions.



**Scheme 1.6.** (a) Rh-catalyzed direct C–H vinylation of styrene derivatives, (b) regioselective oxidative trifluoromethylation of imidazoheterocycles, (c) amine-directed *meta*-selective C–H arylation using Pd/norbornene catalytic system.

## 2. Heterogeneous Catalysts

Heterogeneous catalysis is essential in approximately 85-90% of the industrial processes to afford fine chemicals, bulk chemicals, pharmaceutical drugs, energy materials, and among others.<sup>31</sup> The term 'catalysis' was coined by Baron J. J. Berzelius for the first in 1836.<sup>32</sup> It is defined by the property of some chemicals that permit to enhance the rate of a reaction by reducing the corresponding activation energy. Since catalysts are regenerated through the cycles, they are not a reactant and only small amount is required.<sup>33</sup>

Catalytic processes can be generally categorized into three parts as heterogeneous, homogeneous, or enzymatic way. Herein, we discuss on the chemical catalysts used in organic synthesis, which are differentiated by the phases. Homogeneous catalysts are typically miscible with solvents and also reactants. In sharp contrast, heterogeneous catalysts are usually immiscible with solvents and reagents. Generally, the catalyst is in a solid phase and reactants are in a liquid phase.<sup>34</sup> Thereby, the main advantage of heterogeneous catalyst is the facile separation of products from the reaction mixture, benefitting in continuous chemical processes. Furthermore, heterogeneous catalysts are normally more robust and stable under the extreme operating conditions compared with their homogeneous analogues.<sup>35</sup>

## 2.1 Heterogeneous Catalytic Reactions

The reaction progress within a heterogeneous catalysis can be visualized in Figure 1.4. In a macro-level, the reactants simply enter into the reactor, and then products exit after molecular transformations (Figure 1.4, left). However, the chemistry in a molecular-level is more complicated. The whole reactions are made of (i) the diffusion of substrates into the catalyst pores, (ii) their adsorption, (iii) chemical transformations at the active sites, decomposition of the adsorbed complex on its surface (product-surface), and (iv) release of the products from the catalyst (Figure 1.4, right).<sup>36</sup>

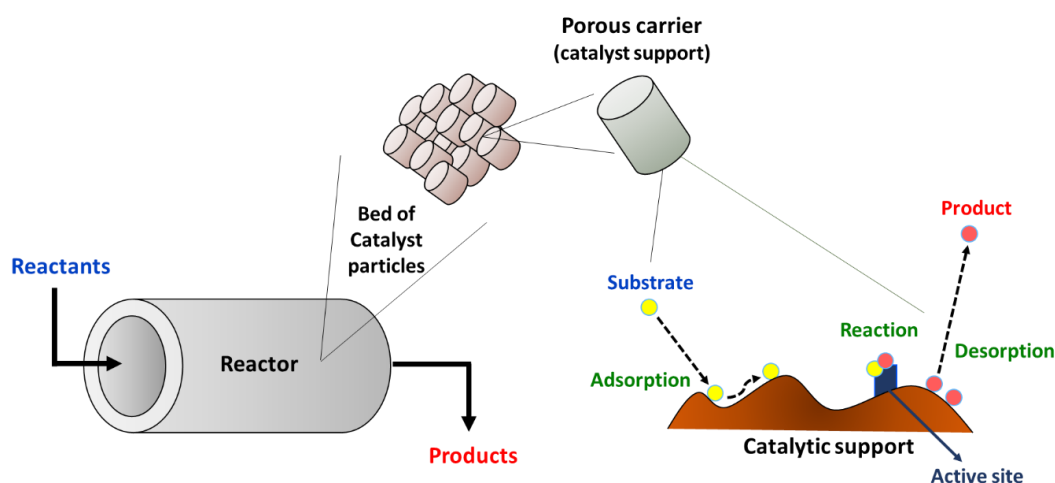


**Figure 1.4.** Schematic representation of the progress of a heterogeneous catalytic reactions. Adapted from reference [36].

## 2.2 Metal-Exchanged Zeolites as Heterogeneous Catalysts

Zeolites are crystalline microporous materials that are constructed from interlinked tetrahedral building units, typically alumina ( $\text{AlO}_4$ ) and silica ( $\text{SiO}_4$ ). Unlike amorphous silica having various pore sizes, zeolites have well-defined structures and pore sizes. The two- or three-dimensional inorganic networks sometimes possess enhanced reactivities by taking active sites within the pores and have become one of the key supports for single-site catalysis. Because counter-cations ( $\text{Na}^+$ ,  $\text{H}^+$ ,  $\text{NH}_4^+$ ) with the frameworks can be ion-exchanged with 3d- or 4d-transition-metals, metal-exchanged zeolites can be applied as efficient catalysts for the cross-coupling reactions.<sup>37</sup>

### 2.2.1 Types of Zeolites

Historically, zeolites are originated from naturally occurring minerals in many parts of mine. However, most forms applied in chemical industry are synthetic zeolites. Zeolite frameworks can be distinguished according to variable physical and chemical properties.<sup>38</sup> Crystal structure and chemical composition can provide basic criteria of the primary differences. Particle size, cation-exchange selectivity, chemical

composition, pore size and volume, surface area, and mechanical strength can differ depending on the zeolite in question. There are diverse examples of natural- and synthetic zeolites, each with a distinctive structure. The commonly accessible pore sizes range from around 3 Å to 10 Å.<sup>39</sup> Herein, we utilized mid- to large pore sized examples include zeolite-β, Y, mordenite (MOR) and ZSM-5.

## 2.2.2. Zeolite Frameworks

### 2.2.2.1. Geometry and Structures

Generally, their primary structure on zeolites is constructed from  $[\text{SiO}_4]$  and  $[\text{AlO}_4]$  tetrahedral building blocks, where silicon or aluminum atoms are located at center and oxygen atoms at corners. The tetrahedral units combine each other to afford more complex units by constructing 4- or 6-membered rings. This large structures are called secondary building units. Moreover, the combination of secondary units can even build up three dimensional cages (Figure 1.5). The chemical compositions of zeolites are determined by Si/Al molar ratio.<sup>40</sup>

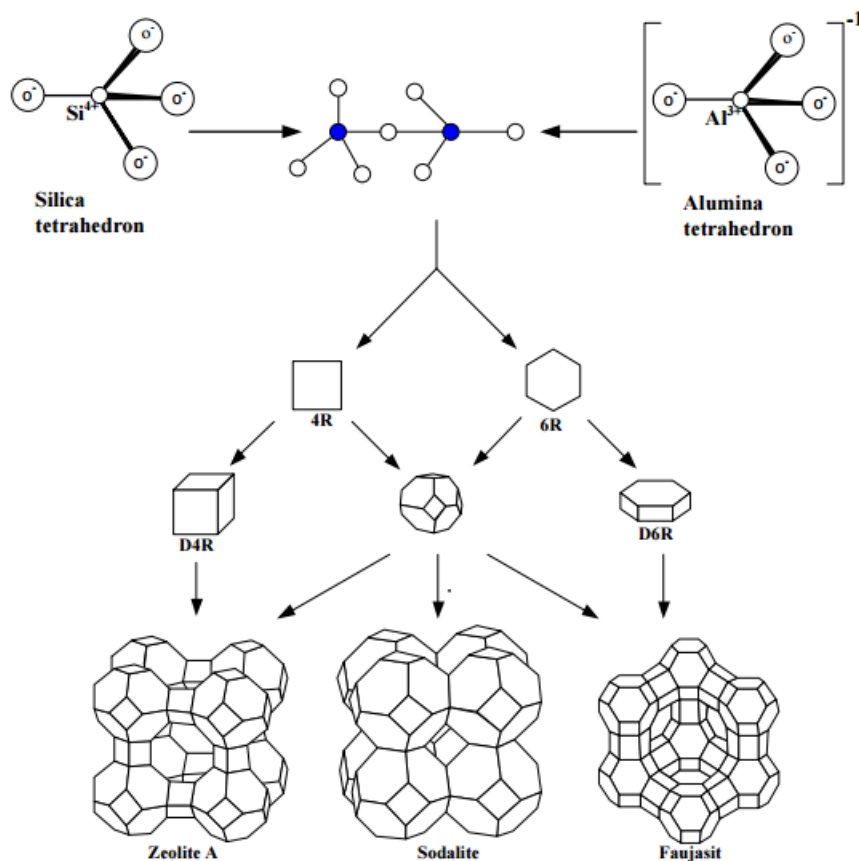


**Figure 1.5.** Structural units of zeolite A, sodalite and faujasite.<sup>41</sup>

### 2.2.2.2. Zeolite Framework Structures

Zeolite frameworks are divided by their lattice structure and the Framework Type Codes (FTC) are often utilized to assign their identification. The codes have been updated and approved, and data-based system is supplied by the Structure Commission of the International Zeolite Association (IZA-SC) (see: the 6<sup>th</sup> edition of the Atlas of Zeolite Framework Types). The similar zeolites can be grouped according to their three dimensional crystalline structures. Figure 1.6 reveals the representative zeolite framework structures used in this thesis, especially for the heterogeneous catalysis.

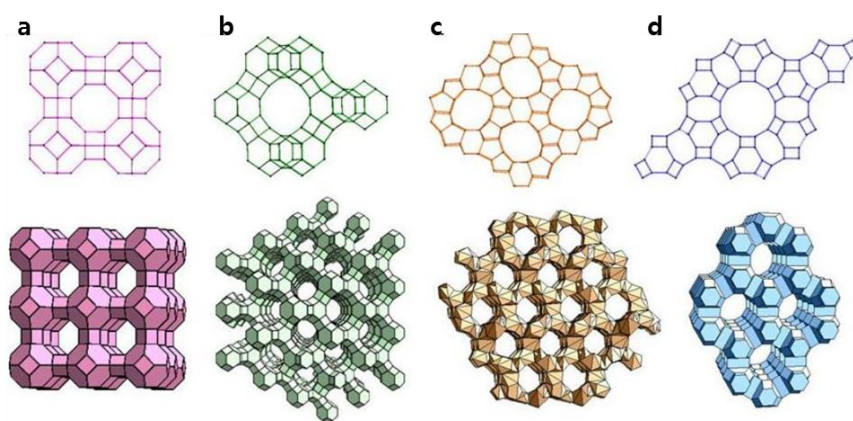


**Figure 1.6.** Some common zeolites frameworks (a) zeolite A (3D, 4.2 Å), (b) zeolite Y (3D, 7.4 Å), (c) zeolite L (1D, 7.1 Å), (d) ZSM-5 (silicalite) (2D, 5.3 ×5.6 Å, 5.1 ×5.5 Å). D stands for the dimensions of channel system.<sup>42</sup>

### 2.2.3 Ion-Exchange and Adsorption Properties of Zeolites

Herein, an ion-exchange reaction (or called metathesis) means the replacement of cations within the zeolite systems. Zeolites provide excellent cation-exchange or adsorption properties since cations are balanced by anionic charges on the surfaces of pores in zeolites.  $[\text{SiO}_4]$  and  $[\text{AlO}_4]$  tetrahedra are interconnected by sharing oxygen atom, and some of Si ions can be replaced by an Al ions. Therefore, the framework has negative charge(s) on the surface, and it can trap cations to establish charge-balance by accommodating  $\text{Na}^+$ ,  $\text{K}^+$ ,  $\text{NH}_4^+$  and  $\text{Ca}^{2+}$  ions.<sup>43</sup> For example, an ion exchange process in zeolites can be applied for ammonium salts removal from waste water. Once ammonium chloride aqueous solution passes through a zeolite package,  $\text{Na}^+$  ions within the zeolite frameworks can be readily exchanged by  $\text{NH}_4^+$  ions (Figure 1.7) generation the purified aqueous solutions to the environment.<sup>44,45</sup> The capacity of adsorbent (See Figure 1.8) and ion exchange property of zeolites are often influenced by their matrix composition (charge), polarity, pore size distribution, and (inner) surface area.<sup>46</sup> Base on these properties, zeolites can even applied to the various areas including catalysis and separations both in academia and industry.

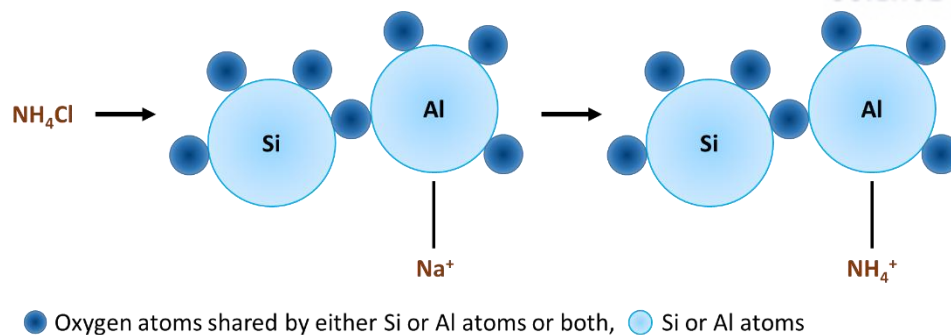


**Figure 1.7.** Schematic presentation of ion-exchange process in the mixture of ammonium chloride solution and sodium-zeolites. Adapted from reference [45].

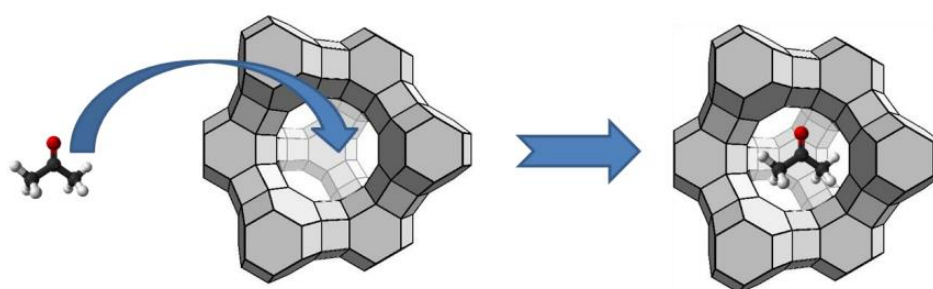


**Figure 1.8.** Adsorption of a small molecule (acetone) inside a zeolite Y pore (window 7.4 Å, cage 13.2 Å).<sup>42</sup>

#### 2.2.4 Single-Site Catalysis by (Metal-Exchanged) Zeolites

To enhance the selectivities of the classical heterogeneous catalysis, current researches have been focusing on the targeted molecular (also referred as single-site) heterogeneous catalysis. Whereas other heterogeneous catalysts have various active sites, zeolites have received a scientific attention as supports due to the defined catalytic sites. Yet, the strict meaning of “single-site” may comprise of one or more atoms.<sup>47</sup> Such single-sites are spatially well-defined and separated from each other within the solid frameworks showing the differences compared with homogenous catalysts. This term also involves a methodology to anchor the molecular active sites to the frameworks.<sup>48</sup> Single-site heterogeneous catalyst can be prepared from metal-cations coordinated to the surface ligands within a rigid framework. These sites are located within the supporting support having different geometries and anchoring patterns could be diverse.<sup>49</sup> Thus, it is challenging work to generate and identify the structurally defined anchored sites. The major difference between homogeneous and single-site heterogeneous catalysts is the existence crystalline structures (channels and pores), which influence the kinetics and selectivities.



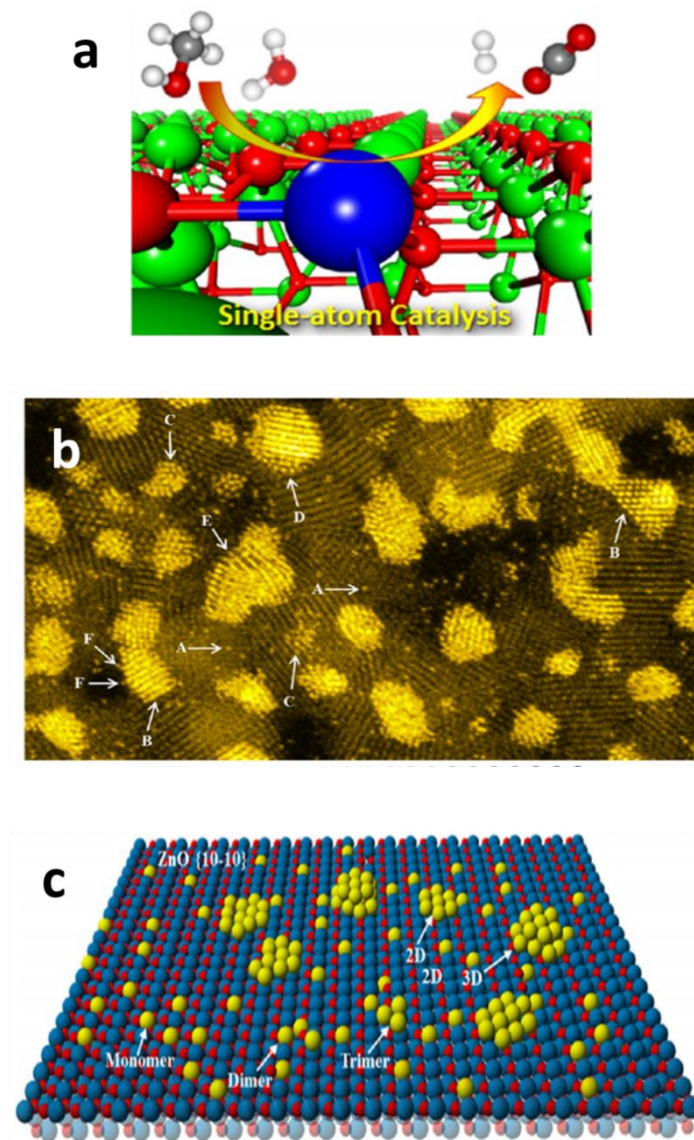


**Figure 1.9.** (a) brief scheme of single-atom catalysis, (b) a HAADF-STEM image of a Pt/ZnO nanobelt model catalyst presenting different Pt atoms, (c) various metallic clusters positioned onto the ZnO surface.<sup>50</sup>

### 3. Microwave Reactions

The development of rapid and efficient synthetic protocols without increasing side products is one of the challenging yet practical issues in industry. Microwave chemistry is a prominent method to allow the organic transformations with shortened reaction time. The reaction time can be substantially reduced from days/hours to minutes/seconds by replacing conventional heat to microwave irradiation. Closed microwave vessel provides a highly-effective heating environment. In addition, the controlling of energy input and output, reaction time and temperature is accurate by avoiding the heat transfer process.<sup>51</sup> For these reasons, microwave heating method is useful for green chemistry and catalysis.<sup>52</sup>

#### 3.1. Physical Background

Like other electromagnetic waves, microwaves are made from orthogonal combination of electric and magnetic fields (Figure 1.10). There are three major factors to be considered for the synthetic applications, practically for the reaction vessel employment. The first unit is an insulator or microwave-transparent vessel including Teflon. There is no loss of the microwaves. The second unit is a conductor (metal) not allowing its penetration. And the third unit is an absorber including water and organic solvents. The physical origin of microwave absorption is from by dielectric heating.<sup>53</sup>

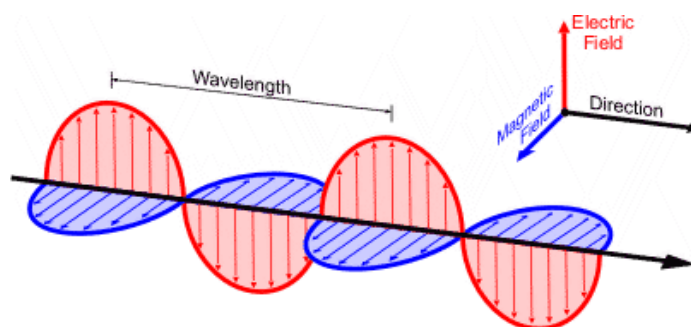


**Figure 1.10.** Electric ( $E$ ) and magnetic ( $H$ ) field components in microwaves. (web source: [http://www.srh.noaa.gov/jetstream/remote/remote\\_intro.html](http://www.srh.noaa.gov/jetstream/remote/remote_intro.html))

Whereas the heating mechanism of polar compounds are linked by the dipolar polarization effect, while the mechanism of charged molecules are by ionic conduction. The common-used materials of microwave vessels are borosilicate glass or Teflon.<sup>54</sup> Unlike conventional heating, microwave heating efficiently generates inside of reaction mixture (Figure 1.11). Therefore, superheating occurs since this interior heat transfer diminish the wall effects by removing the thermal boundary layer. Besides, it is feasible to keep the solution at even higher temperature than their conventional reflux temperature by using closed microwave vessels which are able to tolerate the huge pressures, the superheating effects are distinctly magnified.<sup>55</sup> Thereby, microwave irradiation often allows the reduced reaction time, improved yields, and cleaner reaction profiles.<sup>56</sup> Yet, it is difficult to scale-up chemical reactions.

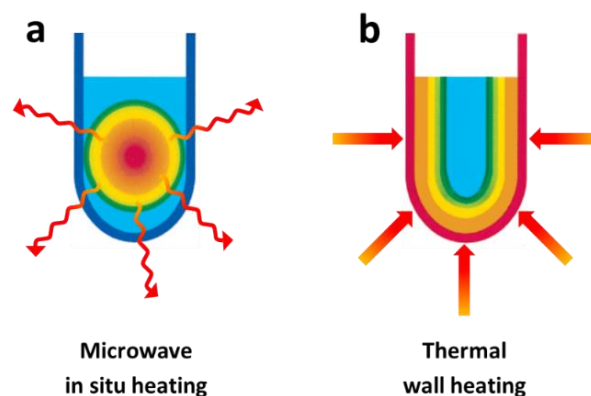
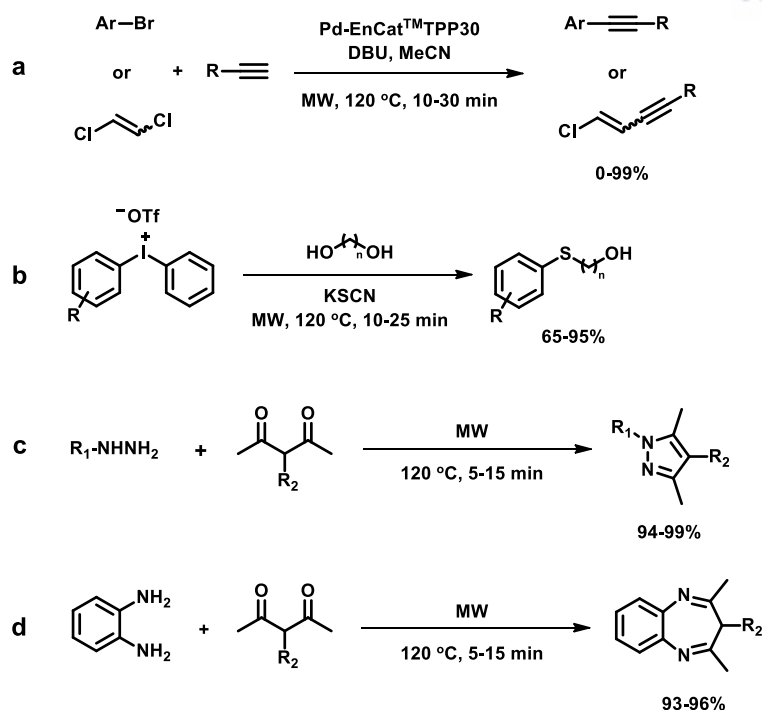


**Figure 1.11.** Schematic representation of heating mechanism (red color stands for higher temperature while blue color indicates lower temperature). Adapted from reference [55].

### 3.2 Microwave-Assisted Organic Synthesis

The Ley group reported the Sonogashira cross-coupling using recyclable palladium catalysts, so-called Pd-EnCat<sup>TM</sup>, under microwave irradiation. This method presented wide substrate scope having 38 examples with moderate to excellent yields. The high catalytic stability of Pd-EnCat<sup>TM</sup> was examined through the reusability test upto 6<sup>th</sup> cycle (Scheme 1.7a).<sup>57</sup> The Leazer group also described practical and rapid method to generate  $\beta$ - and  $\gamma$ -hydroxy sulfides, which can be utilized as candidates of anti-HIV or anticancer agents. Readily available potassium thiocyanate (KSCN) and ethylene glycol/propylene glycol with diaryliodonium salts were employed under catalyst-free conditions (Scheme 1.7b).<sup>58</sup> Moreover, a facile reaction procedure by the same group was reported to prepare pyrazoles and diazepines from 1,3-diketones/ $\beta$ -ketoester under solvent- and catalyst-free conditions using microwave chemistry. A substrate scope studies were given by 17 examples of pyrazole derivatives (Scheme 1.7c)<sup>59</sup> and 5 examples of diazepine derivatives (Scheme 1.7d).<sup>59</sup>



**Scheme 1.7.** (a) Microwave-assisted Sonogashira cross-coupling reaction (Ar = (hetero)aryl, R = (hetero)aryl or alkyl), (b) synthesis of β- and γ-Hydroxy sulfides using diaryliodonium salts, (c,d) synthesis of N-heterocycle compounds (R<sub>1</sub> = Ar and ArCO, R<sub>2</sub> = H, Cl, Et).

#### 4. References

- [1] Lo, J. C., Gui, J., Yabe, Y., Pan, C.-M., Baran, P. S. *Nature* **2014**, *516*, 343–348.
- [2] Nicolaou, K. C., Bulger, P. G., Sarlah, D. *Angew. Chem. Int. Ed.* **2005**, *44*, 4442–4489.
- [3] Johansson Seechurn, C. C. C., Kitching, M. O., Colacot, T. J., Snieckus, V. *Angew. Chem. Int. Ed.* **2012**, *51*, 5062–5085.
- [4] Johansson Seechurn, C. C. C., DeAngelis, A., Colacot, T. J., CHAPTER 1 Introduction to New Trends in Cross-Coupling. In *New Trends in Cross-Coupling: Theory and Applications*, The Royal Society of Chemistry: 2015; pp 1–19.
- [5] Kharasch, M. S., Fields, E. K. *J. Am. Chem. Soc.* **1941**, *63*, 2316–2320.
- [6] Heck, R. F. *J. Am. Chem. Soc.* **1968**, *90*, 5518–5526.
- [7] Sonogashira, K., Tohda, Y., Hagihara, N. *Tet. Lett.* **1975**, *16*, 4467–4470.
- [8] Negishi, E.-i., Baba, S. *J. Chem. Soc., Chem. Commun.* **1976**, 596b–597b.
- [9] Miyaura, N., Suzuki, A. *J. Chem. Soc., Chem. Commun.* **1979**, 866–867.
- [10] Guram, A. S., Rennels, R. A., Buchwald, S. L. *Angew. Chem. Int. Ed.* **1995**, *107*, 1456–1459.
- [11] Louie, J., Hartwig, J. F. *Tet. Lett.* **1995**, *36*, 3609–3612.
- [12] Jana, R., Pathak, T. P., Sigman, M. S. *Chem. Rev.* **2011**, *111*, 1417–1492.

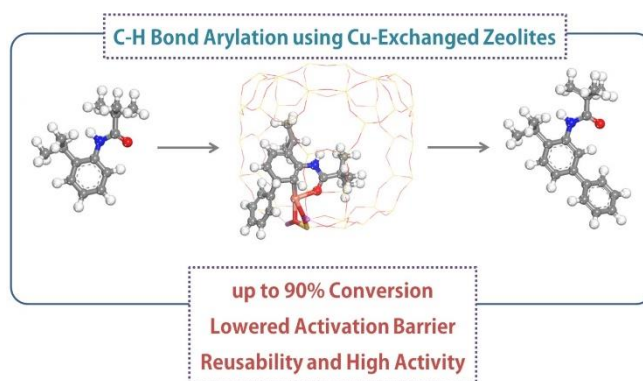
- [13] Zhou, Y., You, W., Smith, K. B., Brown, M. K. *Angew. Chem. Int. Ed.* **2014**, *126*, 3543–3547.
- [14] Muto, K., Yamaguchi, J., Musaev, D. G., Itami, K. *Nat. Commun.* **2015**, *6*, 7508.
- [15] Morita, T., Akita, M., Satoh, T., Kakiuchi, F., Miura, M. *Org. Lett.* **2016**, *18*, 4598–4601.
- [16] Godula, K., Sames, D. *Science* **2006**, *312*, 67–72.
- [17] Labinger, J. A., Bercaw, J. E. *Nature* **2002**, *417*, 507–514.
- [18] Chen, X., Engle, K. M., Wang, D.-H., Yu, J.-Q. *Angew. Chem. Int. Ed.* **2009**, *48*, 5094–5115.
- [19] Park, Y. J., Park, J.-W., Jun, C.-H. *Acc. Chem. Res.* **2008**, *41*, 222–234.
- [20] Wencel-Delord, J., Droge, T., Liu, F., Glorius, F. *Chem. Soc. Rev.* **2011**, *40*, 4740–4761.
- [21] Gensch, T., Hopkinson, M. N., Glorius, F., Wencel-Delord, J. *Chem. Soc. Rev.* **2016**, *45*, 2900–2936.
- [22] Davies, H. M. L., Morton, D. *J. Org. Chem.* **2016**, *81*, 343–350.
- [23] Fujiwara, Y., Moritani, I., Danno, S., Asano, R., Teranishi, S. *J. Am. Chem. Soc.* **1969**, *91*, 7166–7169.
- [24] Tremont, S. J., Rahman, H. U. *J. Am. Chem. Soc.* **1984**, *106*, 5759–5760.
- [25] Hull, K. L., Sanford, M. S. *J. Am. Chem. Soc.* **2007**, *129*, 11904–11905.
- [26] Phipps, R. J., Gaunt, M. J. *Science* **2009**, *323*, 1593–1597.
- [27] Wang, D.-H., Engle, K. M., Shi, B.-F., Yu, J.-Q. *Science* **2010**, *327*, 315–319.
- [28] Otley, K. D., Ellman, J. A. *Org. Lett.* **2015**, *17*, 1332–1335.
- [29] Monir, K., Bagdi, A. K., Ghosh, M., Hajra, A. *J. Org. Chem.* **2015**, *80*, 1332–1337.
- [30] Dong, Z., Wang, J., Dong, G. *J. Am. Chem. Soc.* **2015**, *137*, 5887–5890.
- [31] Chorkendorff, I., Niemantsverdriet, J. W., *Concepts of modern catalysis and kinetics*. John Wiley & Sons: 2006.
- [32] Davis, M. E., Davis, R. J., *Fundamentals of chemical reaction engineering*. Courier Corporation: 2012.
- [33] Binns, C., *Introduction to nanoscience and nanotechnology*. John Wiley & Sons: 2010, Vol. 14.
- [34] Ye, R., Hurlburt, T. J., Sabyrov, K., Alayoglu, S., Somorjai, G. A. *Proc. Natl. Acad. Sci. U. S. A.* **2016**, *113*, 5159–5166.
- [35] Thomas, J. M., Thomas, W. J., *Principles and practice of heterogeneous catalysis*. John Wiley & Sons: 2014.
- [36] Rothenberg, G., *Catalysis: concepts and green applications*. John Wiley & Sons: 2015.
- [37] Weitkamp, J. *Sol. St. Ion.* **2000**, *131*, 175–188.
- [38] Reyad, A. A. D., Aiman, E. A.-R. *Rec. Pat. Chem. Eng.* **2012**, *5*, 20–27.
- [39] Moller, K., Bein, T. *Chem. Soc. Rev.* **2013**, *42*, 3689–3707.
- [40] Margeta, K., Farkas, A., Šiljeg, M., Logar, N. Z., *Natural zeolites in water treatment-how effective is their use*. INTECH Open Access Publisher: 2013.
- [41] Masoudian, S. K., Sadighi, S., Abbasi, A. *Bull. Chem. React. Eng. Catal.* **2013**, *8*, 54–60.

- [42] Zheng, Y., Li, X., Dutta, P. K. *Sensors* **2012**, *12*, 5170.
- [43] Inglezakis, V. J. *J. Coll. Inter. Sci.* **2005**, *281*, 68–79.
- [44] Jorgensen, T. C., Weatherley, L. R. *Wat. Res.* **2003**, *37*, 1723–1728.
- [45] Jha, B., Singh, D. N., Basics of Zeolites. In *Fly Ash Zeolites*, Springer: 2016, pp 5–31.
- [46] Wang, S., Peng, Y. *Chem. Eng. J.* **2010**, *156*, 11–24.
- [47] Thomas, J. M., Raja, R., Lewis, D. W. *Angew. Chem. Int. Ed.* **2005**, *44*, 6456–6482.
- [48] Hlatky, G. G. *Chem. Rev.* **2000**, *100*, 1347–1376.
- [49] Zecchina, A., Bordiga, S., Groppo, E., The Structure and Reactivity of Single and Multiple Sites on Heterogeneous and Homogeneous Catalysts: Analogies, Differences, and Challenges for Characterization Methods. In *Selective Nanocatalysts and Nanoscience*, Wiley-VCH Verlag GmbH & Co. KGaA: 2011, pp 1–27.
- [50] Liu, J. *ACS Catal.* **2017**, *7*, 34–59.
- [51] Oliver Kappe, C. *Chem. Soc. Rev.* **2008**, *37*, 1127–1139.
- [52] Jones, D., Lelyveld, T., Mavrofidis, S., Kingman, S., Miles, N. *Res. Cons. Rec.* **2002**, *34*, 75–90.
- [53] Motasemi, F., Afzal, M. T. *Renew. Sust. Energ. Rev.* **2013**, *28*, 317–330.
- [54] Kappe, C. O. *Angew. Chem. Int. Ed.* **2004**, *43*, 6250–6284.
- [55] Larhed, M., Moberg, C., Hallberg, A. *Acc. chem. Res.* **2002**, *35*, 717–727.
- [56] Horikoshi, S., Serpone, N. *Catal. Sci. Tech.* **2014**, *4*, 1197–1210.
- [57] Sedelmeier, J., Ley, S. V., Lange, H., Baxendale, I. R. *Eur. J. Org. Chem.* **2009**, *2009*, 4412–4420.
- [58] Vaddula, B. R., Varma, R. S., Leazer, J. *Eur. J. Org. Chem.* **2012**, *2012*, 6852–6855.
- [59] Vaddula, B. R., Varma, R. S., Leazer, J. *Tet. Lett.* **2013**, *54*, 1538–1541.

## Chapter II

### C–H Bond Arylation of Anilides inside Copper-Exchanged Zeolites

Syntheses of fine-chemicals using heterogeneous catalysts have tremendous industrial potentials, yet C–H functionalization studies have been largely focused on homogeneous catalysis. We report here the first *meta*-selective C–H bond arylation of anilides inside copper-exchanged zeolites. Mid- or large-pore zeolite frameworks are selected as supports to access large organic molecules, and atomically distributed copper catalysts exhibit high activities (84–90% conversions) toward direct arylation of anilides with diphenyliodonium salt on 0.5 mol% copper concentration. Computational studies indicate the well-fitted copper-aryl complexes inside zeolite frameworks. Electron micrographs, elemental analyses, and reusability study show no observable leaching of catalytically active copper species during the reactions tested. These results demonstrate the practical synthetic potential of copper-exchanged zeolites as promising supported molecular catalysts to afford biaryl motifs-containing compounds with high catalytic activity, chemical stability, and recyclability. This chapter is reproduced from *J. Mol. Catal. A: Chem.* **2016**, 417, 64-70.



#### 1. Introduction

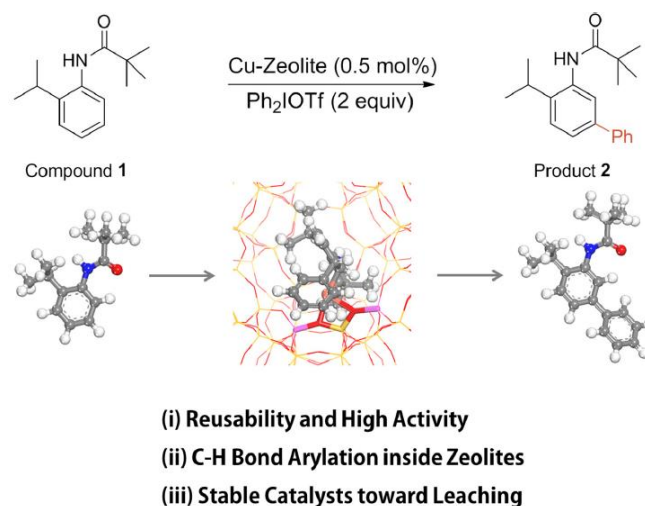
One of the prime goals of synthetic chemists is to develop efficient synthetic methods to construct sophisticated organic scaffolds. Over several decades, transition metal catalysis has expedited retrosynthetic disconnections, inventing original, innovative, and concise molecular transformations.<sup>1</sup> Advances in selective C–H bond functionalization engender new reaction pathways for C–C bond formations.<sup>2-4</sup> Thanks to the pharmaceutical or fine chemical importance of biaryl structural motifs, atom economical methods for aryl–aryl bond formation have been studied extensively. Direct arylation reaction via C–H bond cleavage creates shortened synthetic operations and can also minimize by-

product formation.<sup>5</sup> Pre-coordination allows site-selective transformation of C–H bond, and directing groups predominantly place transition metal in close proximity to arene *ortho* C–H bond.<sup>6,7</sup> Thereby, remote functionalization, e.g. *meta*-selective arylation, distal to directing groups is largely restricted.

Recently, Yang et al., introduced a rationally designed U-shaped nitrile-containing template approach to the direct remote C–H transformation of indolines.<sup>8</sup> An electron-withdrawing sulfonamide linkage was incorporated to prevent *ortho* or *para* C–H functionalization. Furthermore, the nitrile-adjacent germinal alkyl groups were installed to tune *meta*-directing conformations through the Thorpe-Ingold effect. Luo et al. developed a *meta*-selective arylation methodology of phenols via a traceless CO<sub>2</sub> directing group relay strategy.<sup>9</sup> However, template-aided synthesis is accompanied by the extra burden of installation and removal of auxiliary groups. The Gaunt group developed an intriguing *meta*-selective arylation reaction of *N*-protected anilides by using diaryliodonium salts and Cu(OTf)<sub>2</sub> through innate electronic effect.<sup>10,11</sup>

Despite the recent progresses in site-selective C–H functionalization, the reactions have been mostly restricted on homogeneous catalysis due to its molecularly defined catalytic nature and the well-established characterization protocols. In contrast, development of heterogeneous catalysis to synthesize complex organic molecules has been hampered due to uncertainties of catalytic sites and aggregation or leaching of active species during chemical reactions.<sup>12,13</sup> So far, a few groups reported direct arylation methods based on heterogeneous catalysis using metal nanoparticles, metal oxide, or Pd/C.<sup>14-18</sup> Considering the industrial importance, the syntheses of fine chemicals having complex molecular structures via heterogeneous catalysis have enormous potentials. Supported molecular catalysts located at the border between homogeneous and heterogeneous catalysts have been investigated as an emerging class.<sup>19</sup> Atomically distributed active sites inside structurally well-defined supports can exist with near uniformity.<sup>20</sup> Thanks to the superior metal-ion exchange capacity and microporous crystalline structures composed of uniform window and channel sizes, zeolite frameworks are selected as catalyst supports.<sup>21-25</sup> Herein, we describe the first *meta*-selective C–H bond arylation of anilides using copper-exchanged zeolites with high catalytic activities (Scheme 2.1). Kinetic and computational studies are performed to reveal the high catalytic efficiency of the zeolite catalysts to conduct C–H bond arylation. Their chemical stabilities over the reactions are evaluated via transmission electron microscopy (TEM) and energy-dispersive X-ray spectroscopy (EDS) analyses.



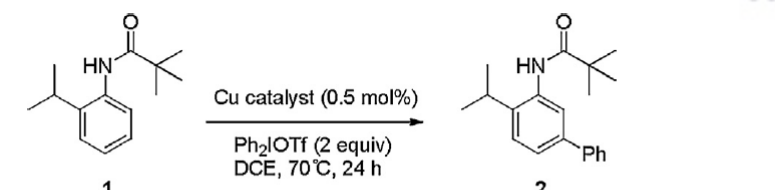


**Scheme 2.1.** Outline of the current direct arylation inside copper-exchanged zeolites.

## 2. Results and Discussion

Direct arylation of pivanilide **1** with diphenyliodonium triflate ( $\text{Ph}_2\text{IOTf}$ ) was performed to examine the catalytic activity of copper<sup>II</sup>-exchanged zeolites (denoted as Cu-zeolite as shown in Table 2.1). Taking into account the accessibility and diffusivity of organic molecules, mid- or large-pore zeolites (beta, Y, and mordenite) were selected. Diaryliodonium salt serves as an aryl transfer agent by generating aryl-copper complexes *in situ* with concomitant removal of aryl iodide.<sup>26,32</sup> In comparison to ceria-supported metallic Cu particles and alumina-supported copper oxide (entries 5 and 6), Cu-zeolites showed higher activities, leading to 84–90% conversions with slight yield variations depending on the types of zeolite framework (entries 1–4). It is noteworthy that C–H functionalization occurred *meta*-selectively on 0.5 mol% Cu concentration; previously reported homogeneous conditions required 10 mol% of  $\text{Cu}(\text{OTf})_2$ .<sup>10</sup>

To explore the synthetic utility of Cu-zeolites, the direct arylation of **1** was performed on 10 times larger scale (Table 2.2). There action afforded arylated compound **2** in 87%. Moreover, recyclability experiments were carried out to reveal the practical and industrial utilities enabling the greener routes in organic synthesis. There was no apparent loss of copper catalytic activity until the 5<sup>th</sup> cycle. In fact, slight activity increasement through the initial recycle tests was observed.



Entry	Catalyst	Cu (wt%) <sup>b</sup>	Cu/Al	Conversion (%) <sup>c</sup>	Yield (%) <sup>d</sup>
1	Cu-β	0.44	0.06	87	84
2	Cu-β	2.94	0.39	90	87
3	Cu-Y	10.34	0.39	88	85
4	Cu-MOR	5.14	0.39	84	80
5	Cu/CeO <sub>2</sub>	10	-	0	0
6	CuO-Al <sub>2</sub> O <sub>3</sub>	13	-	57	55

<sup>a</sup> Reaction conditions: **1** (0.228 mmol), Ph<sub>2</sub>IOTf (0.456 mmol), catalyst (0.5 mol%) in DCE (1.25 mL).  
<sup>b</sup> Copper loaded on the respective solid support.  
<sup>c</sup> Determined by <sup>1</sup>H NMR based on integral values of *tert*-butyl group of **2** with respect to **1**.  
<sup>d</sup> Isolated yield.

**Table 2.1.** Direct arylation of pivanilide **1** with copper catalysts.<sup>a</sup>

First Use	Recycle 1 <sup>st</sup>	Recycle 2 <sup>nd</sup>	Recycle 3 <sup>rd</sup>	Recycle 4 <sup>th</sup>	Recycle 5 <sup>th</sup>
87%	89%	93%	93%	93%	88%

[a] Reaction condition: **1** (2.28 mmol, 0.5 g), Ph<sub>2</sub>IOTf (4.56 mmol), Cu-β (0.5 mol%), in DCE (12.5 mL).

**Table 2.2.** Catalyst reusability study in a 0.5 g scale.<sup>a</sup>

The conversions as a function of reaction time were further examined for Cu-Y, Cu-beta, Cu-mordenite, and Cu(OTf)<sub>2</sub> catalysts on the same copper concentration (0.5 mol%) (Figure 2.1). Cu-Y (10.34 wt%) and Cu-beta (2.94 wt%) gave relatively faster formation of *meta*-arylated product **2**. For Cu-mordenite, an induction period (<1 h) was required before the reaction started and conversion changed slowly with time, highlighting that the reaction rate depended on pore size and interconnections. Noticeably, Cu-Y (10.34 wt%) and Cu-beta (2.94 wt%) revealed even higher conversion rate compared to the analogous homogeneous catalyst (copper triflate) indicating the high catalytic activities of copper ion species in the zeolite frameworks.

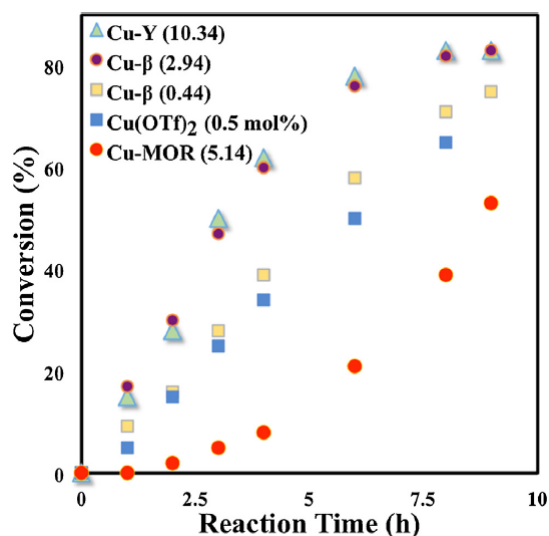


**Figure 2.1.** Conversion vs. reaction time plot on the same Cu<sup>II</sup> concentration (0.5 mol%).

To gain the insight into Cu catalysis, the reaction rate of the direct arylation was evaluated by measurement of initial rates (Figure 2.2a). The plots fitted reasonably well with the pseudo-first-order kinetics in **1**, providing the specific reaction rate constants ( $k$ ) 0.28, 0.25, 0.16, 0.13 and 0.028 h<sup>-1</sup> for Cu-Y, Cu-beta (2.94 wt%), Cu-beta (0.44 wt%), Cu(OTf)<sub>2</sub> (0.5 mol%), and Cu-mordenite, respectively. Cu-Y and Cu-beta (2.94 wt%) have rate constants approximately one order of magnitude higher than Cu-mordenite. These differences among zeolites can be attributed to the diffusion of reactants inside zeolite frameworks (see 4.6. Computational methods).

Both pore sizes and interconnections can affect the overall reaction rates. Cu-Y exhibits a three-dimensionally connected faujasite structure consisting of 7.4 Å pore window. Cu-beta has three-dimensional pore structures with diameters of 7.6 and 6.4 Å. In contrast, Cu-mordenite has straight channels with diameters of 7.0 and 6.5 Å.<sup>33</sup> We believe that the slow reaction rate of Cu-mordenite is mainly attributed to poor internal diffusion of reactants and products due to the one-dimensional pore structure. Furthermore, the apparent activation energy ( $E_a$ ) was estimated experimentally by plotting  $\ln(k)$  vs.  $1/T$ , providing values of 20.7, 21.3 and 28.6 kcal/mol for Cu-Y, Cu-beta, and Cu(OTf)<sub>2</sub> at 0.5 mol% copper concentration, respectively (Figure 2.2b, see also Figure 2.7 and Table 2.5). The activation barriers for Y and beta (2.94 wt%) zeolites are even lower than copper triflate, consistently with conversion- and rate studies.

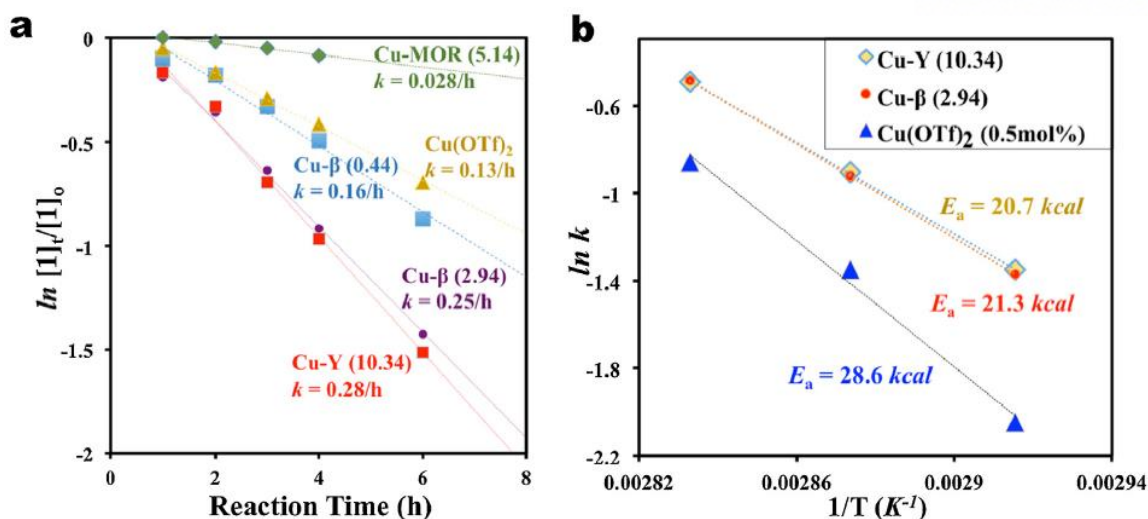


**Figure 2.2.** Kinetic studies of direct arylation using copper catalysts (0.5 mol%). (a) A plot of  $\ln ([1]_t/[1]_0)$  vs. time (b) a plot of  $\ln k$  vs.  $1/T$ .

To clarify the role of copper-ion during the direct arylation, control tests were carried out by preparing a family of pristine and first-row transition metal-exchanged zeolites (e.g., H- $\beta$ , Fe<sup>III</sup>- $\beta$ , Cr<sup>III</sup>- $\beta$ , Ni<sup>II</sup>- $\beta$ , Co<sup>II</sup>- $\beta$ , Mn<sup>II</sup>- $\beta$ , and Zn<sup>II</sup>- $\beta$ ). Under the standard condition, none of them provided **2** even after 48 h at 70 °C clearly indicating the catalytic role of copper. Once the temperature was increased up to 80 °C without a copper catalyst, only negligible amount (below 3% conversion) of **2** was formed after 24 h. Yet, this result explains that *meta*-selectivity comes from the intrinsic electronic reactivity pattern of **1**.<sup>11</sup> The role of copper as a catalyst was further confirmed by the measurement of initial rates while changing the concentration of copper triflate. The plot of  $\ln k$  vs.  $\ln [Cu(OTf)_2]$  (Figure 2.3) showed a linearity indicating the direct involvement of active copper species during the rate-determining step.

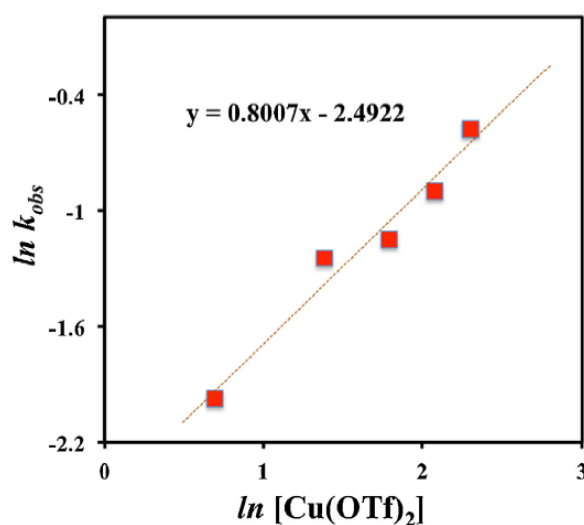


**Figure 2.3.** A plot of  $\ln k$  vs.  $\ln [Cu(OTf)_2]$ .

Recently, Chen et al., proposed the mechanistic picture of  $\text{Cu}(\text{OTf})_2$  catalyzed direct arylation of anilides. The density functional theory (DFT) calculation suggests that the C–H *meta*-selective bond arylation goes through  $\text{Cu}^{\text{II}}\text{--Cu}^{\text{I}}$  reduction, followed by  $\text{Cu}^{\text{I}}/\text{Cu}^{\text{III}}$  cycle with copper-aryl complexes.<sup>34</sup> Encouraged by kinetic examinations and previous reports, molecular structures inside copper-exchanged zeolite frameworks were accessed using DFT methods, performed with DMol3 software package (Figure 2.4). Copper-exchanged zeolite models (beta and Y) were constructed based on the works of the Ma and the Bell groups, respectively (see Figure 2.11).<sup>35,36</sup> Based on earlier reports, we carried out the simulation studies in the following order (see also Figure 2.12): (step 1) Cu(II) exchange, (step 2) reduction of  $\text{Cu}^{\text{II}}\text{--Cu}^{\text{I}}$ , (step 3) reaction of *in situ* generated  $\text{Cu}^{\text{I}}$  with diphenyliodonium salt, (step 4) formation of organocopper complex onto zeolite framework, (step 5) pre-coordination of compound **1** to the complex, (step 6) arylation through carbocupration process, and (step 7) product **2** formation.

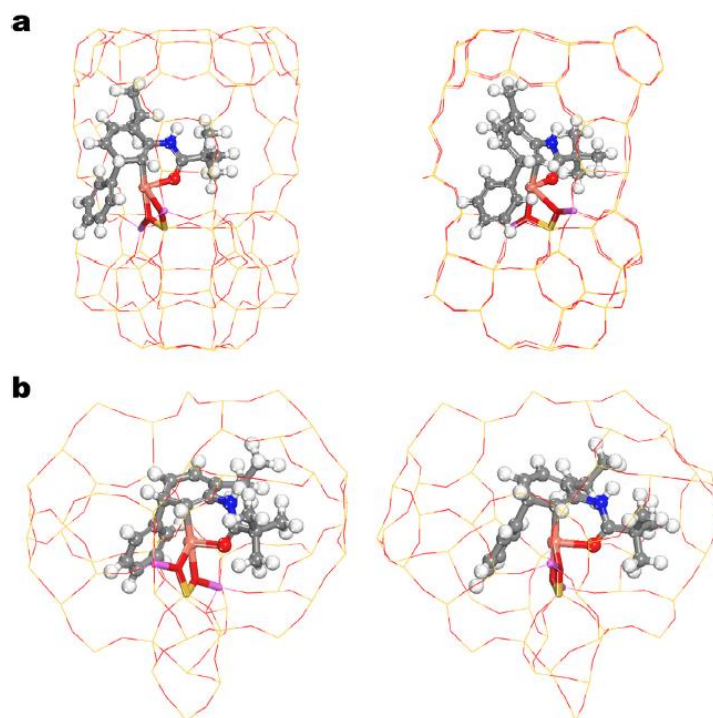


**Figure 2.4.** Copper-aryl intermediate structures well-fitted inside zeolite frameworks. (a) Cu-Y 78T cluster model, and (b) Cu-beta 55T cluster model. Solid lines represent zeolite framework and ball-and-sticks are used to present the copper-aryl complexes. Oxygen: red, nitrogen: blue, carbon: grey, hydrogen: white, copper: reddish orange, silicon: yellow, and aluminum: pink. (For interpretation of the references to color in this figure legend, the reader is referred to the web version of this article.)

Remarkably, the copper-aryl complexes generated through carbocupration process were clearly observed inside Y and beta zeolites resembling the intermediate structure in the copper triflate

homogeneous catalysis. The organocopper intermediates were well-fitted inside zeolite frameworks, which may ascribe the efficient and faster product **2** transformation. In addition, reaction coordinate diagram forming the intermediates represented in Figure 4 was further investigated. Figure 2.13 shows remarkable reactivity differences depending on zeolite frameworks: Cu-Y undergoes facile reaction to form Int1 without requiring activation energy, while Cu-beta has activation energy of ca. 5.14 kcal/mol. Zeolite oxygens in the heterogeneous catalysis act as ligands. Thus, anchoring of the catalytically active species inside zeolite frameworks via metal-ligand coordination can allow the enhanced chemical stability as well as high catalytic activity during the reaction while avoiding the loss of copper ions. To examine the product path out of zeolite frameworks, pore-window size and molecular size of **2** were compared. The pore-rings of Y and beta zeolites are indicated in Figure 2.10. Via the slight bending and torsional motions of product **2** within the activation energy level (ca. 22 kcal/mol), the conformer can pass through the pores at the elevated temperature (70 °C), which widens the Maxwell-Boltzmann distribution of kinetic energy of product **2**.

The leaching and aggregation of catalytically active species in heterogeneous catalysis are major detrimental causes of deactivation.<sup>37</sup> The stability of copper-exchanged zeolites was evaluated by the measurement of copper content through inductively coupled plasma optical emission spectroscopy (ICP-OES) analysis. Cu-beta was chosen due to its high catalytic activity during direct arylation. ICP-OES results of Cu-beta (2.94 wt%) recovered (thoroughly washed with dichloromethane, then dried under vacuum for 1 h) after the reaction were ~2.76 wt%, similar to the fresh catalyst (Tables 2.3 and 2.4). To exclude the possibility of catalytic reactions occurring from the leached copper species, the reaction mixture was filtered after 24 h, then the copper concentration was evaluated in the solution phase showing 0.4 ppm, much lower to perform meaningful catalytic conversions. In addition, ICP-OES analysis on the same reaction mixture indicated an Al content ca. 0.5 ppm (Cu/Al, ca. 0.35) very similar to the Cu/Al ratio (~0.39) of fresh zeolites. This ascribes that the Cu detected in the reaction mixture can be a portion of Cu-zeolites with small particle sizes, which passed through the filtration process, not the isolated free Cu species. These results combined to suggest that no noticeable Cu species leached out of the supports during reaction.

Copper Catalysts	Si/Al	Cu/Al	Na/Al	Cu loading (wt%)
Cu-Y	2.55	0.39	0.20	10.34
Cu-MOR	6.5	0.39	0.23	5.14
Cu-β (before rxn)	12.5	0.39	0.00	2.94
Cu-β (after rxn)	12.5	0.36	0.00	2.76

**Table 2.3.** ICP analysis results of the Cu-exchanged zeolite samples.

Atom	Conc. (mg/L)	Cu/Al
Al	0.106	0.35
Cu	0.088	

**Table 2.4.** ICP analysis results of the reaction solution after reaction using Cu-beta (2.94 wt%).

The stability of the catalysts was further confirmed by high-resolution transition electron microscope (HRTEM) images combined with EDS analysis. As shown in Figure 2.5, we could not find any observable morphological changes in HRTEM images before and after the reaction. There was no Cu cluster formation after direct arylation reaction at 70 °C. Elemental distribution of Cu and Al of Cu-beta zeolite were determined by element maps without significant loss of active copper species (Figure 2.6). These results demonstrated the chemical stability of Cu-zeolite catalysts during the direct arylation reaction tested. Mild reaction conditions, confinement of catalytically active species inside the microporous structure, and coordination bond between framework oxygen and copper ion, may provide the resilience against leaching and aggregation.

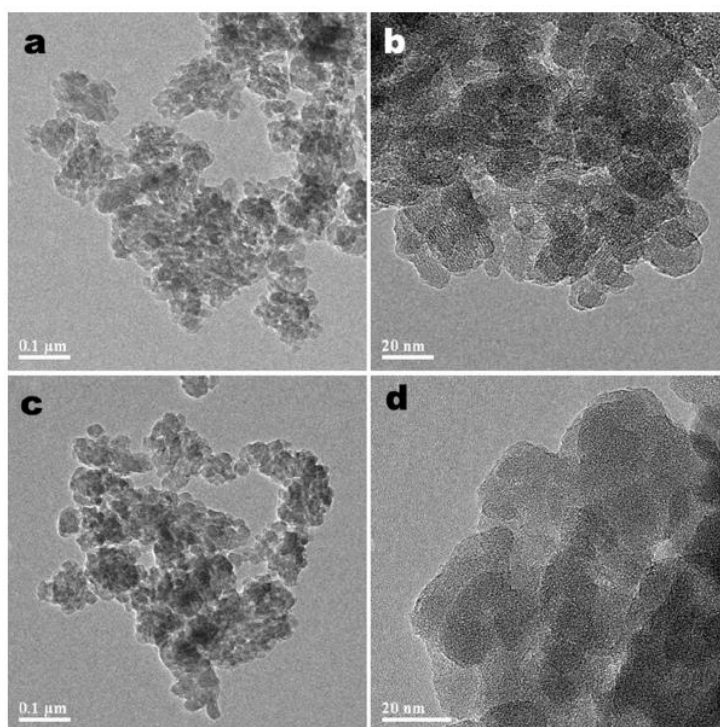


**Figure 2.5.** HRTEM images Cu-beta (2.94 wt%). (a,b) fresh sample, and (c,d) sample after the reaction.

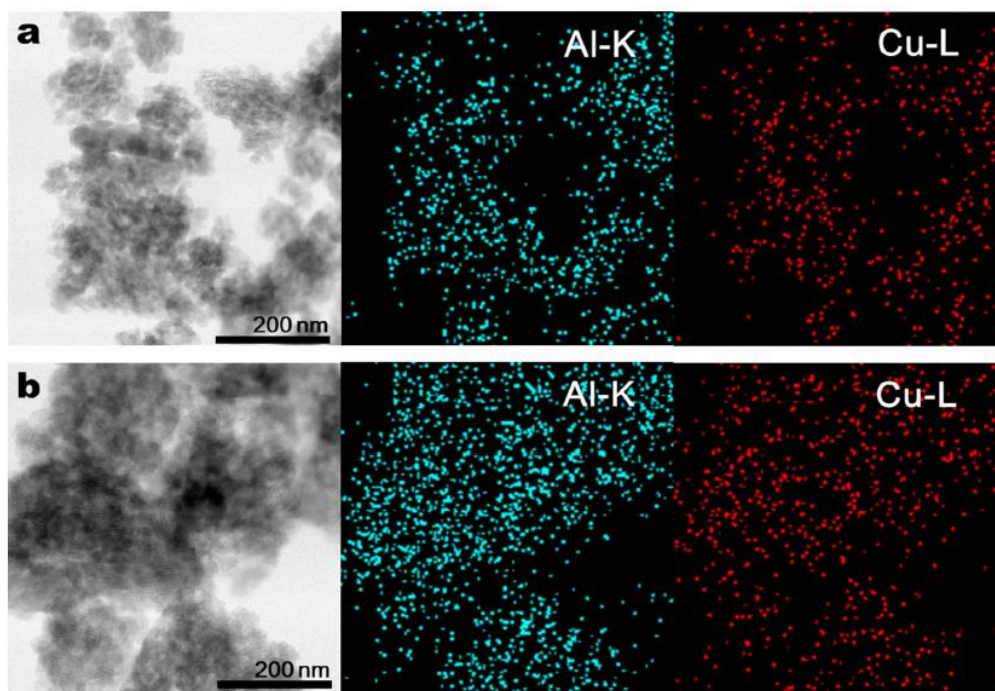


**Figure 2.6.** Bright-field (BF) TEM images (left) and EDS elemental distribution of Al (middle) and Cu (right) of Cu-beta (2.94 wt%). (a) fresh sample and (b) the sample after the direct reaction.

### 3. Conclusions

We demonstrated the first *meta*-selective C–H bond arylation of anilides inside zeolite frameworks. The Cu-zeolites allowed the high catalytic activities showing up to 90% conversion on the low copper concentration (0.5 mol%). To elucidate the catalytic properties of Cu-zeolites, DFT and kinetic studies were carried out demonstrating that intermediates well-fitted inside zeolite frameworks can be formed and apparent activation energies can be reduced than the previous  $\text{Cu}(\text{OTf})_2$  catalyst, respectively. The combined STEM, element maps, and ICP analyses indicated catalytic stability without noticeable leaching of the active Cu-species inside the zeolite frameworks. The coordination between zeolite oxygen and organocopper complex may lead to prevent the loss of catalytically active copper species. Considering industrial or academic importance of heterogeneous reactions, we believe that our chemically stable, reusable, and highly efficient copper-exchanged zeolite catalysts provide novel routes for direct arylation processes.



## 4. Experimental

### 4.1. General Procedures and Materials

The starting material pivanilide **1** was prepared from 2-isopropylaniline (Alfa-Aesar) and pivaloyl chloride (Sigma-Aldrich) based on the reported protocols.<sup>10</sup> Diphenyliodonium triflate (Ph<sub>2</sub>IOTf) was synthesized using reported procedure.<sup>26</sup> Anhydrous 1,2-dichloroethane (DCE) was purchased from Sigma-Aldrich. For TLC, glasses pre-coated (0.25 mm) with Merck silica gel 60 PF<sub>254</sub> were used and visualized using a UV lamp ( $\lambda_{\text{max}}$  254 nm). Flash column chromatography was performed with Merck 9383 Kieselgel 60 silica gel (230–400 mesh). <sup>1</sup>H and <sup>13</sup>C NMR spectra were recorded on an Agilent 400-MR DD2 spectrometer; chemical shifts are given on the  $\delta$ -scale in ppm, and a residual solvent peak was used as a reference.

### 4.2. Preparation and Characterizations of Copper-Zeolites

Beta (CP 814E, Si/Al = 12.5), Y (CBV 100, Si/Al = 2.55), and mordenite (CBV 10A, Si/Al = 6.5) zeolites were obtained from Zeolyst International Co. Cu-zeolites were synthesized by solution ion exchange of Cu<sup>II</sup> ion on various zeolites by using 0.2 M aqueous solution of Cu(NO<sub>3</sub>)<sub>2</sub>.<sup>27</sup> The solution contained twice amount of Cu<sup>II</sup> ion needed for complete ion exchange. After the ion exchange step, the sample was filtered, washed, and then dried at 100 °C overnight. To ensure complete ion exchange, this entire process was repeated twice. Various transition metal ion exchanged beta zeolites were synthesized in the same way using the aqueous solution of the corresponding transition metal nitrate precursors such as Fe(NO<sub>3</sub>)<sub>3</sub>, Cr(NO<sub>3</sub>)<sub>3</sub>, Ni(NO<sub>3</sub>)<sub>2</sub>, Co(NO<sub>3</sub>)<sub>2</sub>, Mn(NO<sub>3</sub>)<sub>2</sub>, and Zn(NO<sub>3</sub>)<sub>2</sub>. All the catalyst samples were then calcined at 500 °C for 2 h using muffle furnace under air atmosphere prior to testing and characterization. The concentration of Cu in the zeolites before and after reaction was determined by ICP-OES (Varian, 720-ES) after acid digestion using hydrofluoric acid. TEM images of Cu-zeolites before and after reaction were collected using the JEOL JEM-2100F microscope operated at 200 kV. Elemental maps for Cu, Al, and Si before and after reaction were obtained by EDS analyzer (Oxford Instrument, X-Max<sup>N</sup> 80 T). TEM samples were prepared by dusting the gently grounded zeolites samples onto a carbon coated Au-grid.

### 4.3. Protocol for the Direct Arylation

A mixture of pivanilide **1** (50 mg, 0.228 mmol), diphenyliodonium triflate (196 mg, 0.456 mmol), copper-zeolite catalyst (0.5 mol%) in DCE (1.25 mL) was taken in a closed glass vial and was extensively stirred (~1000 rpm) at 70 °C for 24 h. After completion of reaction (as indicated by TLC), the glass vial was centrifuged at 4500 rpm for 15 min. The heterogeneous catalyst deposited at the bottom and the clear supernatant liquid was separated and concentrated *in vacuo*. The residue was then subjected to flash column chromatography (*n*-hexane:ethyl acetate, 20:1) to afford the product **2** as a

white solid.

#### 4.4. Zeolite Cluster Models

Zeolite cluster models were constructed to represent zeolite cages or channels based on Cu- $\beta$  55T model, which consists of two crossing 24T,<sup>28</sup> and Cu-Y 78T model, which combined supercage of FAU with 42T model that was previously reported by Zhenget al.<sup>29</sup> Two models were hydrogen-terminated. The partial geometry optimization methods, reported by Barone et al.<sup>30</sup> and Shapovalov and Bell,<sup>31</sup> were applied for the relaxation of the models; the terminating Si atoms were frozen in their crystallographic positions, and the terminating H, Al, and O atoms were relaxed. Subsequently by fixing the coordinates of the terminating hydrogen atoms, the partial optimization was extended to the remaining atoms.

#### 4.5. Kinetic Experiments

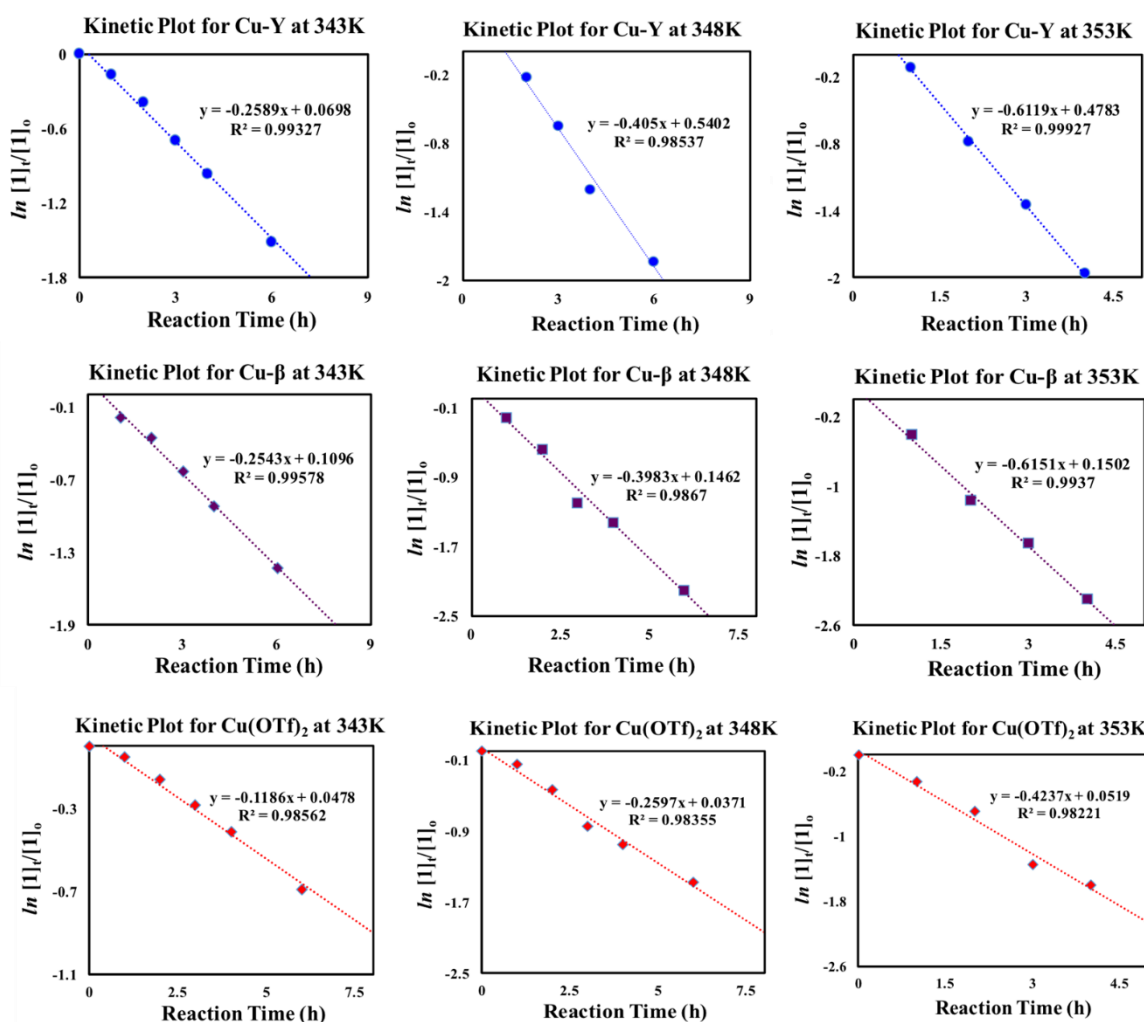


**Figure 2.7.** Kinetic plots for Cu-Y, Cu-beta, and copper triflate at different temperatures.

Entry	T (k)	k [Cu <sup>II</sup> - $\beta$ ] (h <sup>-1</sup> )	k [Cu <sup>II</sup> -Y] (h <sup>-1</sup> )	k [Cu(OTf) <sub>2</sub> ] (h <sup>-1</sup> )
1	343	0.254	0.259	0.119
2	348	0.398	0.405	0.259
3	353	0.615	0.612	0.424

**Table 2.5.** Rate constant ( $k$ ) for Cu<sup>II</sup>- $\beta$ , Cu<sup>II</sup>-Y, and Cu(OTf)<sub>2</sub> zeolites.

## 4.6. Computational Methods

### 4.6.1. Grand Canonical Monte Carlo (GCMC) Simulation

We modeled the unit cells of Cu-Y (10.34 wt%), Cu- $\beta$  (2.94 wt%), and Cu-MOR (5.14 wt%) with 3.8, 15, and 11 of the Si/Al ratio, respectively, by considering the contents of copper. And the unit cells were accordingly extended to have a similar volume (i.e.  $\sim 1.15 \times 10^5 \text{ \AA}^3$ ). With the modeled zeolite frameworks, we applied GCMC method<sup>38</sup> using the Sorption program of Materials Studio 8.0<sup>39</sup> to estimate the amounts of adsorbed molecule (pivanilide **1**) in each zeolite. At two temperatures of 298 K and 343 K, the GCMC simulations have been performed with over  $1 \times 10^6$  equilibrium steps by varying the fugacity from 1 kPa to 1000 kPa to find the adsorption isotherms. The non-bond interactions of adsorbate and zeolite in the GCMC simulation have been treated with van der Waals and Columbic forces using the COMPASS forcefield<sup>40,41</sup> and the Ewald summation method,<sup>42,43</sup> respectively.

### 4.6.2. Results of GCMC Simulation

For Cu-Y, the adsorbate molecules were majorly adsorbed in supercages. For Cu- $\beta$ , most adsorbate molecules were found in pores and connecting space of pore in x-axis and pore in y-axis. But for Cu-MOR, a few adsorbate molecules were found in pores due to the small size of pore. We calculated the free volumes of the zeolites and found the free volume ratios of 1.56:1.22:1 (Cu-Y : Cu- $\beta$  : Cu-MOR) at the similar total volume. But we found the number ratio of the adsorbate molecule **1** based on the free volume, for example, at 298 K and 1000 kPa, to be 1.89:2.08:1 (Cu-Y : Cu- $\beta$  : Cu-MOR) (Figure 2.8). It is also found the similar result of the number ratio to be 1.84:1.92:1 (Cu-Y : Cu- $\beta$  : Cu-MOR) at 343 K and 1000 kPa. Same calculation was carried out for product **2** (see Figure 2.9).

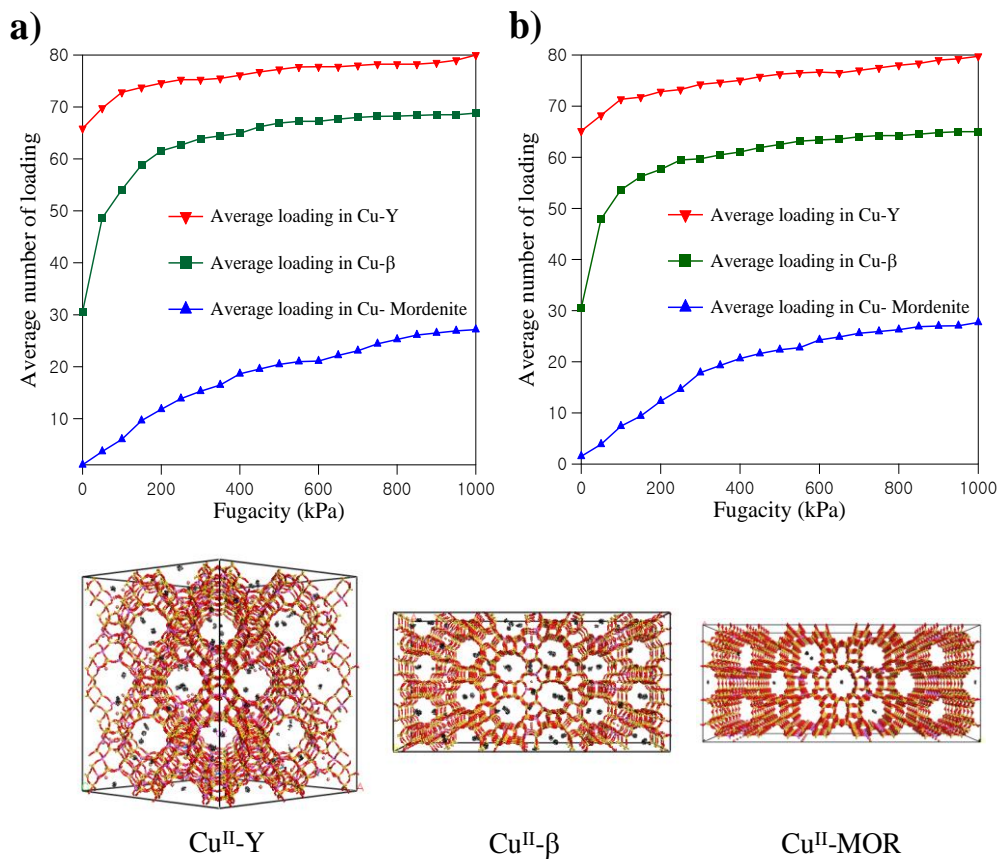


**Figure 2.8.** Adsorption isotherms of **1** in Cu-Y (10.34 wt%), Cu-β (2.94 wt%), and Cu-MOR (5.14 wt%) at (a) 298 K and (b) 343 K. The modeled zeolites are shown with black dots, which represent probable sites of the adsorbate molecule **1** after the GCMC simulation at the fugacity, 1000 kPa.

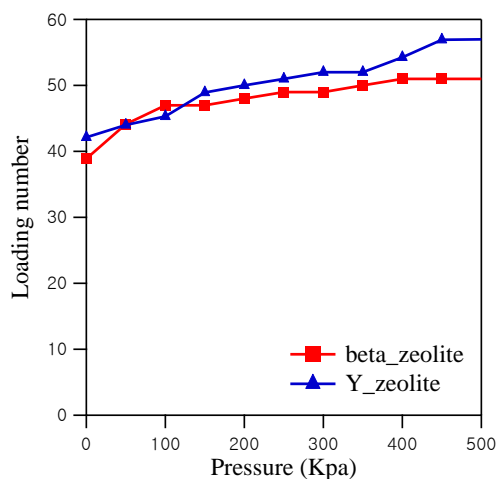


**Figure 2.9.** Adsorption isotherms of product **2**.

### 4.6.3. Pore- and Molecular Size Comparison

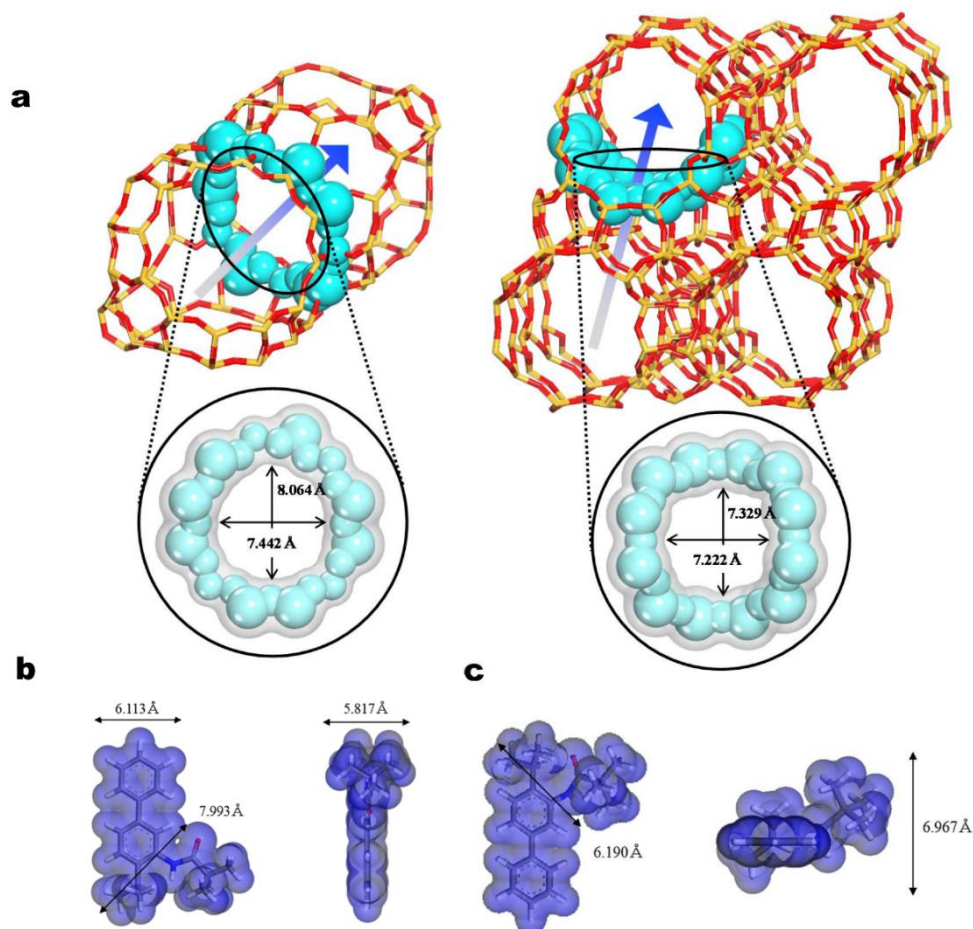


**Figure 2.10.** (a) Zeolite structures (Y: left, beta: right). Cyan colored parts of CPK models represent bottle neck in Y and cross section of beta. Arrow indicates the diffusion path of **2** inside zeolites, (b) the most stable conformer of product **2**, (c) the bent and torsional conformer of product **2**.

### 4.6.4. DFT Calculation

The reaction of diphenyliodonium salt with copper(II) ion has been well documented, where  $\text{Cu}^{\text{I}}$  ion is *in situ* generated from the reduction of  $\text{Cu}^{\text{II}}$  ion, then undergoes  $\text{Cu}^{\text{I}}/\text{Cu}^{\text{III}}$  catalytic cycle forming aryl-copper(III) complexes.<sup>44,45</sup> From previous research on the stable site of  $\text{Cu}^{\text{I}}$  for beta and Y zeolites, Shen *et al.*<sup>46</sup> and Drake *et al.*<sup>47</sup>, respectively, they represent some probable sites for copper ion. The Goursot group compared  $\text{Cu}^{\text{II}}\text{-Y}$  and  $\text{Cu}^{\text{I}}\text{-Y}$  and revealed no differences on copper sites.<sup>48</sup> The autoreduction of  $\text{Cu}^{\text{II}}$  to  $\text{Cu}^{\text{I}}$  inside zeolite frameworks were based on previous work from the Göttl group,<sup>49</sup> which was also described for homogeneous catalysis having  $\text{Cu}^{\text{I}}/\text{Cu}^{\text{III}}$  cycle.<sup>44</sup> Possible position of copper ion and the optimized intermediate structure was estimated by the DFT calculation performed with DMol<sup>3</sup> software package (Biovia Inc.).<sup>50,51</sup> We employed the PBE exchange–correlation functional and the DNP 4.4 basis set with the all–electron relativistic (VPSR) core treatment. Two different criteria for

convergence of energy, force, and displacement were set as  $2 \times 10^{-5}$  Ha,  $0.004 \text{ Ha}/\text{\AA}$ , and  $0.005 \text{ \AA}$  to confirm the position of Cu ion; and as  $1 \times 10^{-5}$  Ha,  $0.002 \text{ Ha}/\text{\AA}$ , and  $0.005 \text{ \AA}$  to estimate reaction intermediate, respectively. To include the dispersion correction of van der Waals effect, the Tkatchenko-Scheffler scheme<sup>52</sup> was used. The COSMO<sup>53</sup> method was applied throughout the calculations with the dielectric constant (i.e. 10.125) of the DCE solvent. To confirm the position of copper ion, two sites (site (i) and site (ii)) were calculated using DFT. For beta zeolite, site (i) is located at 6 ring and site (ii) is located at 5-4-5 ring. For Y zeolite, site (i) is located at 6 ring and site (ii) is located 4-4-4 ring. Figure 2.11 presents four models under our consideration. For both zeolites, site (i) shows lower energy than site (ii). However, the site (i) requires significant amount of activation energy for the coordination with pivanilide **1**. Thus, site (ii) was considered for further calculation to obtain reaction intermediate(s).

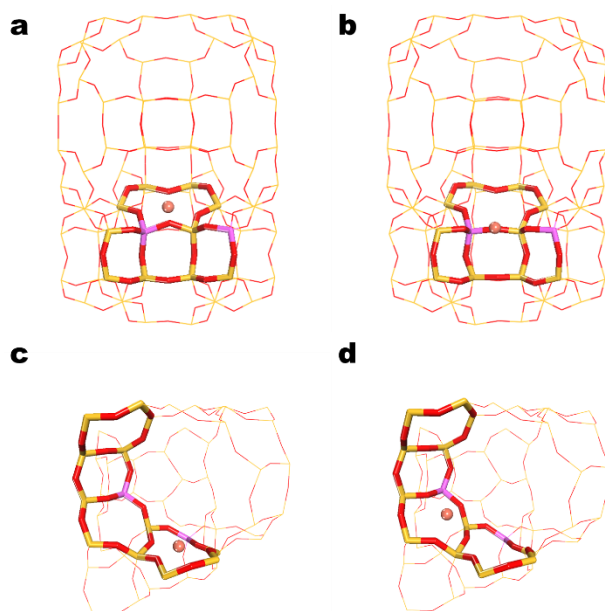


**Figure 2.11.** (a) and (b) Cu-Y models with initial positions of Cu<sup>II</sup> ion at sites (i) and (ii), respectively. (c) and (d) Cu-beta models with initial positions of Cu<sup>II</sup> ion at sites (i) and (ii), respectively.

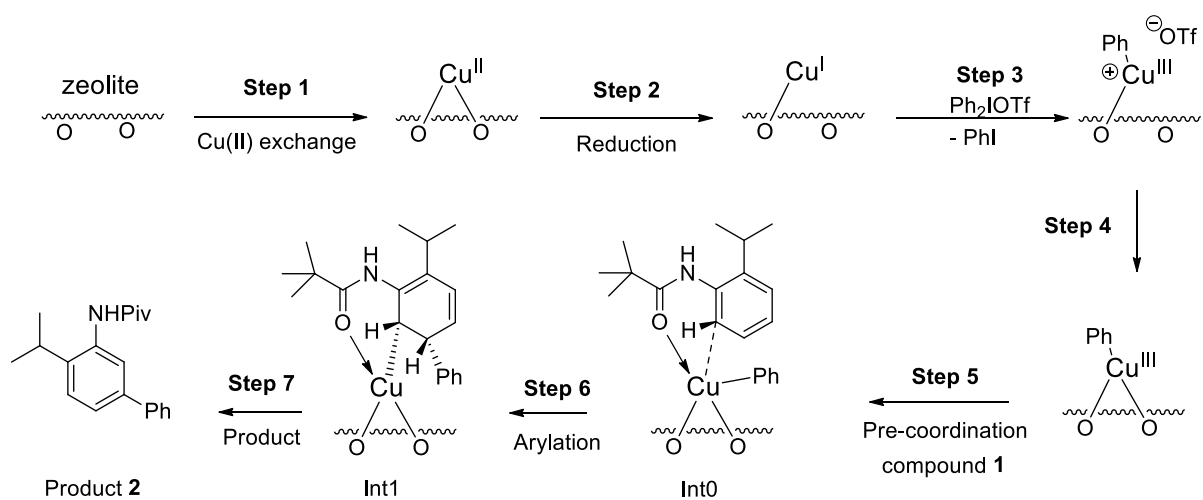


**Figure 2.12.** Schematic representation of simulation processes.

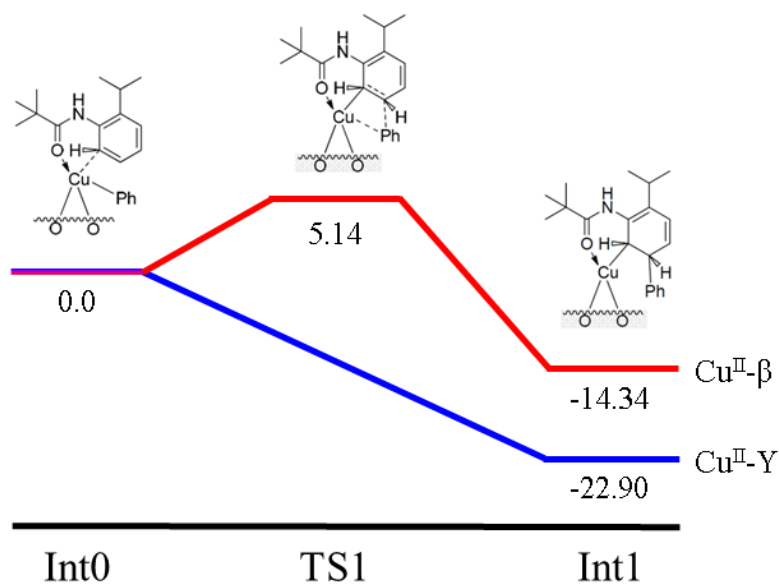


**Figure 2.13.** Reaction coordinate diagram.

#### 4.7. Textural Properties of Zeolites

Pristine zeolites were obtained from a standard supplier, Zeolyst International Co. Table 2.6 informs the textural properties of zeolites.

Zeolite	Pristine model <sup>[a]</sup>	SiO <sub>2</sub> /Al <sub>2</sub> O <sub>3</sub>	Pore size (Å) <sup>[b]</sup>	Surface area (m <sup>2</sup> /g)
Y	CBV-100	5.1	7.4	900
Mordenite	CBV-10A	13	7.0, 6.5	425
beta	CP814E	25	7.6, 6.4	680

<sup>a</sup> Pristine zeolite sample from Zeolyst International® before Cu(II) exchange

<sup>b</sup> Reference [54]

**Table 2.6.** Textural properties of zeolites.

#### 5. References

- [1] B.M. Trost, *Transition Metals for Organic Synthesis*, vol. 1, 2nd ed., VCH, Weinheim, 2008, pp. 3–14.
- [2] J. Yamaguchi, A.D. Yamaguchi, K. Itami, *Angew. Chem. Int. Ed.* **2012**, *51*, 8960–9009.
- [3] L. Ackermann, *Chem. Rev.* **2011**, *111*, 1315–1345.
- [4] S.D. Sarkar, W. Liu, S.I. Kozhushkov, L. Ackermann, *Adv. Synth. Catal.* **2014**, *356*, 1461–1479.
- [5] L. Ackermann, *Modern Arylation Methods*, in: L. Ackermann (Ed.), VCH, Weinheim, 2009, pp. 1–23.
- [6] L.-C. Campeau, D.R. Stuart, K. Fagnou, *Aldrichim. Acta*, **2007**, *40*, 35–41.
- [7] T.W. Lyons, M.S. Sanford, *Chem. Rev.* **2010**, *110*, 1147–1169.
- [8] G. Yang, P. Lindovska, D. Zhu, J. Kim, P. Wang, R.-Y. Tang, M. Movassaghi, J.-Q. Yu, *J. Am. Chem. Soc.* **2014**, *136*, 10807–10813.
- [9] J. Luo, S. Preciado, I. Larrosa, *J. Am. Chem. Soc.* **2014**, *136*, 4109–4112.
- [10] R.J. Phipps, M.J. Gaunt, *Science* **2009**, *323*, 1593–1597.
- [11] L. Ackermann, J. Li, *Nat. Chem.* **2015**, *7*, 686–687.
- [12] A. Motta, I.L. Fragala, T.J. Marks, *J. Am. Chem. Soc.* **2008**, *130*, 16533–16546.
- [13] J.H. Kwak, R. Dagle, G.C. Tustin, Z.R. Zoeller, L.F. Allard, Y. Wang, *J. Phys. Chem. Lett.* **2014**, *5*, 566–572.
- [14] R. Cano, A.F. Schmidt, G.P. McGlacken, *Chem. Sci.* **2015**, *6*, 5338–53446.
- [15] D.-T.D. Tang, K.D. Collins, F. Glorius, *J. Am. Chem. Soc.* **2013**, *135*, 7450–7453.
- [16] W. Zhang, Q. Zeng, X. Zhang, Y. Tian, Y. Yue, Y. Guo, Z. Wang, *J. Org. Chem.* **2011**, *76*, 4741–4745.



- [17] Y. Huang, Z. Lin, R. Cao, *Chem. Eur. J.* **2011**, *17*, 12706–12712.
- [18] E.Y. Lee, J. Park, *ChemCatChem.* **2011**, *3*, 1127–1129.
- [19] P. Serna, B.C. Gates, *Acc. Chem. Res.* **2014**, *47*, 2612–2620.
- [20] M. Flytzani-Stephanopoulos, B.C. Gates, *Annu. Rev. Chem. Biomol. Eng.* **2012**, *3*, 545–574.
- [21] G. Sastre, A. Corma, *J. Mol. Catal. A: Chem.* **2009**, *305*, 3–7.
- [22] A. Corma, *J. Catal.* **2003**, *216*, 298–312.
- [23] R.F. Lobo, *Handbooks of Zeolite Science and Technology*, in: S.M. Auerbach, K.A. Carrado, P.K. Dutta (Eds.), Marcel Dekker, New York, 2003.
- [24] O.Z. Kwon, S.M. Park, M.K. Song, G. Seo, *J. Mol. Catal. A: Chem.* **2009**, *308*, 134–141.
- [25] M. Choi, D.-H. Lee, K. Na, B.-W. Yu, R. Ryoo, *Angew. Chem. Int. Ed.* **2009**, *48*, 3673–3676.
- [26] M. Bielawski, M. Zhu, B. Olofsson, *Adv. Synth. Catal.* **2007**, *349*, 2610–2618.
- [27] J.H. Kwak, T. Varga, C.H.F. Peden, F. Gao, J.C. Hanson, J. Szanyi, *J. Catal.* **2014**, *314*, 83–93.
- [28] C.M. Zicovich-Wilson, A. Corma, P. Viruela, *J. Phys. Chem.* **1994**, *98*, 10863–10870.
- [29] H. Zheng, J. Qi, R. Zhang, Z. Li, B. Wang, M. Ma, *Fuel Process. Technol.* **2014**, *128*, 310–318.
- [30] G. Barone, N. Armata, A. Prestianni, T. Rubino, D. Duca, D.Y. Murzin, *J. Chem. Theory Comput.* **2009**, *5*, 1274–1283.
- [31] V. Shapovalov, A.T. Bell, *J. Phys. Chem. C* **2010**, *114*, 17753–17760.
- [32] E.A. Merritt, B. Olofsson, *Angew. Chem. Int. Ed.* **2009**, *48*, 9052–9070.
- [33] I. Ogino, C.-Y. Chen, B.C. Gates, *Dalton Trans.* **2010**, *39*, 8423–8431.
- [34] B. Chen, X.-L. Hou, Y.-X. Li, Y.-D. Wu, *J. Am. Chem. Soc.* **2011**, *133*, 7668–7671.
- [35] Y. Shen, Q. Meng, S. Huang, S. Wang, J. Gong, X. Ma, *RSC Adv.* **2012**, *2*, 7109–7119.
- [36] I.J. Drake, Y. Zhang, D. Briggs, B. Lim, T. Chau, A.T. Bell, *J. Phys. Chem. B* **2006**, *110*, 11654–11664.
- [37] L. Shao, B. Zhang, W. Zhang, S.Y. Hong, R. Schlögl, D.S. Su, *Angew. Chem. Int. Ed.* **2013**, *52*, 2114–2117.
- [38] Smit, B. *Mol. Phys.* **1995**, *85*, 153–172.
- [39] <http://accelrys.com/products/materials-studio/index.html>.
- [40] Sun, H. *J. Phys. Chem. B* **1998**, *102*, 7338–7364.
- [41] Sun, H. *Comput. Theor. Polym. Sci.* **1998**, *8*, 229–246.
- [42] Ewald, P. *P. Ann. Phys.* **1921**, *64*, 253–287.
- [43] Tosi M. P. *Solid State Phys.* **1964**, *16*, 1–120.
- [44] Chen, B., Hou, X.-L., Li, Y.-X., Wu, Y.-D. *J. Am. Chem. Soc.* **2011**, *133*, 7668–7671.
- [45] Lockhart, T. P. *J. Am. Chem. Soc.* **1983**, *105*, 1940–1946.
- [46] Shen, Y., Meng, Q., Huang, S., Wang, S., Gong, J., Ma, X. *RSC Advances* **2012**, *2*, 7109–7119.
- [47] Drake, I. J., Zhang, Y., Briggs, D., Lim, B., Chau, T., Bell, A. T. *J. Phys. Chem. B* **2006**, *110*,

11654–11664.

[48] Goursot, A., Coq, B., Fajula, F. *J. Catal.* **2003**, *216*, 324–332.

[49] Göttl, F.; Bulo, R. E., Hafner, J., Sautet, P. *J. Phys. Chem. Lett.* **2013**, *4*, 2244–2249.

[50] Delley, B. *J. Chem. Phys.* **1990**, *92*, 508–517.

[51] Delley, B. *J. Chem. Phys.* **2000**, *113*, 7756–7764.

[52] Tkatchenko, A.; Scheffler, M. *Phys. Rev. Lett.* **2009**, *102*, 073005.

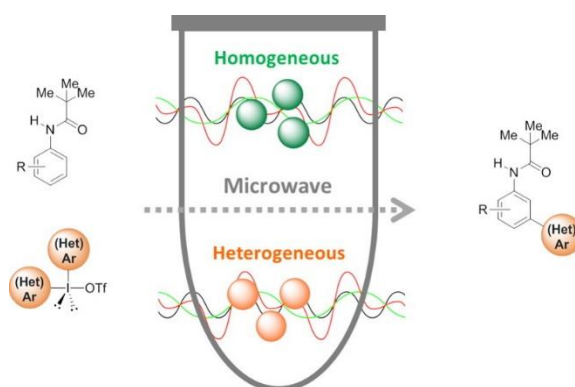
[53] Delley, B. *Mol. Simul.* **2006**, *32*, 117–123.

[54] Ogino, I., Chen, C. -Y., Gates, B. C. *Dalton Trans.* **2010**, *39*, 8423–8431.

## Chapter III

### Efficient Copper Catalysts for C–H Bond Arylation under Microwave Heating: Direct Access to Multi-Substituted Pivanilides

We herein describe a parallel comparison between homogeneous and heterogeneous copper catalysts for microwave-assisted direct C–H bond arylation. These catalytic systems feature enhanced catalytic activities, unique bulky ligand/base effects, mild conditions, and operational simplicity with reduced catalyst loadings and shortened reaction times. A wide range of synthetically challenging multi-substituted pivanilides was directly assembled. Remarkably, copper-exchanged beta-zeolite under ligand-free condition shows good recyclability demonstrating its potential as an efficient and reusable heterogeneous catalytic platform. This chapter is reproduced from *Catal. Commun.* **2017**, *90*, 83-86.



#### 1. Introduction

Recent synthetic innovations have enabled the concise, versatile, and practical synthesis of complex molecular scaffolds. The parameters employed to judge the overall efficiency of a reaction include selectivity, and both atom and step economies.<sup>1-3</sup> Over the past two decades, the metal-catalyzed activation of inert C–H bonds has emerged as a powerful tool to explore unprecedented synthetic routes.<sup>4-8</sup> Site-selective aryl C–H functionalization is particularly appealing to synthetic chemists as it avoids the requirement for functional group manipulation. This approach often demands the presence of directing groups and involves a distinctive cyclometalation step.<sup>9</sup> However, the close proximity between the directing group and metal complex results in the formation of *ortho*-substituted arenes while limiting remote site transformations. Phipps and Gaunt reported a seminal work on a *meta*-arylation strategy that utilized high-valent Cu<sup>III</sup>-aryl species.<sup>10</sup> In this case, the direct arylation of anilides was carried out using Cu(OTf)<sub>2</sub> and diaryliodonium salts to afford biaryl scaffolds. However,

this homogeneous catalytic system required a high catalyst loading (10 mol%) and long reaction times (24–48 h). In addition, catalyst recycling is largely limited in practice due to the difficulty of separation and the instability of active catalysts. Thus, the development of efficient catalytic systems that tackle these issues is necessary.

Over the last few decades, microwave irradiation has been employed as an alternative to conventional heating methods.<sup>11-13</sup> While in conventional conductive heating the energy is transferred from external heat sources, the heating mechanism in microwave irradiation is based on dipolar polarization and ion conduction. As a result, the reaction mixture is heated directly and temperature gradients are minimized. Recently microwave-assisted reactions have been applied to metal catalyzed reactions<sup>14-17</sup> and C–H functionalization methods<sup>18-20</sup> to shorten reaction times. Thus, we herein report our studies into microwave-assisted copper catalysis as an efficient *meta*-selective catalytic platform for direct access to complex aryl-(hetero)aryl structures. Homogeneous and heterogeneous catalysts were compared in terms of yield, substrate scope, bulky ligand effect, and recyclability (Figure 3.1).

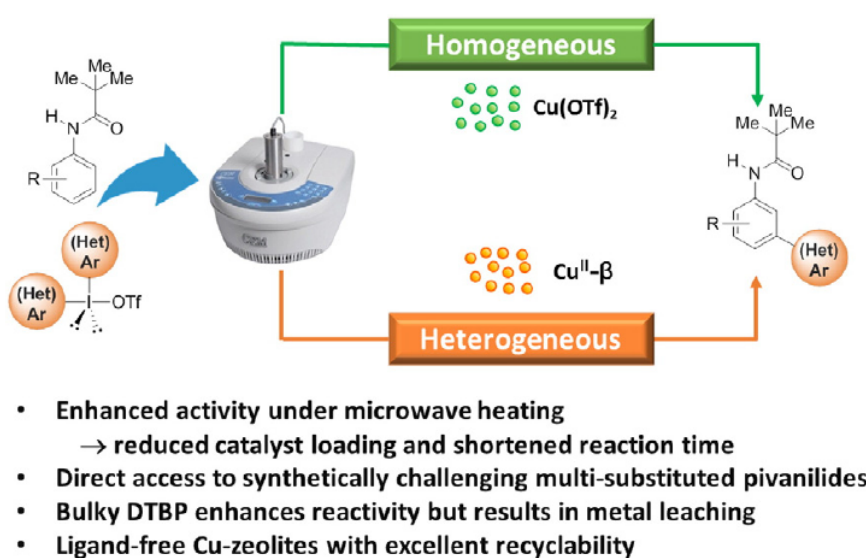
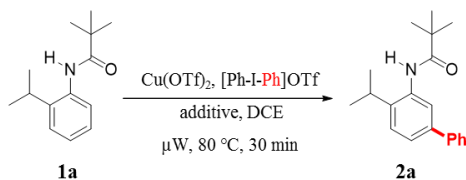


**Figure 3.1.** Outline of microwave-assisted direct arylation via copper catalysis.

## 2. Results and Discussion

We initially investigated the treatment of pivanilide **1a** with  $\text{Cu}(\text{OTf})_2$  (5 mol%) and  $\text{Ph}_2\text{IOTf}$  (2 eq) in DCE at 80 °C. Biaryl product **2a** was exclusively obtained in 71% isolated yield under microwave irradiation over 30 min (Table 3.1, entry 1). Intrigued by the potential roles of nitrogen ligands or bases in copper catalyzed reactions,<sup>21-25</sup> several pyridine based additives were examined (entries 2–7). Pyridine, 2,6-lutidine, and 2,6-diaminopyridine were ineffective; however, the sterically congested DTBP drove the reaction to completion, affording product **2a** in 93% isolated yield (entry 2). These

results may indicate the importance of weak metal-ligand coordination in this transformation.<sup>26,27</sup> Along with this, the dual role of DTBP as a base to quench the in-situ generated TsOH is also suggested.<sup>22</sup> A reduced amount of copper catalyst (entry 3) resulted in poorer conversion, and no product was obtained in the absence of copper catalyst (entry 4).



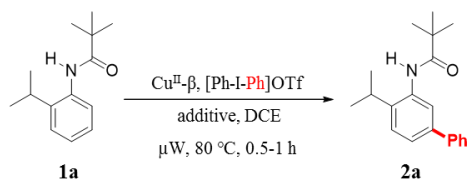
Entry	Catalyst (mol%)	Additive	Conversion (%) <sup>[b]</sup>
1	5	-	75 (71) <sup>[c]</sup>
2	5	DTBP <sup>[a]</sup>	>99 (93) <sup>[c]</sup>
3	2	DTBP	89
4	0	DTBP	NP
5	5	pyridine	NP
6	5	2,6-lutidine	NP
7	5	2,6-diaminopyridine	NP

[a] Reaction conditions: pivanilide **1a** (0.091 mmol), Ph<sub>2</sub>IOTf (2 eq), Cu(OTf)<sub>2</sub> (5 mol%), additive (1 eq) in DCE (0.5 mL) at 80 °C for 30 min in a microwave reactor, MW = Microwave; DCE = dichloroethane; nd = not detected;

[b] Determined by <sup>1</sup>H NMR analysis; [c] Isolated yield

**Table 3.1.** Optimization of the homogeneous direct arylation process.<sup>a</sup>

For the parallel comparison, the microwave-assisted direct arylation reaction was extended to heterogeneous catalysis (Table 3.2). A metal-exchanged zeolite catalyst was selected due to its regular pore structure, chemical stability, and synthetic utility.<sup>28-30,35</sup> Under microwave conditions, we found that 3.5 mol% of copper<sup>II</sup>-exchanged beta-zeolite (Cu<sup>II</sup>-β) at 80 °C afforded product **2a** in 53% conversion over 60 min (entry 2). Under conventional heating conditions, a typical reaction time for this transformation was approximately 24 h.<sup>10,35</sup> Unlike the homogeneous catalytic system, the arylation proceeded with reduced 1 mol% catalyst loadings (entry 3, 90% conversion) and a slightly lower conversion was also obtained with 0.5 mol% catalyst (entry 4, 85%). The optimal catalyst loading of 1 mol% is presumably related to a trade-off between reactant adsorption and internal diffusion within the zeolite pores. A reduction in catalyst loading will result in fewer catalyst particles and an increase in the relative concentration of reactants inside the zeolite pores, thus increasing the probability of a reaction taking place. Yet, a higher concentration of substrates or products within the pores may account for restricted internal diffusion due to the potential coordination between active metals and pivanilides.<sup>31,32</sup>



Entry	Catalyst (mol%)	Time (min)	Additive	Conversion (%) <sup>[b]</sup>
1	3.5	30	-	37
2	3.5	60	-	53
3	1	60	-	90 (86) <sup>[c]</sup>
4	0.5	60	-	85
5	1	60	DTBP	>99 (90) <sup>[c]</sup>

[a] Reaction conditions: pivanilide **1a** (0.091 mmol), Ph<sub>2</sub>IOTf (2 eq), Cu<sup>II</sup>-β (1 mol%), additive (1 eq) in DCE (0.5 mL) at 80 °C for 60 min in a microwave reactor; [b] Determined by <sup>1</sup>H NMR analysis; [c] Isolated yield

**Table 3.2.** Optimization of the heterogeneous direct arylation process.<sup>a</sup>

We then investigated the role of the bulky DTBP additive in the heterogeneous system, and observed a significant increase in conversion (>99%, Table 3.2, entry 5). The enhanced activity in this case can likely be associated with the weak coordination between Cu<sup>II</sup> within the zeolite frameworks and DTBP. However, this dative bond could be detrimental to the catalytic process due to leaching of the active copper ions. Thus, as a key feature of heterogeneous catalysis is recyclability, we investigated the direct arylation reaction using Cu<sup>II</sup>-β both in the presence and absence of DTBP over consecutive runs. As shown in Figure 3.2, the initial cycles where DTBP was present were superior to the ligand-free system. However, after the 5th cycle, the conversion began to drop, suggesting that copper leaching was taking place, as a stable catalytic performance was maintained in the absence of DTBP. We therefore selected ligand-free conditions for subsequent heterogeneous experiments.

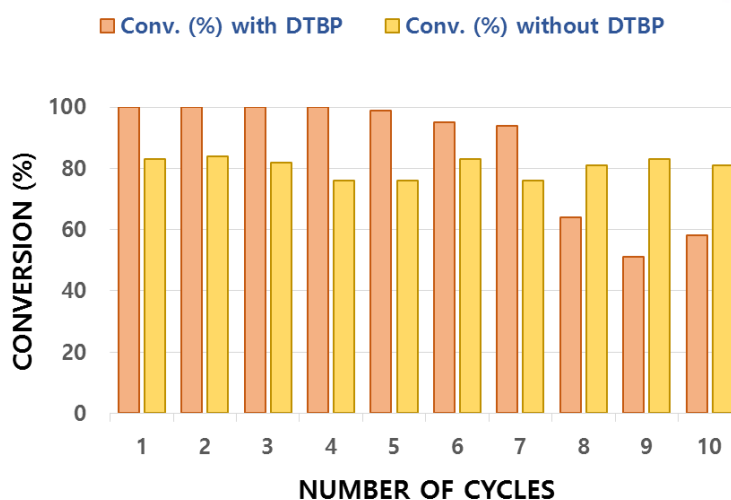
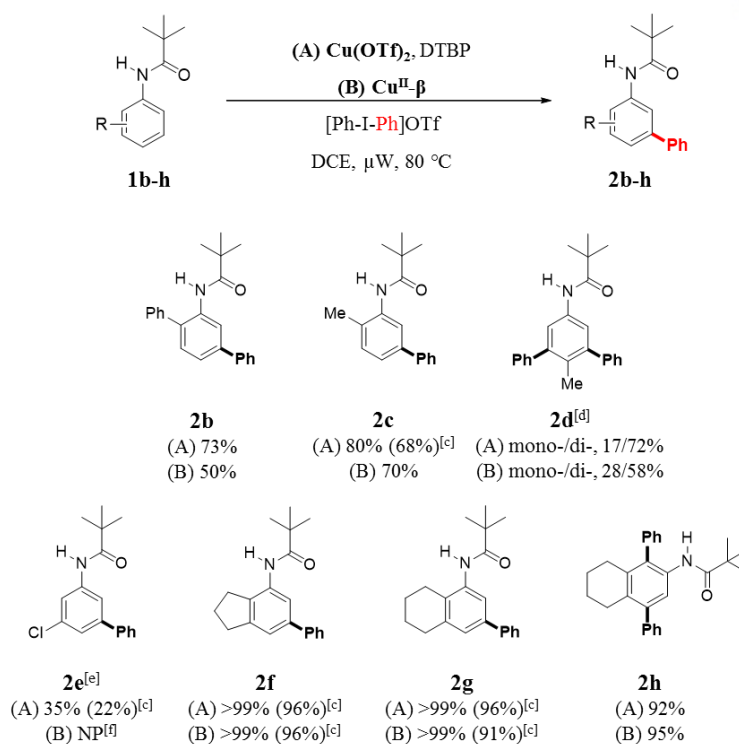


**Figure 3.2.** Recyclability test using  $\text{Cu}^{\text{II}}\text{-}\beta$  in the presence and absence of DTBP.

With the standard arylation conditions established for both homogeneous and heterogeneous systems, we initially explored the scope of substituted pivalilide substrates (Table 3.3). Electron-rich pivalilides (**2b–d** and **2f–h**) readily produced arylation products for both  $\text{Cu}(\text{OTf})_2$  and  $\text{Cu}^{\text{II}}\text{-}\beta$ . For example, the presence of phenyl- and methyl-substituents at the *ortho* position resulted in moderate to good conversions (50–80%), and the symmetrical *meta*-diarylation product was observed for the *para*-methyl substituent (**2d**). However, the *meta*-methyl substituent failed to produce solely *meta*-selectivity, as determined by the presence of different signals with similar exact masses in the GC spectra. These results confirm the electronic effect of the various substituents on the reactivity patterns of the system.<sup>10</sup> In addition, the electron-deficient *N*-(*m*-chlorophenyl)pivalamide (**2e**) exhibited significantly lower reactivity. Upon increasing the reaction time to 4 h, **2e** gave an improved conversion (35%) in the presence of  $\text{Cu}(\text{OTf})_2$ . In contrast, *ortho*-fluoro and *meta*-OTs substituents gave negligible conversions (data not shown). Noticeably, *ortho/meta*-diarylation was also observed with *N*-(5,6,7,8-tetrahydronaphthalen-2-yl)pivalamide (**1h**), and led to the synthetically challenging penta-substituted pivalilide product (**2h**), thereby implying an substituent-site-dependent electronic effect.<sup>10</sup>

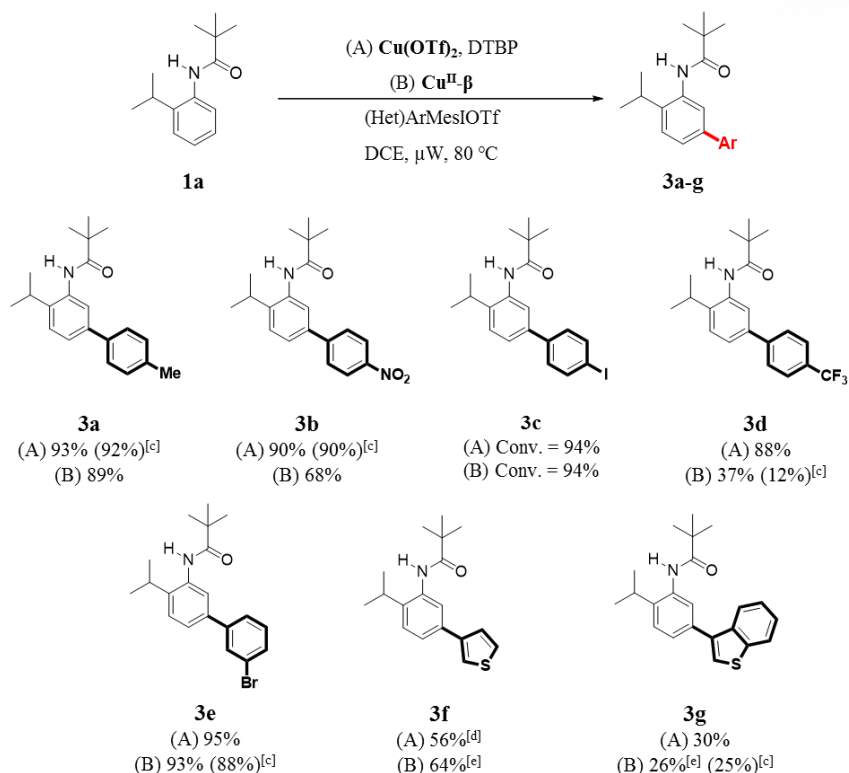


[a] Reaction conditions for homogeneous catalysis: pivanilide **1b-h** (0.091 mmol), Ph<sub>2</sub>IOTf (2 eq), Cu(OTf)<sub>2</sub> (5 mol%), DTBP (1 eq) in DCE (0.5 mL) at 80 °C for 30 min. Reaction conditions for heterogeneous catalysis: pivanilide **1b-h** (0.091 mmol), Ph<sub>2</sub>IOTf (2 eq), Cu<sup>II</sup>-β (1 mol%) in DCE (0.5 mL) at 80 °C for 60 min; [b] Conversions: determined by <sup>1</sup>H NMR analysis; [c] Isolated yield; [d] 4 eq of Ph<sub>2</sub>IOTf; [e] Ph<sub>2</sub>IBF<sub>4</sub> instead of Ph<sub>2</sub>IOTf and 4 h of reaction time

**Table 3.3.** Substrate scope of the direct arylation reaction.<sup>a,b</sup>

We also evaluated the generality of (hetero)aryl transfer using a range of unsymmetrical diaryliodonium salts (Table 3.4). In these hypervalent iodine reagents, smaller aryl moieties are selectively transferred.<sup>33,34</sup> In the majority of cases, the Cu(OTf)<sub>2</sub>/DTBP catalytic system exhibited similar or improved catalytic performances over shorter reaction times (**3a–e**) compared to the Cu<sup>II</sup>-β system. This could be attributed to the large steric congestion imparted by the mesityl-based iodonium salt, which increased the induction period within the catalytic framework. Noticeably, an excellent tolerance of halogen groups (**3c** and **3e**) was observed, with these moieties remaining intact during the copper catalyzed reactions. This allows them to be further utilized as functional handles in subsequent modifications. In addition, the nitro- and trifluoromethyl-(**3b** and **3d**) substituents resulted in reduced conversions via ligand-free heterogeneous catalysis (68% and 37%, respectively). To broaden the synthetic potential of this copper catalyzed arylation method, we performed the direct hetero-arylation of anilides (**3f** and **3g**). Although conversions were moderate for the homogeneous catalysts (**3f**; 56%, 64%) and poor for heterogeneous catalysts (**3g**; 30%, 26%), this direct arylation procedure afforded aryl-(hetero)aryl structures without the requirement for multi-step pre-functionalization.





[a] Reaction conditions for homogeneous catalysis: pivanilide **1b-h** (0.091 mmol), (Het)ArMesOTf (2 eq),  $\text{Cu}(\text{OTf})_2$  (5 mol%), DTBP (1 eq) in DCE (0.5 mL) at 80 °C for 30 min. Reaction conditions for heterogeneous catalysis: pivanilide **1b-h** (0.091 mmol), (Het)ArMesOTf (2 eq),  $\text{Cu}^{\text{II}}\text{-}\beta$  (1 mol%) in DCE (0.5 mL) at 80 °C for 4 h. Mes = mesityl; [b] Conversions: determined by  $^1\text{H}$  NMR analysis; [c] Isolated yield; [d] 1 h of reaction time; [e] 3.5 mol% of  $\text{Cu}^{\text{II}}\text{-}\beta$

**Table 3.4.** Scope of the (hetero)aryl group transfer.<sup>a,b</sup>

### 3. Conclusions

We demonstrated a novel microwave-assisted *meta*-selective direct (hetero)arylation of pivanilides to accelerate copper catalysis. Homogeneous  $\text{Cu}(\text{OTf})_2$  and heterogeneous  $\text{Cu}^{\text{II}}\text{-}\beta$  zeolite catalysts were systematically compared to disclose the characteristics of their catalytic behaviours. Indeed, both systems presented a wide substrate and iodonium salt scope to afford multi-substituted pivanilides in a single operation. In addition, the sterically congested DTBP additive exhibited improved conversion in addition to promoting catalyst leaching. While the  $\text{Cu}(\text{OTf})_2/\text{DTBP}$  system exhibits a high catalytic activity, the ligand free  $\text{Cu}^{\text{II}}\text{-}\beta$  system exhibited improved catalyst stability over consecutive runs. Finally, our results demonstrated that microwave-assisted copper-catalyzed direct arylation protocols provide highly atom and step economical processes, and exhibit remarkable site-selectivity, reduced reaction times, and mild conditions, rendering them attractive candidates for academic and industrial applications.

## 4. Experimental

### 4.1. General

Proton nuclear magnetic resonance ( $^1\text{H}$  NMR) and carbon nuclear magnetic resonance ( $^{13}\text{C}$  NMR) spectra were recorded on an Agilent 400-MR DD2; chemical shifts are given on the  $\delta$ -scale in ppm, and residual solvent peaks were used as references. Infrared (IR) spectra were recorded on a Nicolet iS5 from Thermo Fisher Scientific FT-IR spectrometer. Low resolution mass spectra were acquired from a Bruker HCT Basic System using electrospray ionization (ESI). High resolution mass spectra (HRMS) were measured using a Hybrid LC/Q-TOF system (Bruker BioSciences, maXis 4G). Thin layer chromatography (TLC) was performed using glass plates pre-coated (0.25 mm) with Merck silica gel 60F254. Visualization of the plates was achieved using an ultraviolet lamp ( $\lambda_{\text{max}}$  254 nm). Flash column chromatography was carried out using Merck silica gel 60 (particle size range: 0.040–0.063 mm). ICPOES was taken using a Varian, 720-ES. Direct arylation was carried out in a CEM discover microwave instrument. Microwave reaction vessels are made from Pyrex with silicone septa.

### 4.2. Preparation of the Catalysts and General Protocol for Direct Arylation

Copper(II) triflate (98.0%) was obtained from Tokyo Chemical Industry Co., and beta-zeolite (CP 814E, Si/Al = 12.5) was purchased from Zeolyst International Co. Cu-exchanged zeolites (2.94 wt%) were prepared in accordance with the previously established procedures.<sup>35</sup> A mixture of pivanilide **1a** (0.091 mmol) and diphenyliodonium triflate (0.182 mmol) in dichloroethane (DCE, 0.5 mL) was taken in a microwave vial (10 mL) and stirred for 3 min. To this mixture,  $\text{Cu}(\text{OTf})_2$  (0.005 mmol) or  $\text{Cu}^{\text{II}}\text{-}\beta$  (0.001 mmol) was added and stirred for 1 min. Followed which, in case of  $\text{Cu}(\text{OTf})_2$ , 2,6-di-tert-butylpyridine (DTBP) (0.091 mmol) was added using micro-syringe and again stirred for 1 min. Finally, the microwave vial was then closed with a vial cap and put in a microwave reactor under closed vessel condition (Mode = fixed temperature mode, power = 50 W, temperature = 80 °C, stirring speed = medium, and cooling = on). After 30 min or 1–4 h of reaction time depending on the homogeneous or heterogeneous catalysts, respectively, the crude product was then purified by flash column chromatography (n-hexane:ethyl acetate, 20:1) on silica gel to afford the desired product.

### 4.3. General Procedure for Synthesis of Pivanilide Substrates

To a solution of aromatic amine (8.3 mmol) and  $\text{NaHCO}_3$  (24.8 mmol) in DCM (30 mL) was added pivaloyl chloride (9.1 mmol) in a dropwise manner at room temperature. After completion of the reaction (3–4 h, TLC), the reaction mixture was diluted with DCM. The organic phase was then thoroughly washed with brine, dried over  $\text{Na}_2\text{SO}_4$  then concentrated *in vacuo* to give the desired pivanilide. Analytical data of *N*-(2-isopropylphenyl)pivalamide (**1a**), *N*-([1,1'-biphenyl]-2-yl)pivalamide (**1b**), *N*-(*o*-tolyl)pivalamide (**1c**), *N*-(*p*-tolyl)pivalamide (**1d**), and *N*-(3-

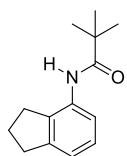
chlorophenyl)pivalamide (**1e**) were matched with previously reported data.<sup>10</sup>

#### 4.4. Recycling Test

After each cycle, the heterogeneous catalyst was recovered by centrifugation of the reaction mixture at 4500 rpm for 30 min. The supernatant reaction mixture was taken out using a glass dropper, following which the solid heterogeneous catalyst was thoroughly washed with DCE. Thereafter, the catalyst was dried at 250 °C for 6 h, and then reused for the next cycle.

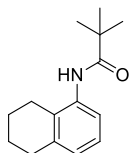
#### 4.5. Synthesis of Pivanilide Substrates

*N*-(2,3-dihydro-1H-inden-4-yl)pivalamide (**1f**)



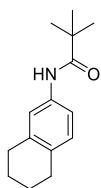
The product was obtained as a light brown solid (1.7 g, 93%). <sup>1</sup>H NMR (400 MHz, CDCl<sub>3</sub>): δ 7.81 (d, *J* = 7.9 Hz, 1H), 7.20 (br s, 1H), 7.15 (t, *J* = 7.8 Hz, 1H), 7.01 (d, *J* = 7.5 Hz, 1H), 2.95 (t, *J* = 7.4 Hz, 2H), 2.80 (t, *J* = 7.4 Hz, 2H), 2.17 – 2.07 (m, 2H), 1.32 (s, 9H); <sup>13</sup>C NMR (100 MHz, CDCl<sub>3</sub>): δ 176.43, 145.21, 134.21, 133.85, 127.44, 120.64, 118.70, 39.82, 33.30, 29.89, 27.83, 24.88; IR  $\nu_{\max}/\text{cm}^{-1}$ : 3246, 2954, 1641, 1506, 1474, 1446, 1430, 1309, 1232, 1190, 925, 769, 668, 535; HRMS (ESI): *m/z* calcd for C<sub>14</sub>H<sub>20</sub>NO [M+H]<sup>+</sup>: 218.1545; found: 218.1539.

*N*-(5,6,7,8-tetrahydronaphthalen-1-yl)pivalamide (**1g**)



The product was obtained as a light redish brown solid (1.8 g, 93%). <sup>1</sup>H NMR (400 MHz, CDCl<sub>3</sub>): δ 7.71 (d, *J* = 8.0 Hz, 1H), 7.19 (br s, 1H), 7.11 (t, *J* = 7.8 Hz, 1H), 6.89 (d, *J* = 7.6 Hz, 1H), 2.77 (t, *J* = 6.0 Hz, 2H), 2.57 (t, *J* = 6.3 Hz, 2H), 1.89 – 1.72 (m, 4H), 1.33 (s, 9H); <sup>13</sup>C NMR (100 MHz, CDCl<sub>3</sub>): δ 176.47, 138.08, 135.62, 127.89, 126.02, 125.95, 120.30, 39.93, 29.95, 27.89, 24.50, 23.08, 22.65; IR  $\nu_{\max}/\text{cm}^{-1}$ : 3269, 2931, 1644, 1516, 1473, 1455, 1435, 1398, 1366, 1331, 1298, 1261, 1184, 937, 773, 765, 710, 674, 559; HRMS (ESI): *m/z* calcd for C<sub>15</sub>H<sub>22</sub>NO [M+H]<sup>+</sup>: 232.1701; found: 232.1697.

*N*-(5,6,7,8-tetrahydronaphthalen-2-yl)pivalamide (**1h**)



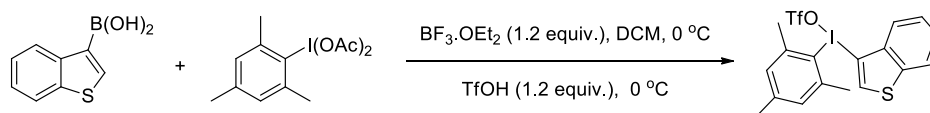
The solid product was gray coloured (1.7 g, 88%). <sup>1</sup>H NMR (400 MHz, CDCl<sub>3</sub>): δ 7.31 (s, 1H), 7.20 (br s, 1H), 7.16 (dd, *J* = 8.2, 2.0 Hz, 1H), 7.00 (d, *J* = 8.2 Hz, 1H), 2.78 – 2.67 (m, 4H), 1.81 – 1.72 (m, 4H), 1.30 (s, 9H); <sup>13</sup>C NMR (100 MHz, CDCl<sub>3</sub>): δ 175.56, 136.91, 134.49, 132.32, 128.54, 119.61, 116.58, 38.65, 28.66, 28.01, 26.79, 22.39, 22.27; IR  $\nu_{\max}/\text{cm}^{-1}$

$^1$ : 3283, 2923, 1645, 1589, 1529, 1501, 1416, 1193, 803, 695, 440; HRMS (ESI):  $m/z$  calcd for  $C_{15}H_{22}NO$   $[M+H]^+$ : 232.1701; found: 232.1698.

#### 4.6. Synthesis and Analytical Data for Iodonium Salts

Diphenyliodonium triflate was synthesized via a one-pot procedure from iodobenzene and benzene using *m*-CPBA as an oxidant at 0-5 °C.<sup>36</sup> Diphenyliodonium tetrafluoroborate was obtained following the reported protocol [*Eur. Pat.*, EP2599771 A1, 2013]. Aryl(mesityl)iodonium triflate salts with aryls-4-methylphenyl, 4-nitrophenyl, 4-iodophenyl, 4-(trifluoromethyl)phenyl, and 3-bromophenyl were purchased from Sigma-Aldrich.

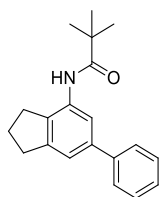
Benzo[*b*]thiophen-3-yl(mesityl)iodonium trifluoromethanesulfonate (iodonium **BT**)<sup>37</sup>



To a solution of benzo[*b*]thien-3-ylboronic acid (1.00 g, 5.62 mmol) in DCM (35 mL) at 0 °C was added dropwise  $BF_3 \cdot OEt_2$  (0.83 mL, 6.74 mmol). After this, reaction mixture was stirred for 15 min, then a solution of 2-diacetoxyiodomesitylene (2.45 g, 6.74 mmol) in DCM (20 mL) was added. This mixture was then stirred for 1 h, and thereafter TfOH (0.60 mL, 6.74 mmol) was added dropwise. The reaction mixture was stirred for another 15 min. Afterwards, DI water was added to quench the reaction, the aqueous layer was washed twice with DCM. The combined organic phase was dried over  $MgSO_4$  and concentrated under reduced pressure. The residue solid was vigorously stirred in diethyl ether for 15 min, and then cooled for 30 min in a freezer. The desired product was isolated *via* filtration and washed with diethyl ether. It was provided as a ochre solid (2.5 g, 84%);  $^1H$  NMR (400 MHz,  $CDCl_3$ ):  $\delta$  8.29 (s, 1H), 7.91 (d,  $J = 8.0$  Hz, 1H), 7.74 (d,  $J = 8.0$  Hz, 1H), 7.53 (t,  $J = 7.5$  Hz, 1H), 7.47 (t,  $J = 7.5$  Hz, 1H), 7.03 (s, 2H), 2.72 (s, 6H), 2.28 (s, 3H);  $^{13}C$  NMR (100 MHz,  $CDCl_3$ ):  $\delta$  144.07, 142.05, 138.72, 137.80, 136.82, 130.46, 126.65, 126.45, 123.28, 122.92, 122.12, 120.21 (q,  $J = 319.9$  Hz), 93.47, 27.22, 20.95; IR  $\nu_{max}/cm^{-1}$ : 3100, 1449, 1278, 1237, 1223, 1159, 1024, 747, 635, 516; HRMS (ESI):  $m/z$  calcd for  $C_{17}H_{16}IS$   $[M-OTf]^+$ : 379.0012; found: 379.0014.

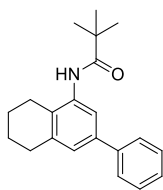
#### 4.7. Synthesis and Analytical Data for Pivanilides by Microwave Reactor

##### *N*-(6-phenyl-2,3-dihydro-1*H*-inden-4-yl)pivalamide (**2f**)



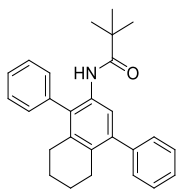
The product was obtained as a white solid [For (A) conversion > 99%; isolated yield = 26 mg, 96%, and for (B) conversion > 99%; isolated yield 26 mg, 96%]. <sup>1</sup>H NMR (400 MHz, CDCl<sub>3</sub>): δ 8.14 (s, 1H), 7.63 – 7.59 (m, 2H), 7.40 – 7.36 (m, 2H), 7.31 – 7.27 (m, 1H), 7.26 (br s, 1H), 7.25 (s, 1H), 3.01 (t, *J* = 7.5 Hz, 2H), 2.84 (t, *J* = 7.4 Hz, 2H), 2.22 – 2.13 (m, 2H), 1.35 (s, 9H); <sup>13</sup>C NMR (100 MHz, CDCl<sub>3</sub>): δ 176.40, 145.67, 141.27, 140.91, 134.28, 132.72, 128.53, 127.25, 126.99, 119.24, 117.71, 39.75, 33.20, 29.55, 27.70, 24.94; IR  $\nu_{\max}$ /cm<sup>-1</sup>: 3326, 2970, 2361, 1739, 1653, 1520, 1448, 1413, 1226, 1027, 869, 763, 699, 561; HRMS (ESI): *m/z* calcd for C<sub>20</sub>H<sub>24</sub>NO [M+H]<sup>+</sup>: 294.1858; found: 294.1852.

##### *N*-(3-phenyl-5,6,7,8-tetrahydronaphthalen-1-yl)pivalamide (**2g**)



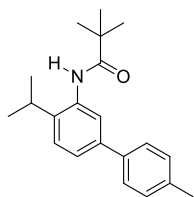
The product was obtained as a white solid [For (A) conversion > 99%; isolated yield = 26 mg, 96% and for (B) conversion > 99%; isolated yield = 24 mg, 91%]. <sup>1</sup>H NMR (400 MHz, CDCl<sub>3</sub>): δ 8.06 (d, *J* = 1.6 Hz, 1H), 7.63 – 7.59 (m, 2H), 7.41 – 7.37 (m, 2H), 7.33 – 7.28 (m, 1H), 7.26 (br s, 1H), 7.15 (s, 1H), 2.85 (t, *J* = 6.1 Hz, 2H), 2.61 (t, *J* = 6.3 Hz, 2H), 1.93 – 1.77 (m, 4H), 1.36 (s, 9H); <sup>13</sup>C NMR (100 MHz, CDCl<sub>3</sub>): δ 176.57, 140.98, 139.07, 138.41, 136.08, 128.70, 127.25, 125.20, 126.74, 124.49, 118.94, 40.04, 30.18, 27.92, 24.40, 23.12, 22.74; IR  $\nu_{\max}$ /cm<sup>-1</sup>: 3326, 2923, 1739, 1652, 1519, 1453, 1411, 1231, 1180, 868, 763, 699, 623, 564; HRMS (ESI): *m/z* calcd for C<sub>21</sub>H<sub>26</sub>NO [M+H]<sup>+</sup>: 308.2014; found: 308.2014.

##### *N*-(1,4-diphenyl-5,6,7,8-tetrahydronaphthalen-2-yl)pivalamide (**2h**)



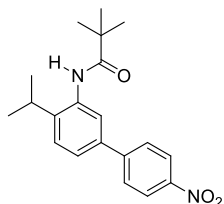
The product was obtained as a white solid [For (A) conversion = 92% and for (B) conversion = 95%]. <sup>1</sup>H NMR (400 MHz, CDCl<sub>3</sub>): δ 8.14 (s, 1H), 7.54 (t, *J* = 7.4 Hz, 2H), 7.47 – 7.42 (m, 1H), 7.39 (d, *J* = 4.4 Hz, 4H), 7.32 (dd, *J* = 8.9, 4.4 Hz, 1H), 7.28 (dd, *J* = 9.3, 2.3 Hz, 2H), 7.01 (br s, 1H), 2.65 (t, *J* = 5.8 Hz, 2H), 2.43 (t, *J* = 5.9 Hz, 2H), 1.72 – 1.62 (m, 4H), 0.96 (s, 9H); <sup>13</sup>C NMR (100 MHz, CDCl<sub>3</sub>): δ 176.10, 142.13, 141.94, 137.35, 135.62, 133.14, 130.86, 130.76, 129.86, 129.53, 129.43, 128.05, 128.00, 126.81, 119.66, 39.66, 29.11, 28.55, 27.29, 23.10, 23.08; IR  $\nu_{\max}$ /cm<sup>-1</sup>: 3421, 2927, 2360, 1738, 1684, 1564, 1512, 1405, 1364, 1216, 775, 698, 522; HRMS (ESI): *m/z* calcd for C<sub>27</sub>H<sub>30</sub>NO [M+H]<sup>+</sup>: 384.2327; found: 384.2324.

*N*-(4-isopropyl-4'-methylbiphenyl-3-yl)pivalamide (**3a**)



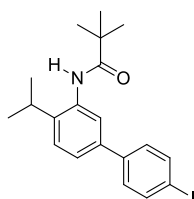
The product was obtained as a white solid [For (A) conversion = 93%; isolated yield = 26 mg, 92% and for (B) conversion = 89%]. <sup>1</sup>H NMR (400 MHz, CDCl<sub>3</sub>): δ 8.10 (d, *J* = 1.8 Hz, 1H), 7.52 (d, *J* = 8.1 Hz, 2H), 7.39 (dd, *J* = 8.1, 1.7 Hz, 2H), 7.33 (d, *J* = 8.1 Hz, 1H), 7.22 (d, *J* = 7.9 Hz, 2H), 3.00 (sept., *J* = 6.8 Hz, 1H), 2.38 (s, 3H), 1.37 (s, 9H), 1.31 (d, *J* = 6.8 Hz, 6H); <sup>13</sup>C NMR (100 MHz, CDCl<sub>3</sub>): δ 176.77, 139.50, 138.19, 137.78, 137.01, 134.88, 129.46, 127.05, 125.88, 123.98, 122.59, 39.88, 28.16, 27.84, 22.95, 21.22; IR  $\nu_{\max}$ /cm<sup>-1</sup>: 3237, 2958, 1738, 1642, 1514, 1367, 1227, 1202, 814, 669, 507; HRMS (ESI): *m/z* calcd for C<sub>21</sub>H<sub>28</sub>NO [M+H]<sup>+</sup>: 310.2171; found: 310.2165.

*N*-(4-isopropyl-4'-nitrobiphenyl-3-yl)pivalamide (**3b**)



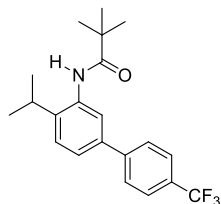
The product was obtained as a lemon yellow solid [For (A) conversion = 90%; isolated yield = 28 mg, 90% and for (B) conversion = 68%]. <sup>1</sup>H NMR (400 MHz, CDCl<sub>3</sub>): δ 8.26 – 8.20 (m, 3H), 7.74 (d, *J* = 8.8 Hz, 2H), 7.48 (br s, 1H), 7.42 – 7.36 (m, 2H), 3.01 (sept., *J* = 6.8 Hz, 1H), 1.37 (s, 9H), 1.31 (d, *J* = 6.8 Hz, 6H); <sup>13</sup>C NMR (100 MHz, CDCl<sub>3</sub>): δ 176.98, 147.16, 147.11, 139.86, 139.81, 137.00, 135.39, 127.83, 126.37, 124.13, 122.60, 40.02, 28.27, 27.81, 22.79; IR  $\nu_{\max}$ /cm<sup>-1</sup>: 3342, 2963, 1738, 1655, 1515, 1424, 1343, 1230, 1170, 856, 850, 823, 696, 630; HRMS (ESI): *m/z* calcd for C<sub>20</sub>H<sub>25</sub>N<sub>2</sub>O<sub>3</sub> [M+H]<sup>+</sup>: 341.1865; found: 341.1860.

*N*-(4'-iodo-4-isopropyl-[1,1'-biphenyl]-3-yl)pivalamide (**3c**)



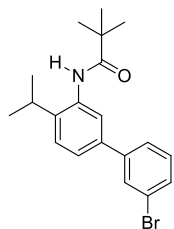
The product was obtained as a ivory white solid [For (A) conversion = 94% and for (B) conversion = 94%]. <sup>1</sup>H NMR (400 MHz, CDCl<sub>3</sub>): δ 8.11 (s, 1H), 7.72 (d, *J* = 8.1 Hz, 2H), 7.41 (br s, 1H), 7.36 (s, 1H), 7.34 (s, 3H), 2.99 (sept., *J* = 6.8 Hz, 1H), 1.37 (s, 9H), 1.31 (d, *J* = 6.8 Hz, 6H); <sup>13</sup>C NMR (100 MHz, CDCl<sub>3</sub>): δ 176.83, 140.19, 138.74, 138.33, 137.82, 135.10, 129.07, 126.10, 123.77, 122.32, 93.03, 39.94, 28.19, 27.83, 22.88; IR  $\nu_{\max}$ /cm<sup>-1</sup>: 3235, 2957, 1738, 1644, 1474, 1226, 1201, 1171, 1004, 816, 674, 505; HRMS (ESI): *m/z* calcd for C<sub>20</sub>H<sub>25</sub>INO [M+H]<sup>+</sup>: 422.0981; found: 422.0976.

*N*-(4-isopropyl-4'-(trifluoromethyl)-[1,1'-biphenyl]-3-yl)pivalamide (**3d**)



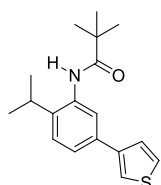
The product was obtained as a white solid [For (A) conversion = 88% and for (B) conversion = 37%]. <sup>1</sup>H NMR (400 MHz, CDCl<sub>3</sub>): δ 8.18 (s, 1H), 7.72 (d, *J* = 8.1 Hz, 2H), 7.65 (d, *J* = 8.4 Hz, 2H), 7.45 (br s, 1H), 7.41 – 7.35 (m, 2H), 3.01 (sept., *J* = 6.8 Hz, 1H), 1.37 (s, 9H), 1.31 (d, *J* = 6.8 Hz, 6H); <sup>13</sup>C NMR (100 MHz, CDCl<sub>3</sub>): δ 176.72, 144.08, 139.01, 137.90, 135.06, 129.18 (q, *J* = 32.4 Hz), 127.33, 126.04, 125.55 (q, *J* = 3.8 Hz), 124.31 (q, *J* = 271.9 Hz), 123.95, 122.52, 39.82, 28.08, 27.67, 22.70; IR  $\nu_{\max}/\text{cm}^{-1}$ : 3245, 2963, 1738, 1645, 1518, 1324, 1164, 1122, 1105, 1071, 846, 824, 669, 596, 509; HRMS (ESI): *m/z* calcd for C<sub>21</sub>H<sub>25</sub>F<sub>3</sub>NO [M+H]<sup>+</sup>: 364.1888; found: 364.1883.

*N*-(3'-bromo-4-isopropylbiphenyl-3-yl)pivalamide (**3e**)



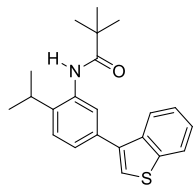
The product was obtained as a white solid [For (A) conversion = 95% and for (B) conversion = 93%; isolated yield = 30 mg, 88%]. <sup>1</sup>H NMR (400 MHz, CDCl<sub>3</sub>): δ 8.10 (s, 1H), 7.75 – 7.74 (m, 1H), 7.54 (d, *J* = 7.8 Hz, 1H), 7.46 – 7.40 (m, 2H), 7.35 (d, *J* = 0.8 Hz, 2H), 7.27 (t, *J* = 7.9 Hz, 1H), 3.01 (sept., *J* = 6.8 Hz, 1H), 1.37 (s, 9H), 1.31 (d, *J* = 6.8 Hz, 6H); <sup>13</sup>C NMR (100 MHz, CDCl<sub>3</sub>): δ 176.82, 142.87, 139.02, 138.03, 135.08, 130.25, 130.21, 130.11, 126.07, 125.92, 124.07, 122.87, 122.62, 39.90, 28.18, 27.81, 22.86; IR  $\nu_{\max}/\text{cm}^{-1}$ : 3332, 2971, 1646, 1553, 1524, 1489, 1468, 1388, 1234, 1196, 1169, 883, 781, 696, 636, 560; HRMS (ESI): *m/z* calcd for C<sub>20</sub>H<sub>25</sub>BrNO [M+H]<sup>+</sup>: 374.1120; found: 374.1112.

*N*-(2-isopropyl-5-(thiophen-3-yl)phenyl)pivalamide (**3f**)



(A) Reaction time was doubled to 1 h and (B) 3.5 mol% Cu<sup>II</sup>-β was used. The product was obtained as a brown solid [For (A) conversion = 56% and for (B) conversion = 64%]. <sup>1</sup>H NMR (400 MHz, CDCl<sub>3</sub>): δ 8.12 (d, *J* = 1.9 Hz, 1H), 7.45 (dd, *J* = 2.9, 1.3 Hz, 1H), 7.41 – 7.37 (m, 3H), 7.34 (dd, *J* = 5.0, 2.9 Hz, 1H), 7.29 (d, *J* = 8.1 Hz, 1H), 2.98 (sept., *J* = 6.8 Hz, 1H), 1.36 (s, 9H), 1.29 (d, *J* = 6.8 Hz, 6H); <sup>13</sup>C NMR (100 MHz, CDCl<sub>3</sub>): δ 176.77, 142.02, 138.16, 135.01, 134.42, 126.63, 126.04, 125.94, 123.55, 122.00, 120.44, 39.95, 28.21, 27.87, 22.93; IR  $\nu_{\max}/\text{cm}^{-1}$ : 3346, 2961, 2360, 1738, 1651, 1508, 1477, 1459, 1362, 1227, 853, 822, 776, 605; HRMS (ESI): *m/z* calcd for C<sub>18</sub>H<sub>24</sub>NOS [M+H]<sup>+</sup>: 302.1579; found: 302.1574.

*N*-(5-(benzo[*b*]thiophen-3-yl)-2-isopropylphenyl)pivalamide (**3g**)



Conversion was improved when the mole percent was increased to 3.5 mol% using (B) Cu<sup>II</sup>-β. The product was obtained as a ochre solid [For (A) conversion = 30% and for (B) conversion = 26%; isolated yield = 8 mg, 25%]. <sup>1</sup>H NMR (400 MHz, CDCl<sub>3</sub>): δ 8.05 (s, 1H), 8.00 (dd, *J* = 7.3, 1.2 Hz, 1H), 7.90 (dd, *J* = 7.0, 1.0 Hz, 1H), 7.44 – 7.38 (m, 5H), 7.37 – 7.35 (m, 1H), 3.04 (sept., *J* = 6.9 Hz, 1H), 1.37 (s, 9H), 1.34 (d, *J* = 6.9 Hz, 6H); <sup>13</sup>C NMR (100 MHz, CDCl<sub>3</sub>): δ 176.76, 140.76, 138.89, 138.03, 137.64, 134.86, 134.33, 125.87, 125.82, 124.58, 124.51, 124.42, 123.60, 123.21, 122.94, 39.89, 28.30, 27.86, 22.97; IR *v*<sub>max</sub>/cm<sup>-1</sup>: 3333, 2957, 1738, 1647, 1534, 1508, 1414, 1286, 1250, 1191, 1170, 757, 731, 649, 631, 423; HRMS (ESI): *m/z* calcd for C<sub>22</sub>H<sub>26</sub>NOS [M+H]<sup>+</sup>: 352.1735; found: 352.1732.

## 5. References

- [1] T. Newhouse, P.S. Baran, R.W. Hoffmann, *Chem. Soc. Rev.* **2009**, 38, 3010–3021.
- [2] P.A. Wender, V.A. Verma, T.J. Paxton, T.H. Pillow, *Acc. Chem. Res.* **2008**, 41, 40–49.
- [3] B.M. Trost, *Acc. Chem. Res.* **2008**, 35, 695–705.
- [4] T. Gensch, M.N. Hopkinson, F. Glorius, J. Wencel-Delord, *Chem. Soc. Rev.* **2016**, 45, 2900–2936.
- [5] R. Cano, A.F. Schmidt, G.P. McGlacken, *Chem. Sci.* **2015**, 6, 5338–5346.
- [6] J. Yamaguchi, A.D. Yamaguchi, K. Itami, *Angew. Chem. Int. Ed.* **2012**, 51, 8960–9009.
- [7] D. Alberico, M.E. Scott, M. Lautens, *Chem. Rev.* **2007**, 107, 174–238.
- [8] K. Godula, D. Sames, *Science* **2006**, 312, 67–72.
- [9] M. Albrecht, *Chem. Rev.* **2010**, 110, 576–623.
- [10] R.J. Phipps, M.J. Gaunt, *Science* **2009**, 323, 1593–1597.
- [11] C.O. Kappe, *Chem. Soc. Rev.* **2008**, 37, 1127–1139.
- [12] C.O. Kappe, *Angew. Chem. Int. Ed.* **2004**, 43, 6250–6284.
- [13] B.A. Roberts, C.R. Strauss, *Acc. Chem. Res.* **2005**, 38, 653–661.
- [14] C.S. Sundar, K.U.M. Rao, N.B. Reddy, M.V.N. Reddy, S.S. Prasad, C.S. Reddy, *Catal. Sci. Technol.* **2012**, 2, 1382–1385.
- [15] L. Bai, J.-X. Wang, *Adv. Synth. Catal.* **2008**, 350, 315–320.
- [16] Y. Kabri, A. Gellis, P. Vanelle, *Eur. J. Org. Chem.* **2009**, 4059–4066.
- [17] M. Massaro, S. Riela, G. Cavallaro, C.G. Colletti, S. Milioto, R. Noto, F. Parisi, G. Lazzara, *J. Mol. Catal. A Chem.* **2015**, 408, 12–19.
- [18] N.R. Deprez, D. Kalyani, A. Krause, M.S. Sanford, *J. Am. Chem. Soc.* **2006**, 128, 4972–4973.

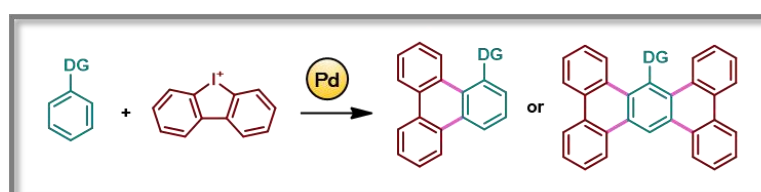


- [19] J.C. Lewis, J.Y. Wu, R.G. Bergman, J.A. Ellman, *Angew. Chem. Int. Ed.* **2006**, *45*, 1589–1591.
- [20] K. Takamatsu, K. Hirano, T. Satoh, M. Miura, *Org. Lett.* **2014**, *16*, 2892–2895.
- [21] M.R. Kuram, W.G. Kim, K. Myung, S.Y. Hong, *Eur. J. Org. Chem.* **2016**, 438–442.
- [22] R.J. Phipps, N.P. Grimster, M.J. Gaunt, *J. Am. Chem. Soc.* **2008**, *130*, 8172–8174.
- [23] R.J. Phipps, L. McMurray, S. Ritter, H.A. Duong, M.J. Gaunt, *J. Am. Chem. Soc.* **2012**, *134*, 10773–10776.
- [24] A. Quali, J.-F. Spindler, A. Jutand, M. Taillefer, *Adv. Synth. Catal.* **2007**, *349*, 1906–1916.
- [25] P. Gamez, I.W.C.E. Arends, J. Reedijk, R.A. Sheldon, *Chem. Commun.* **2003**, 2414–2415.
- [26] Y.-H. Zhang, B.-F. Shi, J.-Q. Yu, *J. Am. Chem. Soc.* **2009**, *131*, 5072–5074.
- [27] K.M. Engle, T.-S. Mei, M. Wasa, J.-Q. Yu, *Acc. Chem. Res.* **2012**, *45*, 788–802.
- [28] J.H. Kwak, J.H. Lee, S.D. Burton, A.S. Lipton, H.F. Peden, J. Szanyi, *Angew. Chem. Int. Ed.* **2013**, *52*, 9985–9989.
- [29] B. Wichterlova, J. Dedecek, A. Vondrova, *J. Phys. Chem.* **1995**, *99*, 1065–1067.
- [30] M. Choi, D.-H. Lee, K. Na, B.-W. Yu, R. Ryoo, *Angew. Chem. Int. Ed.* **2009**, *48*, 3673–3676.
- [31] M.E. Davis, R.J. Davis, *Fundamentals of Chemical Reaction Engineering*, McGraw-Hill, 2003.
- [32] M. Campanati, G. Fornasari, V. Vaccari, *Catal. Today* **2003**, *77*, 299–314.
- [33] E.A. Merritt, B. Olofsson, *Angew. Chem. Int. Ed.* **2009**, *48*, 9052–9070.
- [34] T.B. Petersen, R. Khan, B. Olofsson, *Org. Lett.* **2011**, *13*, 3462–3465.
- [35] B.P. Mathew, H.J. Yang, H. Jeon, J.H. Lee, J.C. Kim, T.J. Shin, K. Myung, S.K. Kwak, J.H. Kwak, S.Y. Hong, *J. Mol. Catal. A Chem.* **2016**, *417*, 64–70.
- [36] M. Bielawski, M. Zhu, B. Olofsson, *Adv. Syn. Catal.* **2007**, *349*, 2610–2618.
- [37] B.S.L. Collins, M.G. Suero, M.J. Gaunt, *Angew. Chem. Int. Ed.* **2013**, *52*, 5799–5802.

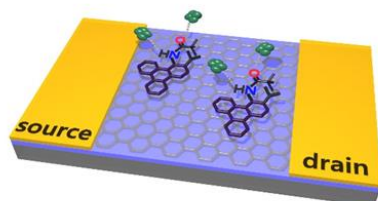
## Chapter IV

### An Annulative Synthetic Strategy for Building Triphenylene Frameworks by Multiple C–H Bond Activations

C–H activation is a versatile tool for appending aryl groups to aromatic systems. However, heavy demands on multiple catalytic cycle operations and site-selectivity have limited its use for graphene segment synthesis. A Pd-catalyzed one-step synthesis of functionalized triphenylene frameworks is disclosed, which proceeds by 2- or 4-fold C–H arylation of unactivated benzene derivatives. A Pd<sub>2</sub>(dibenzylideneacetone)<sub>3</sub> catalytic system, using cyclic diaryliodonium salts as  $\pi$ -extending agents, leads to site-selective inter- and intramolecular tandem arylation sequences. Moreover, N-substituted triphenylenes are applied to a field-effect transistor sensor for rapid, sensitive, and reversible alcohol vapor detection. This chapter is reproduced from *Angew. Chem. Int. Ed.* **2017**, 56, 5007–5011.



*Synthesis and Application of Substituted Triphenylenes*

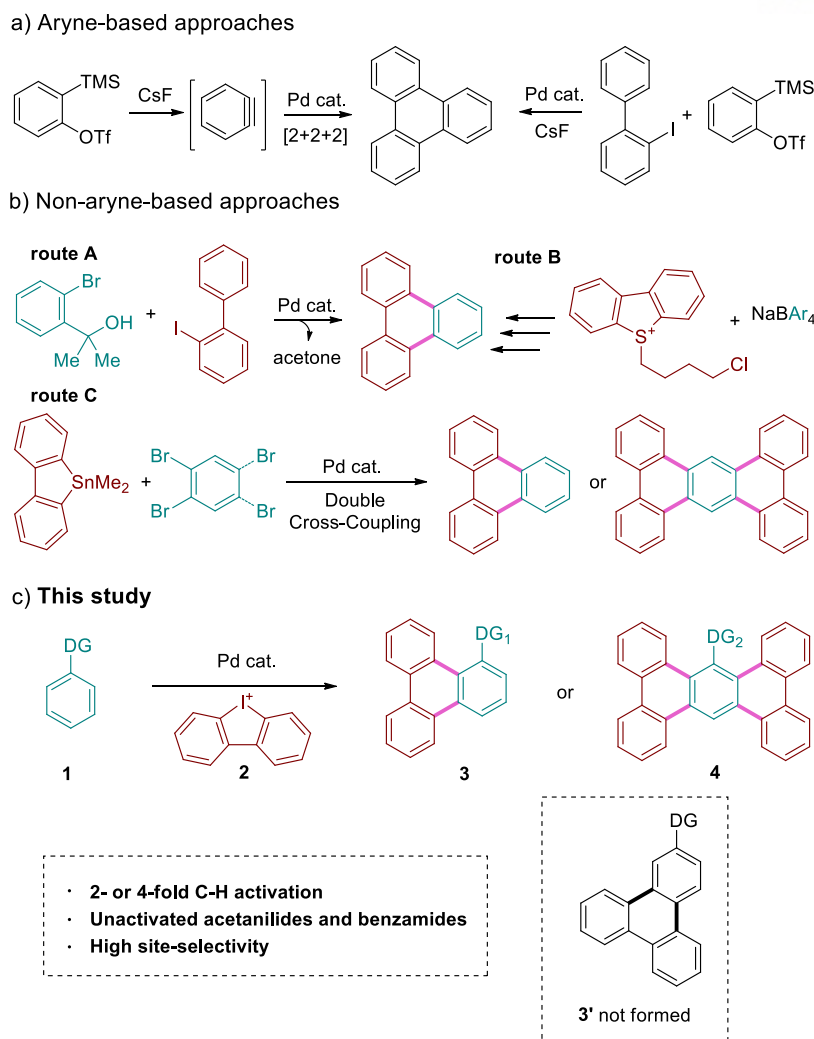


#### 1. Introduction

Graphene is a fundamentally and industrially important synthetic carbon allotrope that has been applied to a vast array of applications since its isolation by Geim and Novoselov in 2004.<sup>1-4</sup> The development of synthetic methods for accessing (functionalized) graphene and its molecular segment has been a recent theme for synthetic chemists in pursuit of two-dimensional nanostructures with finely tuned properties.<sup>1</sup> Although top-down synthetic routes are well established for producing large-scale graphene materials, bottom-up synthetic approaches, including the Diels–Alder reaction, cross-coupling reactions, surface-mediated synthesis, and C–H activation, are logical choices to access atomically precise graphene segments—also known as polycyclic aromatic hydrocarbons (PAHs).<sup>1,5-11</sup>

Among the 35 parent structural units of PAHs, triphenylene belongs to a branched all-benzoid category.<sup>12</sup> Pd-catalyzed annulation approaches to triphenylene moieties are based on aryne chemistry.<sup>13-17</sup> For example, Perez et al. have reported [2+2+2] cyclotrimerization of benzyne (Scheme 4.1a).<sup>16</sup> The Larock group introduced annulation of arynes using 2-halobiaryls.<sup>17</sup> Alternatively, Nishihara et al. have reported a non-benzyne route using *o*-bromobenzyl alcohol as an annulating agent (route A, Scheme 4.1b).<sup>18</sup> Yorimitsu et al. developed a multi-step transformation approach from dibenzothiophenes (route B, Scheme 4.1b).<sup>19</sup> Shimizu and coworkers introduced [4+2]-type aromatic annulation between 9-stannafluorenes and di-/tetra-halogenated compounds (route C, Scheme 4.1b).<sup>20</sup> However, these methods for tailored triphenylene synthesis typically require laborious prefunctionalization steps. Therefore, the development of concise synthetic strategies to provide triphenylene frameworks from unactivated substrates is an important synthetic goal in graphene chemistry.

Herein, we show that unactivated and readily available arene substrates can undergo Pd-catalyzed 2- or even 4-fold C–H arylation to afford substituted triphenylenes **3** or phenanthro[9,10-*b*]triphenylenes **4**, respectively (Scheme 1c). To our knowledge, this is the first example of a straightforward p-extension strategy utilized to provide triphenylene frameworks from acetanilides and benzamides. The N-substituted triphenylenes obtained are incorporated into an alcohol field-effect transistor (FET) sensor, which exhibits a rapid and reversible response.



**Scheme 4.1.** Synthesis of triphenylene frameworks.

## 2. Results and Discussion

Over the last few decades, direct arylation methods have emerged aided by bench-stable hypervalent iodine compounds.<sup>21,22</sup> It was anticipated that **2**, with cyclic geometry, has the potential for 2-fold C–H arylation of **1** toward aromatic annulation (Figure 4.1). Simple amide moieties were chosen as the directing groups (DGs) owing to 1) their wide prevalence in natural products and functional organic materials, 2) the effective facilitation of  $sp^2$  C–H activation, and 3) increased processability for FET applications. In cycle I, cyclic diaryliodonium salt **2** undergoes successive single-electron reductions by  $Pd^0$  to form X- $Pd^{II}$ -aryl complex **A**, as previously suggested by the Glorius group.<sup>23</sup> Subsequently, cyclopalladation of arene **1** would afford **C**, which can undergo reductive elimination to give aryl iodide **D**. In cycle II, oxidative addition, concerted metalation–deprotonation, and subsequent reductive elimination, regenerate  $Pd^0$  and afford the desired product **3**.

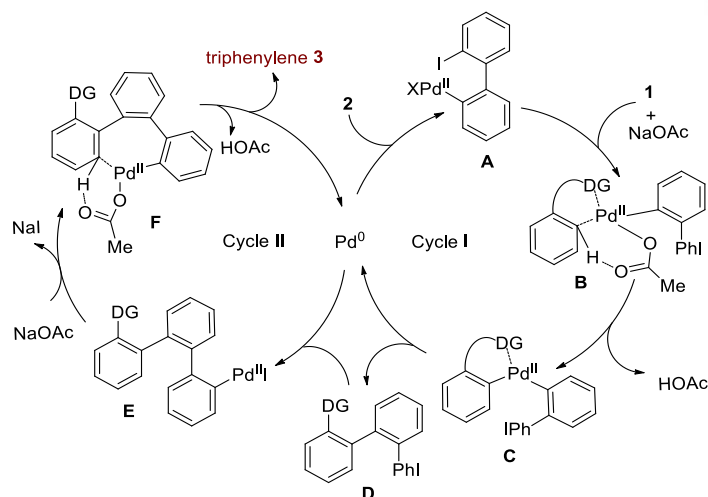
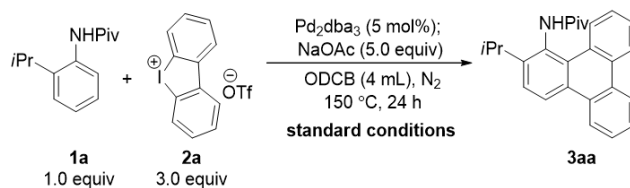


**Figure 4.1.** Proposed 2-fold C–H arylation mechanism.

To examine the feasibility of this strategy, various reaction parameters were surveyed. The optimized conditions provided annulated product **3aa** in 85% yield (Table 4.1). In the absence of catalyst (entry 2), there was no reactivity. Changes in the palladium source or catalyst loading caused diminished yields (entries 3–5). A control reaction without NaOAc showed no reactivity (entry 6). Other weak bases, such as AgOAc and KOAc, were ineffective (entries 8 and 9). Addition of external oxidants, such as K<sub>2</sub>S<sub>2</sub>O<sub>8</sub> or air, led to reduced yields (entries 10 and 11). The presence of radical scavengers (butylated hydroxytoluene (BHT) and 2,2,6,6-tetramethyl-1-piperidinyloxy (TEMPO)) affected the reaction yields drastically (entries 12 and 13), indicating the potential involvement of a radical pathway. A probable thermal reduction of Pd(OAc)<sub>2</sub> to Pd<sup>0</sup> may account for a moderate yield (55%, entry 5).<sup>23</sup> However, an alternative mechanistic pathway involving a Pd<sup>II</sup>/Pd<sup>IV</sup> manifold cannot be ruled out completely.<sup>22,24</sup> When other solvents were used, such as toluene or *N,N*-dimethylformamide (DMF), the reaction did not progress (entries 14 and 15). Reduction of the reaction volume (2 mL) only caused a moderate drop in yield (52%, entry 16). Finally, decreasing the concentration of **2a** (1.5 equiv, entry 17) and reducing the reaction temperature (100 °C, entry 18) led to moderate and poor yields, respectively.



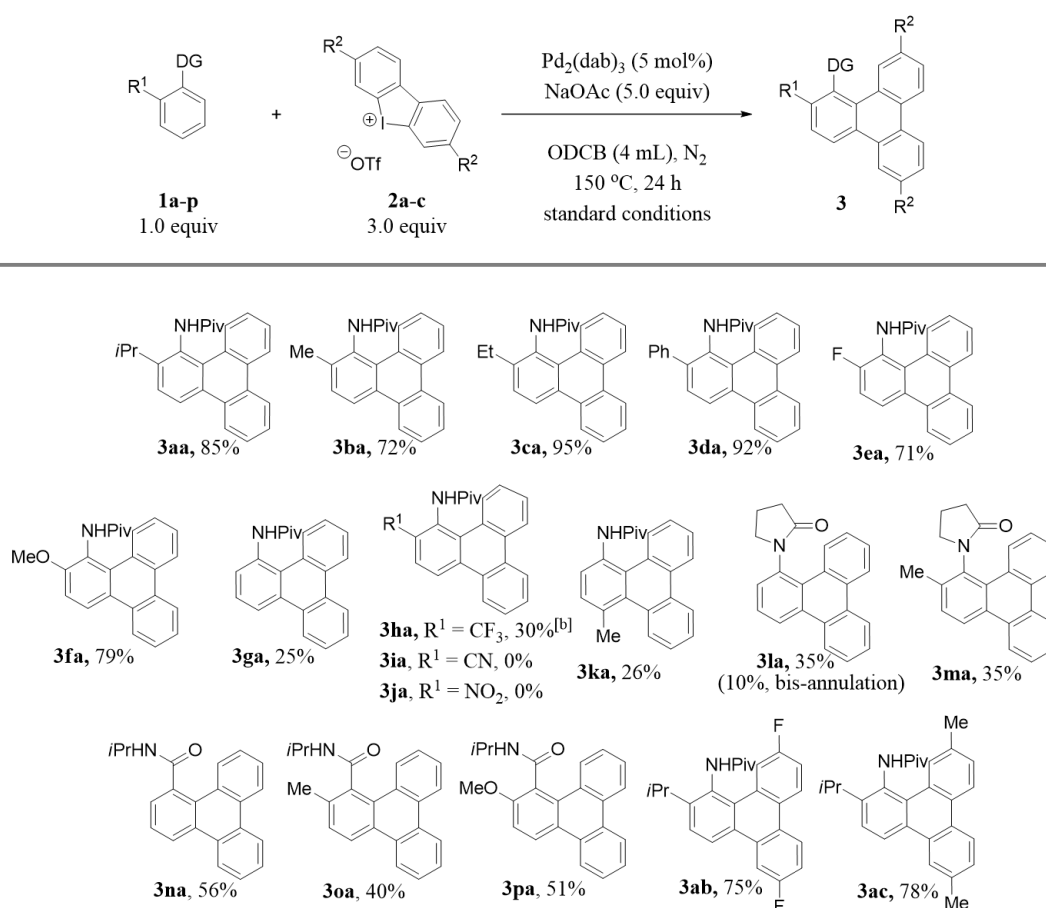
Entry	Deviations from standard conditions	Yield [%] <sup>[b]</sup>
1	None	85
2	no $[\text{Pd}_2\text{dba}_3]$	0
3	with 1.5 mol% $[\text{Pd}_2\text{dba}_3]$	52
4	$\text{Pd}(\text{PPh}_3)_4$ instead of $[\text{Pd}_2\text{dba}_3]$	39
5	$\text{Pd}(\text{OAc})_2$ instead of $[\text{Pd}_2\text{dba}_3]$	55
6	no NaOAc	0
7	1 equiv of NaOAc instead of 5 equiv	trace
8	AgOAc instead of NaOAc	0
9	KOAc instead of NaOAc	trace
10	$\text{K}_2\text{S}_2\text{O}_8$ (1 equiv) added	64
11	under air	31
12	BHT (1 equiv) added	27
13	TEMPO (1 equiv) added	9 <sup>[c]</sup>
14	toluene instead of ODCB	trace
15	DMF instead of ODCB	0
16	2 mL of ODCB instead of 4 mL	52
17	1.5 equiv of <b>2a</b> instead of 3.0 equiv	51
18	at 100 °C	8 <sup>[c]</sup>

[a] Experiments were performed with **1a** (0.228 mmol), **2a** (3 equiv),  $[\text{Pd}_2\text{dba}_3]$  (tris(dibenzylideneacetone)dipalladium(0), 5 mol%), NaOAc (5 equiv) in 1,2-dichlorobenzene (ODCB, 4 mL) at 150 °C for 24 h under nitrogen. [b] Isolated yields. [c] GC yield using n-dodecane as an internal standard.

**Table 4.1.** Optimization of 2-fold C–H arylation.<sup>a</sup>

With the optimized conditions in hand, our subsequent goal was to investigate the reaction scope. Arenes with *ortho*-alkyl groups, including *i*Pr (**1a**), methyl (**1b**), and ethyl (**1c**), gave good yields of the corresponding triphenylenes. Functional groups with  $\pi$ -electron donors, such as *ortho*-phenyl (**1d**), *ortho*-fluoro (**1e**), and *ortho*-OMe (**1f**) were tolerated, furnishing the annulated products in moderate to good yields. However, electron-withdrawing trifluoromethyl, cyano, and nitro groups resulted in poorer reactivity (**3ha**, 30%; **3ia** and **3ja**, no product). Pivanilide (**1g**) with no *ortho*-substituent gave a poor yield (**3ga**, 25%). Subsequently, the 2-fold arylation was attempted with *meta*-substituted substrates

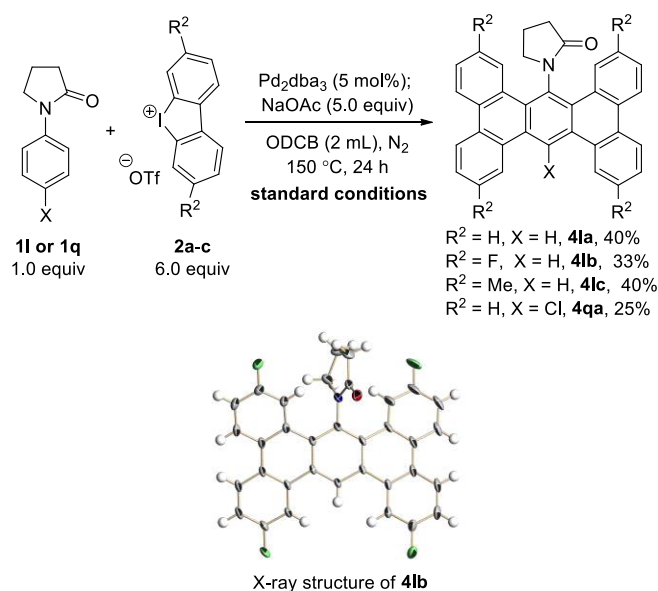
with methyl and cyano groups (data not shown), but no product formation was observed. The *para*-substituted substrate **1k** was subjected to the reaction conditions, but a poor isolated yield was obtained (26%). Additionally, the compatibility of this method with other simple but electron-deficient benzamide substrates was examined. Benzamide-based triphenylene derivatives (**3na**, **3oa**, and **3pa**) were obtained in moderate yields (56%, 40%, and 51%, respectively) with incomplete conversion of the corresponding substrates. Cyclic diaryliodonium salts **2b** and **2c** bearing difluoro and dimethyl groups provided good yields to afford **3ab** and **3ac**, respectively. Given the difficulties in constructing a diverse array of tailored triphenylenes, arising from the planar and (un)symmetrical structures,<sup>15,19</sup> the reaction scope of this approach is comparable to that of previously reported methods.<sup>16-20</sup> Overall, the electronic nature of the substrates bearing amide DGs (and substituents) significantly affects the efficiency of the annulation.



[a] Standard reaction conditions and isolated yields. [b] Experiment was performed with **1h** (0.228 mmol), **2a** (3+2 equiv),  $[\text{Pd}_2\text{dab}_3]$  (5+2.5 mol%), NaOAc (5 equiv) in ODCB (4 mL) at  $150\text{ }^\circ\text{C}$  for 48 h under nitrogen.

**Table 4.2.** Reaction scope.<sup>a</sup>

With the aim of using alternative DGs, we reacted 1-phenylpyrrolidin-2-one (**11**) with **2a**. Particularly noteworthy is the formation of phenanthro[9,10-*b*]triphenylene product **41a** arising from 4-fold C–H arylation in 10% isolated yield along with product **31a** (35% yield, Table 4.2). To enhance the yield of the bis-annulated (or 4-fold C–H arylated) product, we doubled the number of equivalents of **2a** (6.0 equiv) and reduced the volume of 1,2-dichlorobenzene (ODCB; 2 mL), as shown in Scheme 4.2. With these changes, the yield of the bis-annulated product improved moderately to 40%. However, we still observed mono-annulation with the reduced amount (18%). We performed additional reactions with **2b** and **2c**, and observed phenanthro[9,10-*b*]triphenylene derivative formation in 33% and 40% yields, respectively. Single-crystal X-ray diffraction analysis unambiguously confirmed the structure of **41b**.<sup>25</sup> Interestingly, chlorinated substrate **1q** gave bis-annulated product **41qa**, albeit with a poor isolated yield (25%). The photophysical properties of compounds **4** were also studied (see, Figure 4.5 and Table 4.4).



**Scheme 4.2.** Synthesis of phenanthro[9,10-*b*]triphenylene **4** frameworks.

To highlight the applicability of substituted triphenylenes, readily soluble and processable **3aa** was incorporated into graphene-based FETs for application as a chemical gas sensor as part of our ongoing research on the functionalization of nanostructured carbons.<sup>26-28</sup> Graphene FETs were fabricated on a Si wafer as a bottom gate structure (gate: doped Si; dielectric layer: 300 nm-thick SiO<sub>2</sub>), and then **3aa** was non-covalently immobilized on the graphene channel with  $\pi$ – $\pi$  interactions, as shown in Figure 4.2a.<sup>26,29</sup> Figure 4.2b presents the transfer curves of graphene FETs before and after **3aa** coating (see, Figure 4.3). The pristine FET showed ambipolar behavior consistent with the expected semimetallic characteristics of graphene,<sup>30-32</sup> with a positive charge neutrality point of approximately 38 V (black curve in Figure 4.2b). The hole (electron) mobility of the graphene FET was 2940 cm<sup>2</sup>V<sup>-1</sup>s<sup>-1</sup> (2520 cm<sup>2</sup>V<sup>-1</sup>s<sup>-1</sup>) for a



channel length of 70 nm and width of 5 nm. After **3aa** coating, the graphene FET showed a leftward  $V_{\text{Dirac}}$  shift because of its negative charge transfer effect, with negligible change in mobility. The similar slopes (*trans*-conductance ( $g_m$ )) of the two curves in Figure 4.2b indicate that graphene segment structured **3aa** can induce charge transfer without causing additional scatterings on the graphene channel. Figure 4.2c reveals that the response of the **3aa**-functionalized sensor to ethanol vapor at 1000 ppm is fast and completely reversible. The sensitivity was maintained upon multiple exposures. Hydrogen bonding with the amide functionality of **3aa** may give rise to ethanol binding on the **3aa**-functionalized graphene channel, which effectively raises the Henry's law constant at the graphene surface (Figure 4.2a).<sup>33,34</sup> Graphene without **3aa**-functionalization showed a weaker response and poor reversibility when exposed to ethanol vapor (see, Figure 4.4). Figure 4.2d compares the sensitivities of the sensor to ethanol,  $\text{NH}_3$ ,  $\text{CO}_2$ , and  $\text{H}_2$  at room temperature (same concentration, 1000 ppm). The **3aa**-functionalized sensor is three to five times more sensitive to ethanol than to the other analytes.

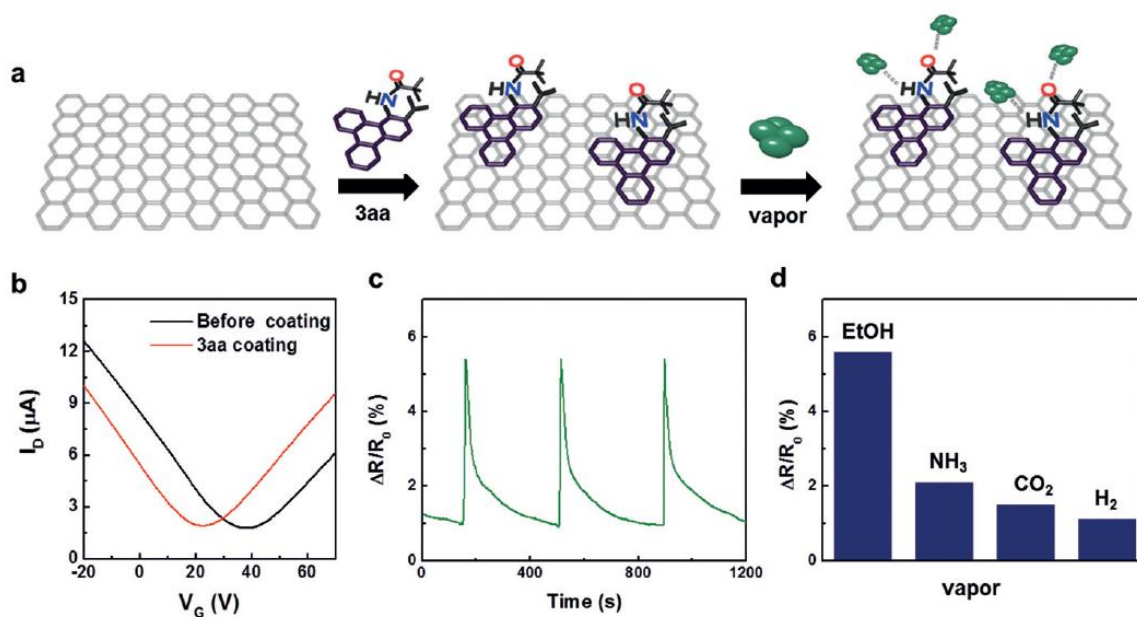


**Figure 4.2.** (a) Interaction of **3aa** with the graphene surface, (b) Transfer characteristics ( $V_D=0.1$  V), (c) Real-time response, (d) Sensor sensitivities.

### 3. Conclusions

In conclusion, a palladium-catalyzed 2- or 4-fold C–H arylation strategy to afford functionalized triphenylenes and phenanthro[9,10-*b*]triphenylenes from unactivated arenes was demonstrated for the first time. This annulative  $\pi$ -extension method features inter- and intramolecular tandem arylation sequences employing cyclic diaryliodonium salts by multiple C–H activations. *N*-substituted triphenylenes with good processability were incorporated into an alcohol FET sensor that showed a

rapid and reversible response. This study is expected to bridge synthetic organic chemistry and nanoscience by providing a one-step synthetic route to access various triphenylene frameworks.

## 4. Experimental

### 4.1. General Methods

All reagents were purchased from standard suppliers (Sigma-Aldrich, Alfa Aesar, or TCI) and were used without further purification. Annulation reactions were performed in oven-dried schlenk tubes (capacity, 10 or 25 mL) under inert conditions.  $^1\text{H}$ ,  $^{13}\text{C}$ , and  $^{19}\text{F}$  NMR spectra were recorded on an Agilent VNMRS 600. All chemical shifts are quoted on the  $\delta$ -scale in ppm, and residual solvent peaks were used as references. For  $^{19}\text{F}$  NMR,  $\alpha,\alpha,\alpha$ -trifluorotoluene (-63.72 ppm, 0.05% in benzene- $d_6$ ) was used as an external reference. GC analysis was performed on an Agilent Technologies GCMS 7890A equipped with a BR-ms column (30 m x 0.25 mm i.d., 0.25  $\mu\text{m}$  film thickness, pressure = 20.0 kPa, detector = EI, 300  $^\circ\text{C}$ ) with helium gas as carrier. Infrared (IR) spectra were recorded on a Nicolet iS5 from Thermo Fisher Scientific FT-IR spectrometer using the attenuated total reflectance (ATR) mode. Low resolution mass spectrometry (MS) spectra were acquired from a Bruker 1200 Series & HCT Basic System using electrospray ionization (ESI). High resolution mass spectrometry (HRMS) spectra were measured using a Q Exactive<sup>TM</sup> Plus Hybrid Quadrupole-Orbitrap<sup>TM</sup> mass spectrometer from Thermo Scientific. UV/VIS absorption spectra were recorded on an Agilent 8453 UV-Visible spectrometer. Fluorescence emission spectra were recorded on a SpectraMax<sup>®</sup> i3x Multi-Mode Detection Platform from Molecular Devices. Thin layer chromatography (TLC) was performed using glass plates pre-coated (0.25 mm) with Merck silica gel 60 F254. Visualization of the plate was achieved using an ultraviolet lamp ( $\lambda_{\text{max}}$ , 254 nm). Flash column chromatography was carried out using Merck silica gel 60 (0.040-0.063 mm).

### 4.2. Synthesis of Arene Substrates

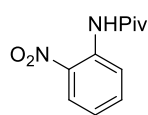
#### 4.2.1. General Procedure for the Preparation of Pivalilide Substrates

To a solution of aromatic amine (8.3 mmol) and  $\text{NaHCO}_3$  (24.8 mmol) in dichloromethane (DCM, 30 mL) was added pivaloyl chloride (9.1 mmol) in a dropwise manner at room temperature (RT). After completion of the reaction (3-4 h, TLC), the reaction mixture was diluted with DCM. The organic phase was washed with brine, dried over  $\text{Na}_2\text{SO}_4$  then concentrated *in vacuo* to give the desired pivalilide.

*N*-(2-isopropylphenyl)pivalamide (**1a**),<sup>35</sup> *N*-(*o*-tolyl)pivalamide (**1b**),<sup>35</sup> *N*-(2-ethylphenyl)pivalamide (**1c**),<sup>36</sup> *N*-([1,1'-biphenyl]-2-yl)pivalamide (**1d**),<sup>35</sup> *N*-(2-fluorophenyl)pivalamide (**1e**),<sup>35</sup> *N*-(2-methoxyphenyl)pivalamide (**1f**),<sup>35</sup> *N*-phenylpivalamide (**1g**),<sup>35</sup> *N*-(2-(trifluoromethyl)phenyl)pivalamide (**1h**),<sup>37</sup> *N*-(2-cyanophenyl)pivalamide (**1i**),<sup>38</sup> and *N*-(*p*-

tolyl)pivalamide (**1k**)<sup>35</sup> and were matched with previously reported data.

#### *N*-(2-nitrophenyl)pivalamide (**1j**)



The product was obtained as a yellow solid (1.7 g, 92%). <sup>1</sup>H NMR (600 MHz, CDCl<sub>3</sub>) δ = 10.73 (br s, 1H), 8.83 (d, *J* = 8.5 Hz, 1H), 8.22 (d, *J* = 8.4 Hz, 1H), 7.64 (t, *J* = 7.8 Hz, 1H), 7.16 (t, *J* = 7.8 Hz, 1H), 1.36 (s, 9H); <sup>13</sup>C NMR (150 MHz, CDCl<sub>3</sub>) δ = 177.83, 135.97, 135.43, 125.73, 122.91, 122.07, 40.57, 27.43; IR  $\nu_{\max}$ /cm<sup>-1</sup>: 3370, 3119, 2962, 2871, 1704, 1606, 1582, 1494, 1455, 1424, 1331, 1265, 1229, 1136, 1080, 1040, 922, 860, 786, 744; HRMS (ESI) *m/z* calcd for C<sub>11</sub>H<sub>15</sub>N<sub>2</sub>O<sub>3</sub> [M+H]<sup>+</sup> 223.1083; found 223.1073.

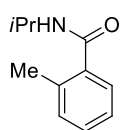
#### 4.2.2. General Procedure for the Preparation of 2-Pyrrolidinone Substrates

**Method I** (for **1l** and **1q**): A schlenk tube was charged with Pd<sub>2</sub>dba<sub>3</sub> (0.5 mol%), Xantphos (1.5 mol%), the solid reactant(s) (1.0 mmol of aryl bromide), and Cs<sub>2</sub>CO<sub>3</sub> (1.4 mmol). The schlenk tube was evacuated and backfilled with argon for two times. The liquid reactant(s) (1.2 mmol of 2-pyrrolidinone) and 1,4-dioxane (1 mL) were added and stirred at 100 °C for 16 h. The reaction mixture was then cooled to RT, diluted with DCM (10 mL), filtered, and concentrated *in vacuo*. The crude material was purified by flash column chromatography (n-hexane/ethyl acetate, 1:1); **Method II** (for **1m**): A schlenk tube was charged with 2-pyrrolidone (16.2 mmol), 2-iodotoluene (5.4 mmol), CuI (0.5 mmol), *N,N*-dimethylglycine (1.1 mmol), and K<sub>2</sub>HPO<sub>4</sub> (10.8 mmol). The tube was evacuated and backfilled with argon for two times. DMF (3.0 mL) was added under argon. The reaction mixture was stirred at 150 °C for 24 h. The cooled mixture was diluted with DI water and ethyl acetate. The aqueous layer was extracted with ethyl acetate for three times. The combined organic layers were washed with brine, dried over Na<sub>2</sub>SO<sub>4</sub>, and concentrated *in vacuo*. The residue was purified by flash column chromatography (n-hexane/ethyl acetate, 3:1 → 2:1). 1-phenylpyrrolidin-2-one (**1l**),<sup>39</sup> 1-(*o*-tolyl)pyrrolidin-2-one (**1m**),<sup>40</sup> and 1-(4-chlorophenyl)pyrrolidin-2-one (**1q**)<sup>41</sup> were matched with previously reported data.

#### 4.2.3. General Procedure for the Preparation of *N*-Isopropylbenzamide Substrates

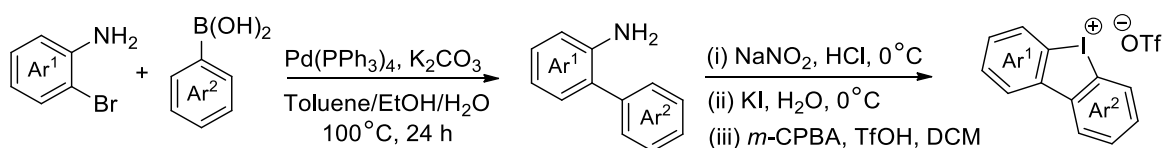
To a solution of K<sub>2</sub>CO<sub>3</sub> (2.073 g, 15 mmol, 1.5 equiv) and isopropylamine (1.03 mL, 1.2 equiv) in anhydrous acetonitrile (20 mL) was added aromatic acid chloride (10 mmol), and the mixture was stirred magnetically at 70 °C. After completion of the reaction (2 h, TLC), the mixture was cooled to RT; filtered off and the solvent was evaporated to dryness *in vacuo* to afford the corresponding *N*-isopropyl benzamide derivative. *N*-isopropylbenzamide (**1n**) and *N*-isopropyl-2-methoxybenzamide (**1p**) were matched with the previously reported data.<sup>42</sup>

### *N*-isopropyl-2-methylbenzamide (**10**)



The product was obtained as a white solid (1.2 g, 68%).  $^1\text{H}$  NMR (600 MHz,  $\text{CDCl}_3$ )  $\delta$  = 7.25 – 7.22 (m, 2H), 7.12 (dd,  $J$  = 16.3, 7.8 Hz, 2H), 5.86 (br s, 1H), 4.23 – 4.13 (m, 1H), 2.36 (s, 3H), 1.18 (d,  $J$  = 6.5 Hz, 6H);  $^{13}\text{C}$  NMR (150 MHz,  $\text{CDCl}_3$ )  $\delta$  = 169.32, 136.92, 135.60, 130.73, 129.48, 126.55, 125.56, 41.60, 22.68, 19.55; IR  $\nu_{\text{max}}/\text{cm}^{-1}$ : 3278, 3019, 2972, 2929, 2875, 2158, 1633, 1534, 1455, 1365, 1344, 1300, 1286, 1170, 1150, 1131, 1036, 886, 843, 799, 777, 744, 722; HRMS (ESI)  $m/z$  calcd for  $\text{C}_{11}\text{H}_{16}\text{NO}$   $[\text{M}+\text{H}]^+$  178.1232; found 178.1223.

### 4.3. Synthesis of Cyclic Diaryliodonium Salts



A 250 mL three-necked flask equipped with a magnetic stir bar was charged with an arylboronic acid (7.5 mmol, 1.5 equiv),  $\text{K}_2\text{CO}_3$  (2.75 g, 20.0 mmol, 4.0 equiv),  $\text{Pd}(\text{PPh}_3)_4$  (577 mg, 0.5 mmol, 10 mol%), toluene (40 mL), DI water (8 mL), and ethanol (10 mL). To the resulting solution was added *ortho*-bromoaniline derivative (5.0 mmol), and the reaction mixture was heated at 100 °C for 16 h. After cooling to RT, the biphasic mixture was diluted with satd. aqueous  $\text{NH}_4\text{Cl}$  (30 mL) and DCM (30 mL). The aqueous phase was extracted with DCM, and the combined organic layers were washed with DI water and satd. aqueous  $\text{NaHCO}_3$ , dried over  $\text{Na}_2\text{SO}_4$ , and then concentrated *in vacuo*. The residue was purified by flash column chromatography to afford the desired 2-aminobiaryl derivative.

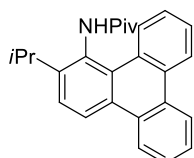
2-Aminobiaryl derivative (5 mmol) was suspended in DI water (5 mL) at 0 °C and HCl (12 N; 1 mL) was added. After slow addition of a solution of  $\text{NaNO}_2$  (10 mmol) in DI water (1.3 mL), the reaction mixture was stirred for 45 min at 0 °C. A solution of ice cooled KI (12.5 mmol) in DI water (2 mL) was added, and then it was allowed to warm to RT overnight. The reaction mixture was extracted with ether, and the organic layers were washed with diluted HCl solution (aqueous, 1 M), satd.  $\text{NaHCO}_3$ , satd.  $\text{Na}_2\text{S}_2\text{O}_5$ , and brine. After drying over  $\text{Na}_2\text{SO}_4$  and concentration *in vacuo*, the crude product was purified by column chromatography (n-hexane) to yield 2-iodobiaryl derivative as an oil. In a 250 mL round-bottom flask, 1.6 equiv (11.4 mmol) of *m*-chloroperbenzoic acid (*m*-CPBA) was taken. To this, a solution of 2-iodobiaryl derivative (7.14 mmol) in anhydrous DCM (22 mL) was added, followed by dropwise addition of TfOH (3.25 equiv) with constant stirring at RT. Thereafter, the reaction mixture was stirred for 1.5 h, and then solvent was evaporated *in vacuo* at RT. The residue was diluted with ether (~30 mL) and stirred for 30 min at RT to afford solid precipitate. This solid was then filtered and washed thoroughly with ether to yield the required cyclic diaryliodonium salts.

$^1\text{H}$  and  $^{13}\text{C}$  NMR spectra for the following known cyclic diaryliodonium salts showed good

agreement with the literature data.<sup>43</sup> Diphenyliodonium trifluoromethanesulfonate (**2a**), 3,7-Difluorodibenzo[*b,d*]iodol-5-ium trifluoromethanesulfonate (**2b**), 3,7-Dimethyldibenzo[*b,d*]iodol-5-ium trifluoromethanesulfonate (**2c**).

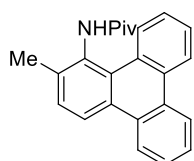
#### 4.4. Substituted Triphenylenes and Phenanthro[9,10-*b*]triphenylenes

##### *N*-(2-isopropyltriphenylen-1-yl)pivalamide (**3aa**)



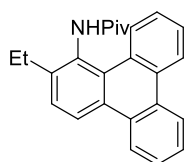
The product was obtained as a white solid (72 mg, 85%). <sup>1</sup>H NMR (600 MHz, CDCl<sub>3</sub>) δ = 8.75 (d, *J* = 8.0 Hz, 1H), 8.59 – 8.52 (m, 4H), 7.63 – 7.57 (m, 4H), 7.49 (br s, 1H), 7.43 (t, *J* = 7.1 Hz, 1H), 3.27 – 3.23 (septet, *J* = 6.6 Hz, 1H), 1.43 (s, 9H), 1.32 (d, *J* = 6.6 Hz, 6H); <sup>13</sup>C NMR (150 MHz, CDCl<sub>3</sub>) δ = 176.77, 145.69, 131.13, 130.67, 130.07, 130.04, 130.00, 129.44, 128.04, 127.40, 127.27, 127.25, 127.23, 125.66, 124.94, 123.61, 123.40, 123.17, 122.74, 39.70, 28.71, 27.82, 23.53; IR  $\nu_{\max}$ /cm<sup>-1</sup>: 3262, 2962, 2359, 1637, 1507, 1435, 1400, 1257, 1181, 1060, 933, 814, 751, 731, 723; HRMS (ESI) *m/z* calcd for C<sub>26</sub>H<sub>28</sub>NO [M+H]<sup>+</sup> 370.2165; found 370.2162.

##### *N*-(2-methyltriphenylen-1-yl)pivalamide (**3ba**)

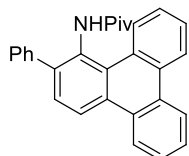


The product was obtained as a yellow ocher solid (56 mg, 72%). <sup>1</sup>H NMR (600 MHz, CDCl<sub>3</sub>) δ = 8.67 (d, *J* = 8.4 Hz, 1H), 8.52 – 8.50 (m, 2H), 8.44 – 8.41 (m, 1H), 8.30 (d, *J* = 8.3 Hz, 1H), 7.58 – 7.57 (m, 3H), 7.52 (t, *J* = 7.5 Hz, 1H), 7.35 – 7.30 (m, 2H), 2.25 (s, 3H), 1.36 (s, 9H); <sup>13</sup>C NMR (150 MHz, CDCl<sub>3</sub>) δ = 176.23, 136.07, 132.06, 130.78, 129.89, 129.88, 129.62, 129.56, 129.06, 127.46, 127.16, 127.14, 126.95, 126.94, 125.48, 123.20, 123.19, 122.93, 121.79, 39.46, 27.61, 18.99; IR  $\nu_{\max}$ /cm<sup>-1</sup>: 3266, 2955, 2868, 1647, 1570, 1515, 1486, 1437, 1395, 1364, 1258, 1179, 933, 905, 809, 745, 720; HRMS (ESI) *m/z* calcd for C<sub>24</sub>H<sub>24</sub>NO [M+H]<sup>+</sup> 342.1858; found 342.1852.

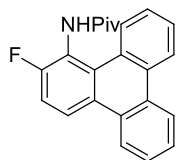
##### *N*-(2-ethyltriphenylen-1-yl)pivalamide (**3ca**)



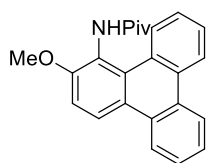
The product was obtained as an orange solid (77 mg, 95%). <sup>1</sup>H NMR (600 MHz, CDCl<sub>3</sub>) δ = 8.73 (d, *J* = 8.4 Hz, 1H), 8.56 – 8.51 (m, 2H), 8.48 – 8.47 (m, 1H), 8.43 (d, *J* = 8.5 Hz, 1H), 7.59 – 7.58 (m, 3H), 7.55 (t, *J* = 7.5 Hz, 1H), 7.44 (d, *J* = 8.4 Hz, 1H), 7.38 – 7.34 (m, 1H), 2.68 (q, *J* = 7.6 Hz, 2H), 1.37 (s, 9H), 1.23 (t, *J* = 7.6 Hz, 3H); <sup>13</sup>C NMR (150 MHz, CDCl<sub>3</sub>) δ = 176.51, 141.23, 131.51, 130.83, 129.95, 129.89, 129.74, 129.21, 127.82, 127.58, 127.18, 127.12, 126.99, 125.50, 123.28, 123.23, 122.97, 122.26, 39.46, 30.88, 27.56, 25.07; IR  $\nu_{\max}$ /cm<sup>-1</sup>: 3291, 2965, 2926, 2866, 2360, 1641, 1506, 1435, 1396, 1366, 1261, 1179, 1058, 940, 818, 752, 722; HRMS (ESI) *m/z* calcd for C<sub>25</sub>H<sub>26</sub>NO [M+H]<sup>+</sup> 356.2009; found 356.2006.

*N*-(2-phenyltriphenylen-1-yl)pivalamide (**3da**)

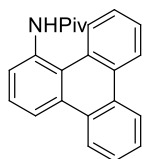
The product was obtained as a white solid (85 mg, 92%).  $^1\text{H NMR}$  (600 MHz,  $\text{CDCl}_3$ )  $\delta$  = 8.96 (dd,  $J$  = 8.5, 1.2 Hz, 1H), 8.59 – 8.56 (m, 4H), 7.64 – 7.62 (m, 2H), 7.60 – 7.57 (m, 2H), 7.55 – 7.53 (m, 1H), 7.50 – 7.47 (m, 2H), 7.44 – 7.39 (m, 4H), 1.06 (s, 9H);  $^{13}\text{C NMR}$  (150 MHz,  $\text{CDCl}_3$ )  $\delta$  = 175.70, 139.85, 139.12, 131.39, 131.10, 130.66, 130.32, 129.81, 129.20, 129.10, 128.58, 128.49, 127.60, 127.44, 127.42, 127.27, 127.25, 126.31, 125.72, 123.56, 123.19, 121.67, 39.25, 27.10; IR  $\nu_{\text{max}}/\text{cm}^{-1}$ : 3331, 3259, 3056, 2961, 2924, 1735, 1640, 1496, 1430, 1391, 1259, 1089, 1017, 943, 822, 797, 748, 720; HRMS (ESI)  $m/z$  calcd for  $\text{C}_{29}\text{H}_{26}\text{NO}$   $[\text{M}+\text{H}]^+$  404.2009; found 404.2005.

*N*-(2-fluorotriphenylen-1-yl)pivalamide (**3ea**)

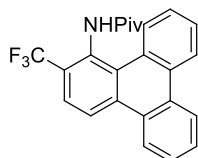
The product was obtained as a yellow solid (56 mg, 71%).  $^1\text{H NMR}$  (600 MHz,  $\text{CDCl}_3$ )  $\delta$  = 8.89 (d,  $J$  = 8.4 Hz, 1H), 8.56 – 8.50 (m, 2H), 8.45 – 8.40 (m, 2H), 7.62 – 7.56 (m, 3H), 7.52 (br s, 1H), 7.43 – 7.38 (m, 1H), 7.31 (t,  $J$  = 8.8 Hz, 1H), 1.42 (s, 9H);  $^{13}\text{C NMR}$  (150 MHz,  $\text{CDCl}_3$ )  $\delta$  = 177.01, 157.69 (d,  $J$  = 246.2 Hz), 131.02, 129.70, 129.48, 129.11 (d,  $J$  = 3.2 Hz), 128.76, 127.86 (d,  $J$  = 2.5 Hz), 127.80, 127.54, 127.31, 126.68, 126.08, 123.49 (t,  $J$  = 4.7 Hz), 123.35, 123.28, 121.51 (d,  $J$  = 13.7 Hz), 114.96 (d,  $J$  = 23.0 Hz), 39.70, 27.65;  $^{19}\text{F NMR}$  (564 MHz,  $\text{CDCl}_3$ )  $\delta$  = -119.82 (dd,  $J$  = 8.3, 5.9 Hz); IR  $\nu_{\text{max}}/\text{cm}^{-1}$ : 3275, 2961, 1655, 1607, 1484, 1437, 1398, 1366, 1278, 1158, 1092, 912, 881, 813, 750, 720; HRMS (ESI)  $m/z$  calcd for  $\text{C}_{23}\text{H}_{21}\text{FNO}$   $[\text{M}+\text{H}]^+$  346.1602; found 346.1601.

*N*-(2-methoxytriphenylen-1-yl)pivalamide (**3fa**)

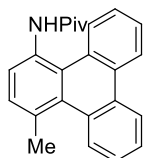
The product was obtained as a yellow ocher solid (64 mg, 79%).  $^1\text{H NMR}$  (600 MHz,  $\text{CDCl}_3$ )  $\delta$  = 9.01 (d,  $J$  = 8.4 Hz, 1H), 8.54 (t,  $J$  = 8.8 Hz, 2H), 8.40 (t,  $J$  = 9.4 Hz, 2H), 7.68 (br s, 1H), 7.59 – 7.55 (m, 3H), 7.40 (t,  $J$  = 7.6 Hz, 1H), 7.12 (d,  $J$  = 9.0 Hz, 1H), 3.86 (s, 3H), 1.39 (s, 9H);  $^{13}\text{C NMR}$  (150 MHz,  $\text{CDCl}_3$ )  $\delta$  = 176.69, 153.20, 130.66, 130.09, 129.96, 129.46, 127.98, 127.25, 127.16, 126.53, 126.44, 125.79, 124.96, 123.30, 123.20, 122.97, 122.25, 110.68, 56.20, 39.62, 27.55; IR  $\nu_{\text{max}}/\text{cm}^{-1}$ : 3402, 2922, 1678, 1602, 1481, 1459, 1402, 1305, 1272, 1167, 1125, 1104, 1018, 930, 803, 749, 719; HRMS (ESI)  $m/z$  calcd for  $\text{C}_{24}\text{H}_{24}\text{NO}_2$   $[\text{M}+\text{H}]^+$  358.1802; found 358.1799.

*N*-(triphenylen-1-yl)pivalamide (**3ga**)

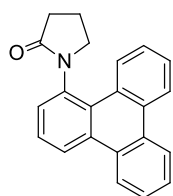
The product was obtained as a brown solid (19 mg, 25%).  $^1\text{H}$  NMR (600 MHz,  $\text{CDCl}_3$ )  $\delta$  = 8.73 (d,  $J$  = 8.3 Hz, 1H), 8.63 (d,  $J$  = 8.2 Hz, 1H), 8.57 (dd,  $J$  = 9.2, 5.8 Hz, 2H), 8.45 (d,  $J$  = 8.1 Hz, 1H), 8.18 (d,  $J$  = 7.8 Hz, 1H), 7.97 (br s, 1H), 7.66 – 7.60 (m, 4H), 7.52 (t,  $J$  = 7.6 Hz, 1H), 1.43 (s, 9H);  $^{13}\text{C}$  NMR (150 MHz,  $\text{CDCl}_3$ )  $\delta$  = 176.18, 134.69, 131.98, 131.27, 130.04, 129.91, 128.54, 127.77, 127.66, 127.45, 127.39, 126.70, 126.06, 124.32, 124.17, 123.73, 123.21, 120.18, 40.02, 27.78; IR  $\nu_{\text{max}}/\text{cm}^{-1}$ : 3275, 2962, 2925, 2868, 1655, 1604, 1578, 1519, 1478, 1434, 1398, 1366, 1286, 1259, 1173, 1024, 938, 801, 746, 720; HRMS (ESI)  $m/z$  calcd for  $\text{C}_{23}\text{H}_{22}\text{NO}$   $[\text{M}+\text{H}]^+$  328.1696; found: 328.1694.

*N*-(2-(trifluoromethyl)triphenylen-1-yl)pivalamide (**3ha**)

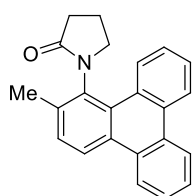
The product was obtained using the general procedure, except the iodonium salt was added in two parts (3.0 + 2.0 equiv) and  $\text{Pd}_2\text{dba}_3$  also was added in two parts (5.0 + 2.5 mol%) for a total reaction time of 48 h. The product was obtained as a yellow ocher solid (27 mg, 30%).  $^1\text{H}$  NMR (600 MHz,  $\text{CDCl}_3$ )  $\delta$  = 8.98 (d,  $J$  = 8.4 Hz, 1H), 8.53 (t,  $J$  = 7.7 Hz, 3H), 8.47 (d,  $J$  = 8.0 Hz, 1H), 8.09 (br s, 1H), 7.81 (d,  $J$  = 8.6 Hz, 1H), 7.66 – 7.63 (m, 1H), 7.61 – 7.58 (m, 2H), 7.43 – 7.39 (m, 1H), 1.35 (s, 9H);  $^{13}\text{C}$  NMR (150 MHz,  $\text{CDCl}_3$ )  $\delta$  = 175.64, 134.85, 132.75, 130.97, 130.71, 129.03, 128.98, 128.74, 128.53, 127.95, 127.44, 126.17, 126.01, 125.44 (q,  $J$  = 28.7 Hz), 124.36 (q,  $J$  = 273.0 Hz), 123.92, 123.69, 123.39 (q,  $J$  = 5.5 Hz), 123.28, 122.01, 39.46, 27.22;  $^{19}\text{F}$  NMR (564 MHz,  $\text{CDCl}_3$ )  $\delta$  = -60.23 (s); IR  $\nu_{\text{max}}/\text{cm}^{-1}$ : 3291, 2970, 1655, 1603, 1499, 1486, 1401, 1330, 1293, 1187, 1165, 1118, 1021, 945, 826, 754, 737, 723; HRMS (ESI)  $m/z$  calcd for  $\text{C}_{24}\text{H}_{21}\text{F}_3\text{NO}$   $[\text{M}+\text{H}]^+$  396.1570; found 396.1565.

*N*-(4-methyltriphenylen-1-yl)pivalamide (**3ka**)

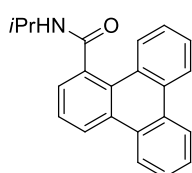
The product was obtained as a brown solid (20 mg, 26%).  $^1\text{H}$  NMR (600 MHz,  $\text{CDCl}_3$ )  $\delta$  = 8.58 (d,  $J$  = 8.2 Hz, 1H), 8.53 – 8.49 (m, 2H), 8.42 (d,  $J$  = 8.1 Hz, 1H), 8.04 (d,  $J$  = 7.9 Hz, 1H), 7.95 (br s, 1H), 7.60 – 7.53 (m, 3H), 7.46 (t,  $J$  = 7.6 Hz, 1H), 7.42 (d,  $J$  = 7.9 Hz, 1H), 2.95 (s, 3H), 1.38 (s, 9H);  $^{13}\text{C}$  NMR (150 MHz,  $\text{CDCl}_3$ )  $\delta$  = 175.91, 132.51, 131.63, 131.03, 130.82, 130.78, 130.52, 129.00, 127.79, 127.23, 126.87, 126.34, 126.24, 126.20, 124.80, 123.98, 123.32, 122.11, 39.74, 27.56, 25.12; IR  $\nu_{\text{max}}/\text{cm}^{-1}$ : 3290, 2961, 2868, 2241, 1652, 1585, 1505, 1481, 1428, 1366, 1301, 1258, 1191, 1159, 1091, 1017, 908, 802, 755, 727; HRMS (ESI)  $m/z$  calcd for  $\text{C}_{24}\text{H}_{24}\text{NO}$   $[\text{M}+\text{H}]^+$  342.1852; found 342.1851.

1-(triphenylen-1-yl)pyrrolidin-2-one (**3la**)

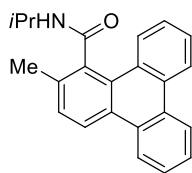
The product was obtained as a brown oil (25 mg, 35%).  $^1\text{H NMR}$  (600 MHz,  $\text{CDCl}_3$ )  $\delta$  = 8.69 (d,  $J$  = 8.4 Hz, 1H), 8.61 – 8.56 (m, 4H), 7.69 – 7.61 (m, 4H), 7.59 – 7.52 (m, 2H), 3.81 (td,  $J$  = 9.7, 3.5 Hz, 1H), 3.43 (dd,  $J$  = 17.6, 8.0 Hz, 1H), 2.80 – 2.66 (m, 2H), 2.32 – 2.18 (m, 2H);  $^{13}\text{C NMR}$  (150 MHz,  $\text{CDCl}_3$ )  $\delta$  = 175.37, 136.18, 132.39, 130.55, 129.96, 129.72, 128.46, 128.31, 127.62, 127.60, 127.49, 127.45, 126.80, 126.42, 125.61, 123.61, 123.46, 123.17, 122.72, 50.27, 31.77, 18.94; IR  $\nu_{\text{max}}/\text{cm}^{-1}$ : 2925, 1732, 1683, 1597, 1577, 1463, 1435, 1395, 1302, 1234, 1096, 1044, 1016, 811, 750, 726; HRMS (ESI)  $m/z$  calcd for  $\text{C}_{22}\text{H}_{18}\text{NO}$   $[\text{M}+\text{H}]^+$  312.1383; found 312.1382.

1-(2-methyltriphenylen-1-yl)pyrrolidin-2-one (**3ma**)

The product was obtained as a brown oil (26 mg, 35%).  $^1\text{H NMR}$  (600 MHz,  $\text{CDCl}_3$ )  $\delta$  = 8.62 (d,  $J$  = 8.1 Hz, 1H), 8.61 – 8.56 (m, 1H), 8.55 (d,  $J$  = 8.3 Hz, 3H), 7.69 – 7.60 (m, 3H), 7.56 (t,  $J$  = 7.5 Hz, 2H), 3.62 (td,  $J$  = 9.9, 4.9 Hz, 1H), 3.38 (dd,  $J$  = 17.5, 7.9 Hz, 1H), 2.88 (dd,  $J$  = 13.8, 5.7 Hz, 2H), 2.41 (s, 3H), 2.33 – 2.22 (m, 2H);  $^{13}\text{C NMR}$  (150 MHz,  $\text{CDCl}_3$ )  $\delta$  = 177.19, 135.99, 132.89, 130.94, 130.62, 130.23, 129.65, 129.61, 128.14, 127.72, 127.53, 127.44, 126.92, 126.89, 125.39, 123.50, 123.38, 123.25, 123.07, 49.78, 31.08, 19.19, 18.61; IR  $\nu_{\text{max}}/\text{cm}^{-1}$ : 2915, 2360, 1772, 1685, 1607, 1463, 1435, 1417, 1290, 1205, 1151, 752, 733, 721; HRMS (ESI)  $m/z$  calcd for  $\text{C}_{23}\text{H}_{20}\text{NO}$   $[\text{M}+\text{H}]^+$  326.1539; found 326.1535.

*N*-isopropyltriphenylene-1-carboxamide (**3na**)

The product was obtained as a yellow ocher solid (40 mg, 56%).  $^1\text{H NMR}$  (600 MHz,  $\text{CDCl}_3$ )  $\delta$  = 8.66 (d,  $J$  = 8.2 Hz, 1H), 8.62 – 8.58 (m, 3H), 8.51 (d,  $J$  = 8.3 Hz, 1H), 7.71 (d,  $J$  = 7.2 Hz, 1H), 7.67 – 7.61 (m, 4H), 7.53 (t,  $J$  = 7.6 Hz, 1H), 5.52 (d,  $J$  = 7.3 Hz, 1H), 4.41 – 4.32 (m, 1H), 1.18 (d,  $J$  = 6.6 Hz, 6H);  $^{13}\text{C NMR}$  (150 MHz,  $\text{CDCl}_3$ )  $\delta$  = 171.62, 135.83, 131.13, 130.63, 129.99, 129.45, 128.32, 128.26, 128.22, 127.71, 127.68, 127.51, 126.98, 126.62, 126.39, 124.33, 123.47, 123.19, 123.15, 42.16, 22.25; IR  $\nu_{\text{max}}/\text{cm}^{-1}$ : 3292, 3063, 2959, 2922, 2852, 1734, 1629, 1527, 1455, 1364, 1260, 1171, 1017, 780, 746, 724; HRMS (ESI)  $m/z$  calcd for  $\text{C}_{22}\text{H}_{20}\text{NO}$   $[\text{M}+\text{H}]^+$  314.1545; found 314.1538.

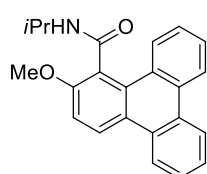
*N*-isopropyl-2-methyltriphenylene-1-carboxamide (**3oa**)

The product was obtained as a white solid (30 mg, 40%).  $^1\text{H NMR}$  (600 MHz,  $\text{CDCl}_3$ )  $\delta$  = 8.80 (d,  $J$  = 8.3 Hz, 1H), 8.58 (dt,  $J$  = 14.9, 8.1 Hz, 4H), 7.66 – 7.61 (m, 3H), 7.54 (t,  $J$  = 7.4 Hz, 1H), 7.50 (d,  $J$  = 8.3 Hz, 1H), 5.44 (d,  $J$  = 7.0 Hz, 1H), 4.44 – 4.35 (m, 1H), 2.58 (s, 3H), 1.15 (d,  $J$  = 6.7 Hz, 6H);  $^{13}\text{C NMR}$  (150 MHz,  $\text{CDCl}_3$ )  $\delta$



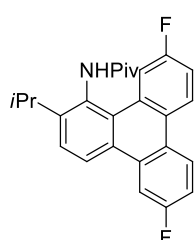
= 171.58, 135.69, 134.75, 130.78, 129.79, 129.77, 129.75, 129.03, 128.97, 127.79, 127.57, 127.55, 127.44, 127.15, 126.69, 123.69, 123.34, 123.24, 123.20, 42.03, 21.85, 20.02; IR  $\nu_{\max}/\text{cm}^{-1}$ : 3254, 3063, 2970, 2917, 2851, 1628, 1533, 1446, 1363, 1287, 1249, 1158, 1129, 905, 813, 745, 720; HRMS (ESI)  $m/z$  calcd for  $\text{C}_{23}\text{H}_{22}\text{NO}$   $[\text{M}+\text{H}]^+$  328.1696; found 328.1691.

#### *N*-isopropyl-2-methoxytriphenylene-1-carboxamide (**3pa**)



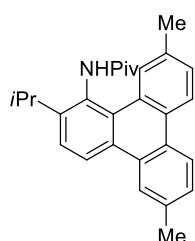
The product was obtained as a yellow solid (40 mg, 51%).  $^1\text{H}$  NMR (600 MHz,  $\text{CDCl}_3$ )  $\delta$  = 8.82 (d,  $J$  = 8.3 Hz, 1H), 8.60 – 8.53 (m, 3H), 8.46 – 8.42 (m, 1H), 7.63 – 7.56 (m, 3H), 7.51 (t,  $J$  = 7.3 Hz, 1H), 7.23 (d,  $J$  = 9.1 Hz, 1H), 5.65 (d,  $J$  = 7.9 Hz, 1H), 4.49 – 4.43 (m, 1H), 3.94 (s, 3H), 1.21 (d,  $J$  = 6.6 Hz, 6H);  $^{13}\text{C}$  NMR (150 MHz,  $\text{CDCl}_3$ )  $\delta$  = 169.19, 156.35, 130.96, 129.68, 129.00, 128.58, 128.46, 127.63, 127.37, 126.67, 126.52, 125.32, 124.55, 123.56, 123.10, 123.03, 122.85, 111.66, 56.51, 41.85, 22.35; IR  $\nu_{\max}/\text{cm}^{-1}$ : 3309, 2965, 2929, 2360, 1637, 1593, 1522, 1488, 1449, 1426, 1319, 1270, 1241, 1170, 1118, 1019, 902, 803, 755, 718; HRMS (ESI)  $m/z$  calcd for  $\text{C}_{23}\text{H}_{22}\text{NO}_2$   $[\text{M}+\text{H}]^+$  344.1645; found 344.1645.

#### *N*-(6,11-difluoro-2-isopropyltriphenylene-1-yl)pivalamide (**3ab**)



The product was obtained as a white solid (69 mg, 75%).  $^1\text{H}$  NMR (600 MHz,  $\text{CDCl}_3$ )  $\delta$  = 8.55 (dd,  $J$  = 12.5, 2.7 Hz, 1H), 8.44 – 8.37 (m, 3H), 8.09 (dd,  $J$  = 11.2, 2.6 Hz, 1H), 7.62 (d,  $J$  = 8.6 Hz, 1H), 7.61 (br s, 1H), 7.31 – 7.27 (m, 2H), 3.23 (septet,  $J$  = 6.9 Hz, 1H), 1.43 (s, 9H), 1.32 (d,  $J$  = 6.9 Hz, 6H);  $^{13}\text{C}$  NMR (150 MHz,  $\text{CDCl}_3$ )  $\delta$  = 176.68, 162.29 (d,  $J$  = 202.3 Hz), 160.67 (d,  $J$  = 200.1 Hz), 145.93, 131.49 (d,  $J$  = 8.1 Hz), 130.98, 130.79 (d,  $J$  = 8.1 Hz), 129.66 (d,  $J$  = 3.4 Hz), 127.74 (d,  $J$  = 3.1 Hz), 127.09 (d,  $J$  = 2.2 Hz), 126.10 (d,  $J$  = 2.1 Hz), 125.51, 125.45, 125.25 (d,  $J$  = 8.7 Hz), 123.05, 115.63 (d,  $J$  = 23.0 Hz), 115.45 (d,  $J$  = 22.7 Hz), 112.54 (d,  $J$  = 24.1 Hz), 109.00 (d,  $J$  = 22.9 Hz), 39.70, 28.81, 27.66, 23.43;  $^{19}\text{F}$  NMR (564 MHz,  $\text{CDCl}_3$ )  $\delta$  = -114.41 – -114.50 (m), -115.65 – -115.69 (m); IR  $\nu_{\max}/\text{cm}^{-1}$ : 3285, 2955, 2925, 2868, 1648, 1619, 1514, 1490, 1417, 1388, 1260, 1216, 1186, 1171, 1049, 973, 881, 852, 814, 796; HRMS (ESI)  $m/z$  calcd for  $\text{C}_{26}\text{H}_{26}\text{F}_2\text{NO}$   $[\text{M}+\text{H}]^+$  406.1977; found 406.1974.

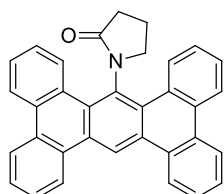
#### *N*-(2-isopropyl-6,11-dimethyltriphenylene-1-yl)pivalamide (**3ac**)



The product was obtained as a white solid (69 mg, 78%).  $^1\text{H}$  NMR (600 MHz,  $\text{CDCl}_3$ )  $\delta$  = 8.54 (d,  $J$  = 8.7 Hz, 2H), 8.42 (d,  $J$  = 8.4 Hz, 1H), 8.38 (d,  $J$  = 8.3 Hz, 1H), 8.29 (s, 1H), 7.59 (d,  $J$  = 8.6 Hz, 1H), 7.51 (br s, 1H), 7.40 – 7.38 (m, 2H), 3.22 (septet,  $J$  = 6.9 Hz, 1H), 2.57 (s, 3H), 2.49 (s, 3H), 1.43 (s, 9H), 1.32 (d,  $J$  = 6.9 Hz, 6H);  $^{13}\text{C}$  NMR (150 MHz,  $\text{CDCl}_3$ )  $\delta$  = 176.79, 145.47, 136.57, 134.61, 130.53, 130.17, 129.64, 129.19, 129.02, 128.65, 128.64, 128.17, 127.82, 127.07, 124.70, 123.45, 123.36, 122.91, 122.71, 39.63,

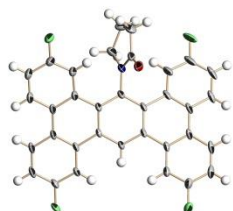
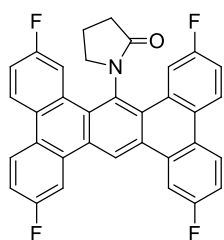
28.65, 27.85, 23.58, 22.05, 21.96; IR  $\nu_{\max}/\text{cm}^{-1}$ : 3264, 2960, 2922, 2855, 1735, 1638, 1508, 1457, 1418, 1376, 1257, 1176, 1082, 1025, 942, 866, 803; HRMS (ESI)  $m/z$  calcd for  $\text{C}_{28}\text{H}_{32}\text{NO}$   $[\text{M}+\text{H}]^+$  398.2478; found 398.2475.

1-(tribenzo[*f,k,m*]tetraphen-9-yl)pyrrolidin-2-one (**4la**)

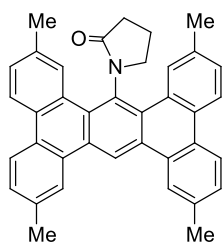


The product was obtained as a brown solid (42 mg, 40%).  $^1\text{H}$  NMR (600 MHz,  $\text{CDCl}_3$ )  $\delta$  = 9.57 (s, 1H), 8.65 – 8.61 (m, 2H), 8.59 – 8.53 (m, 4H), 8.32 (d,  $J$  = 8.1 Hz, 2H), 7.69 – 7.60 (m, 6H), 7.48 – 7.46 (m, 2H), 3.93 (t,  $J$  = 7.1 Hz, 2H), 2.72 (t,  $J$  = 8.4 Hz, 2H), 2.41 – 2.34 (m, 2H);  $^{13}\text{C}$  NMR (150 MHz,  $\text{CDCl}_3$ )  $\delta$  = 175.64, 131.28, 130.74, 130.59, 130.04, 128.90, 127.87, 127.73, 127.67, 126.58, 126.36, 125.40, 124.14, 124.12, 123.32, 116.02, 49.07, 31.76, 18.61; IR  $\nu_{\max}/\text{cm}^{-1}$ : 3066, 1688, 1494, 1444, 1406, 1282, 1236, 1164, 1048, 907, 750, 723; HRMS (ESI)  $m/z$  calcd for  $\text{C}_{34}\text{H}_{24}\text{NO}$   $[\text{M}+\text{H}]^+$  462.1852; found 462.1842.

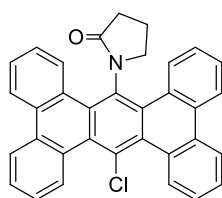
1-(2,7,11,16-tetrafluorotribenzo[*f,k,m*]tetraphen-9-yl)pyrrolidin-2-one (**4lb**)



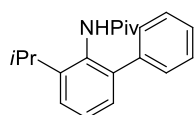
The product was obtained as a brown solid (40 mg, 33%). The structure of 4lb was also determined by single-crystal X-ray diffraction, and deposited in the Cambridge Crystallographic Data Centre (CCDC 1523986).  $^1\text{H}$  NMR (600 MHz,  $\text{CDCl}_3$ )  $\delta$  = 9.15 (s, 1H), 8.35 (dd,  $J$  = 9.0, 6.1 Hz, 2H), 8.31 (dd,  $J$  = 8.9, 5.5 Hz, 2H), 8.12 (dd,  $J$  = 10.5, 2.1 Hz, 2H), 7.94 (dd,  $J$  = 12.1, 2.4 Hz, 2H), 7.31 – 7.25 (m, 4H), 3.92 (t,  $J$  = 7.2 Hz, 2H), 2.79 (t,  $J$  = 8.5 Hz, 2H), 2.50 – 2.44 (m, 2H);  $^{13}\text{C}$  NMR (150 MHz,  $\text{CDCl}_3$ )  $\delta$  = 175.85, 162.44 (d,  $J$  = 161.3 Hz), 160.81 (d,  $J$  = 159.3 Hz), 131.98, 131.09 (d,  $J$  = 8.0 Hz), 130.63 (d,  $J$  = 3.1 Hz), 129.62 (d,  $J$  = 8.5 Hz), 127.40 (d,  $J$  = 1.7 Hz), 126.50 (d,  $J$  = 2.8 Hz), 126.41 (d,  $J$  = 1.8 Hz), 125.96 (d,  $J$  = 8.7 Hz), 125.27 (d,  $J$  = 8.6 Hz), 116.93, 116.32 (d,  $J$  = 22.8 Hz), 116.03 (d,  $J$  = 22.4 Hz), 111.29 (d,  $J$  = 24.3 Hz), 109.84 (d,  $J$  = 22.7 Hz), 48.78, 31.49, 18.51;  $^{19}\text{F}$  NMR (564 MHz,  $\text{CDCl}_3$ )  $\delta$  = -113.15 – -113.28 (m), -114.31 – -114.43 (m); IR  $\nu_{\max}/\text{cm}^{-1}$ : 2922, 2852, 1693, 1616, 1590, 1497, 1414, 1268, 1242, 1199, 1182, 1006, 931, 858, 799, 786, 772; HRMS (ESI)  $m/z$  calcd for  $\text{C}_{34}\text{H}_{20}\text{F}_4\text{NO}$   $[\text{M}+\text{H}]^+$  534.1476; found 534.1469.

1-(2,7,11,16-tetramethyltribenzo[*f,k,m*]tetraphen-9-yl)pyrrolidin-2-one (**4lc**)

The product was obtained as a brown solid (47 mg, 40%). <sup>1</sup>H NMR (600 MHz, CDCl<sub>3</sub>) δ = 9.54 (s, 1H), 8.43 – 8.39 (m, 6H), 8.11 (s, 2H), 7.44 (dd, *J* = 16.6, 8.1 Hz, 4H), 3.94 (t, *J* = 7.1 Hz, 2H), 2.70 (t, *J* = 8.5 Hz, 2H), 2.64 (s, 6H), 2.50 (s, 6H), 2.40 – 2.37 (m, 2H); <sup>13</sup>C NMR (150 MHz, CDCl<sub>3</sub>) δ = 175.29, 136.90, 135.21, 131.14, 130.65, 129.72, 129.14, 129.07, 128.86, 128.61, 128.33, 126.55, 125.69, 124.08, 123.70, 123.03, 116.01, 48.91, 31.72, 21.99, 21.81, 18.50; IR  $\nu_{\max}/\text{cm}^{-1}$ : 2916, 1693, 1613, 1588, 1413, 1375, 1282, 1035, 869, 789, 735; HRMS (ESI) *m/z* calcd for C<sub>38</sub>H<sub>32</sub>NO [M+H]<sup>+</sup> 518.2478; found 518.2481.

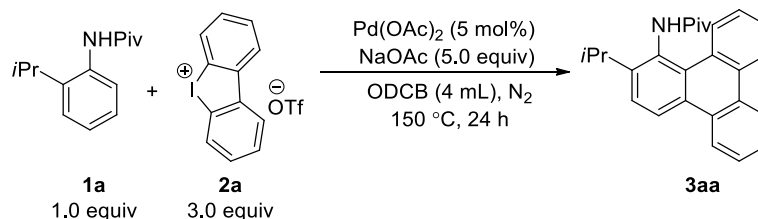
1-(18-chlorotribenzo[*f,k,m*]tetraphen-9-yl)pyrrolidin-2-one (**4qa**)

The product was obtained as a lemon solid (28 mg, 25%). <sup>1</sup>H NMR (600 MHz, CDCl<sub>3</sub>) δ = 8.96 (d, *J* = 8.2 Hz, 2H), 8.46 (dd, *J* = 8.1, 2.4 Hz, 4H), 8.04 (d, *J* = 8.2 Hz, 2H), 7.61 (dt, *J* = 16.1, 7.5 Hz, 4H), 7.51 (t, *J* = 7.3 Hz, 2H), 7.43 (t, *J* = 7.3 Hz, 2H), 3.93 (t, *J* = 7.1 Hz, 2H), 2.57 (t, *J* = 8.3 Hz, 2H), 2.32 – 2.25 (m, 2H); <sup>13</sup>C NMR (150 MHz, CDCl<sub>3</sub>) δ = 175.23, 131.79, 131.19, 129.92, 129.34, 128.99, 128.73, 128.49, 128.42, 128.19, 127.59, 127.22, 126.11, 125.56, 124.65, 124.38, 123.86, 49.80, 31.81, 18.96; IR  $\nu_{\max}/\text{cm}^{-1}$ : 3059, 2921, 2858, 2359, 1698, 1479, 1441, 1396, 1282, 1233, 1051, 1010, 860, 795, 745, 736, 721; HRMS (ESI) *m/z* calcd for C<sub>34</sub>H<sub>23</sub>ClNO [M+H]<sup>+</sup> 496.1463; found 496.1461.

**4.5. ortho-Arylation under the Standard Conditions***N*-(3-isopropyl-[1,1'-biphenyl]-2-yl)pivalamide

In an oven-dried schlenk tube, 2-isopropylpivanilide (50 mg, 0.228 mmol), Ph<sub>2</sub>IOTf (3.0 equiv), NaOAc (5.0 equiv), and Pd<sub>2</sub>dba<sub>3</sub> (5 mol%) was weighed. This solid mixture was then alternatively subjected to vacuum and nitrogen conditions for maintaining an inert atmosphere. To this mixture, ODCB (2 mL) was added and then stirred (1,000 rpm) at 150 °C for 24 h. After completion of reaction (on the basis of TLC), the reaction mixture was filtered through celite and washed using DCM. Thereafter, the organic layer was concentrated and purified by flash column chromatography (n-hexane/ethyl acetate, 1:0 → 10:1). The product was obtained as a ivory solid (65 mg, 97%). <sup>1</sup>H NMR (600 MHz, CDCl<sub>3</sub>) δ = 7.38 – 7.33 (m, 5H), 7.31 – 7.28 (m, 2H), 7.17 (dd, *J* = 7.1, 1.6 Hz, 1H), 6.78 (br s, 1H), 3.08 (septet, *J* = 6.9 Hz, 1H), 1.26 (d, *J* = 6.9 Hz, 6H), 1.08 (s, 9H); <sup>13</sup>C NMR (150 MHz, CDCl<sub>3</sub>) δ = 177.28, 146.87, 140.57, 140.16, 131.66, 128.97, 128.04, 127.59, 127.14, 125.30, 38.94, 28.57, 27.40, 23.53; IR  $\nu_{\max}/\text{cm}^{-1}$ : 3290, 2959, 2868, 1645, 1505, 1456, 1434, 1362, 1223, 1172, 943, 810, 795, 757, 738; HRMS (ESI) *m/z* calcd for C<sub>20</sub>H<sub>26</sub>NO [M+H]<sup>+</sup> 296.2009; found 296.2009.

#### 4.6. Radical Route in Pd-Catalyzed Reaction: Control Reaction



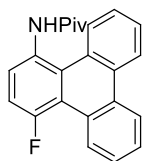
To confirm radical formation in Pd-catalyzed reaction,  $\text{Pd(OAc)}_2$  instead of  $\text{Pd}_2\text{dba}_3$  was used and BHT or TEMPO (1.0 equiv) as a radical scavenger was added under standard conditions. The isolated yield was reduced to 23% or 21%, respectively.

#### 4.7. Additional Annulative $\pi$ -Extension Reactions

This section contains the miscellaneous reaction scope of the palladium-catalyzed annulative  $\pi$ -extension. We have carried out the annulation reactions with several substrates to investigate the electronic influences of substituents and directing groups (Table 4.3). In general, NHPiv group was identified as a good directing group, and *ortho*-substituents were critical to furnish the corresponding products in good to excellent yields (Table 4.2). Non-*ortho*-substituted substrate **1r** was subjected to the mono- or bis-annulation reaction conditions to afford the annulated **3ra** or **4ra**, albeit in low yield, respectively. The reactions employing phthalimide- or Weinreb amide-based substrates **1s** and **1t** were also conducted. However, these removable or modifiable directing groups were not suited to yield the desired products. Halogenated substrates **1v** and **1w** exhibited the formation of various side products. The desired Pd-catalyzed C–H arylation might be hampered because the substrates can undergo competing oxidative addition. Substrates **1u** and **1x** gave the corresponding products via two-fold C–H arylation.

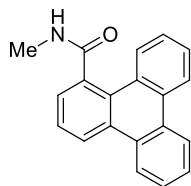


#### *N*-(4-fluorotriphenylene-1-yl)pivalamide (**3ua**)



The product was obtained as a yellow solid (15 mg, 19%). <sup>1</sup>H NMR (600 MHz, CDCl<sub>3</sub>) δ = 9.00 – 8.95 (m, 1H), 8.61 (d, *J* = 8.4 Hz, 1H), 8.55 (t, *J* = 7.9 Hz, 2H), 8.04 (dd, *J* = 8.7, 4.8 Hz, 1H), 7.86 (br s, 1H), 7.67 – 7.60 (m, 3H), 7.49 – 7.45 (m, 1H), 7.32 (dd, *J* = 13.4, 8.8 Hz, 1H), 1.40 (s, 9H); <sup>13</sup>C NMR (150 MHz, CDCl<sub>3</sub>) δ = 176.15, 158.52 (d, *J* = 251.7 Hz), 131.33, 130.06, 127.90, 127.78 (d, *J* = 2.5 Hz), 127.71, 127.69 (d, *J* = 2.1 Hz), 126.62, 126.30 (d, *J* = 3.6 Hz), 125.92, 125.17 (d, *J* = 10.4 Hz), 124.01, 122.76, 121.86 (d, *J* = 7.8 Hz), 120.29 (d, *J* = 8.5 Hz), 115.44 (d, *J* = 22.4 Hz), 114.50 (d, *J* = 26.9 Hz), 39.69, 27.53; <sup>19</sup>F NMR (564 MHz, CDCl<sub>3</sub>) δ = -111.99 – -112.02 (m); IR *v*<sub>max</sub>/cm<sup>-1</sup>: 3294, 2959, 2927, 2869, 1652, 1508, 1482, 1465, 1430, 1228, 1163, 924, 807, 758, 726; HRMS (ESI) *m/z* calcd for C<sub>23</sub>H<sub>21</sub>FNO [M+H]<sup>+</sup> 346.1602; found 346.1597.

#### *N*-methyltriphenylene-1-carboxamide (**3xa**)



The product was obtained as a yellow solid (10 mg, 15%). <sup>1</sup>H NMR (600 MHz, CDCl<sub>3</sub>) δ = 8.68 (d, *J* = 8.0 Hz, 1H), 8.64 – 8.58 (m, 3H), 8.39 (d, *J* = 8.2 Hz, 1H), 7.73 – 7.72 (m, 1H), 7.68 – 7.62 (m, 4H), 7.56 – 7.53 (m, 1H), 5.67 (br s, 1H), 2.98 (d, *J* = 4.9 Hz, 3H); <sup>13</sup>C NMR (150 MHz, CDCl<sub>3</sub>) δ = 173.30, 135.37, 131.16, 130.72, 129.97, 129.41, 128.26, 128.14, 127.74, 127.67, 127.57, 127.08, 126.69, 126.49, 124.47, 123.48, 123.26, 123.22, 27.08; IR *v*<sub>max</sub>/cm<sup>-1</sup>: 3309, 3060, 2923, 2853, 2360, 1640, 1578, 1546, 1489, 1409, 1310, 1261, 1159, 803, 753, 712; HRMS (ESI) *m/z* calcd for C<sub>20</sub>H<sub>16</sub>NO [M+H]<sup>+</sup> 286.1226; found 286.1221.

## 4.8. Fabrication of Alcohol FET Sensors

### 4.8.1. CVD Synthesis and Transfer of Graphene

A Cu foil (Alfa Aesar, item No.: 13382) was loaded into the CVD chamber under vacuum (10 mTorr). And then, the furnace was heated up to 1,000 °C under 200 sccm Ar and 500 sccm H<sub>2</sub>. Graphene synthesis was carried out for 5 min under 12 sccm of CH<sub>4</sub> and 500 sccm of H<sub>2</sub>, and then the chamber was cooled down. To transfer the graphene onto Si substrate, poly(methyl methacrylate) (MicroChem Corp., 950 PMMA) was used as supporting layer. Cu foil was completely etched by a diluted solution (FeCl<sub>3</sub> solution (aq. 35%): HCl solution (aq. 42%): H<sub>2</sub>O = 1 : 1 : 20 vol%). After rinsing the graphene-PMMA with DI water, the graphene-PMMA layer was transferred onto Si substrate with the subsequent removal of PMMA by acetone rinsing.

### 4.8.2. Fabrication of Field-Effect Transistors

Photoresist was patterned on Si substrate with 300 nm thick SiO<sub>2</sub>, and Cr/Au (3 nm/100 nm) electrodes were made by thermal evaporation. Then, graphene was transferred onto the Cr/Au electrodes and

patterned by photolithography. Graphene film was dry-etched using oxygen reactive ion etching (RIE) plasma for channel. Graphene channel was surface functionalized by dip coating in a solution of **3aa** in DCM ( $\sim 1.0$  mg/mL) via  $\pi$ - $\pi$  stacking with subsequent DCM rinsing.<sup>44,45</sup>

### 4.8.3. Electrical Characterizations

Electrical characterizations were conducted using a probe station (Keithley 4200-SCS semiconductor parametric analyzer) to measure transfer and output characteristics of devices. All devices were characterized at 0.1 V of drain bias.

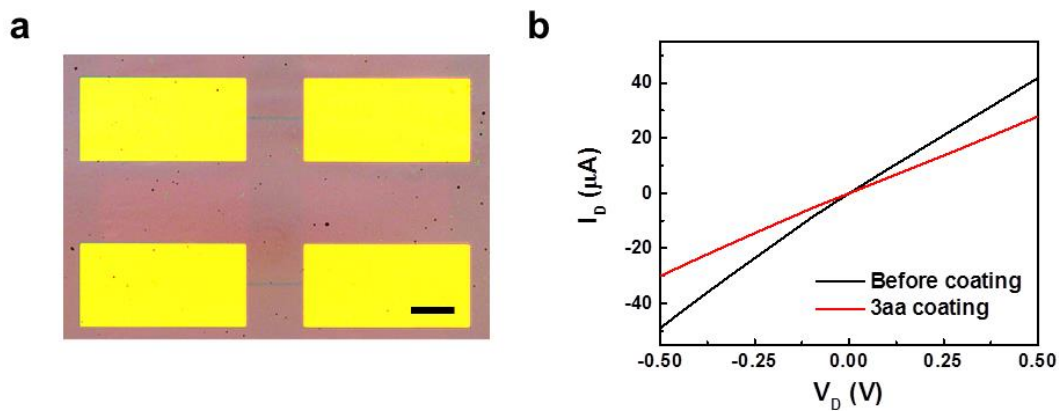


**Figure 4.3.** (a) Optical microscope image of the graphene channel FETs. The width of the channel is 5  $\mu\text{m}$ , and the length of the channel is 70  $\mu\text{m}$ . Scale bar, 50  $\mu\text{m}$ , (b) Output ( $I_D$ - $V_D$ ) characteristics of the graphene FETs before and after **3aa** coating ( $V_G = 0$  V).

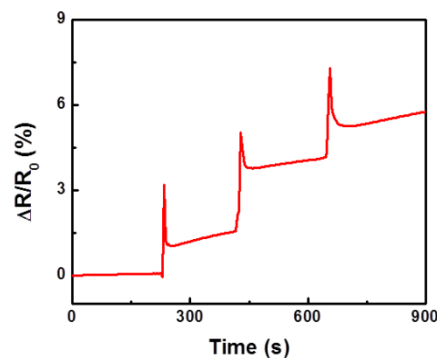


**Figure 4.4.** Real-time response of the graphene sensor to ethanol vapor without **3aa**-functionalization at a fixed concentration (1,000 ppm) ( $V_G = 0$  V).

#### 4.9. The Photophysical Properties of Compounds **4**

The photophysical properties of compounds **4** were examined by UV/Vis and fluorescence spectroscopy. The absorption maxima ( $\lambda_{\text{abs}}$ ) of compounds **4** were between 310 and 325 nm. Emission maxima ( $\lambda_{\text{em}}$ ) were between 410 and 461 nm. Compared to the spectra of triphenylene, red shifts in both the absorption and emission are ascribed to the larger  $\pi$ -conjugation.

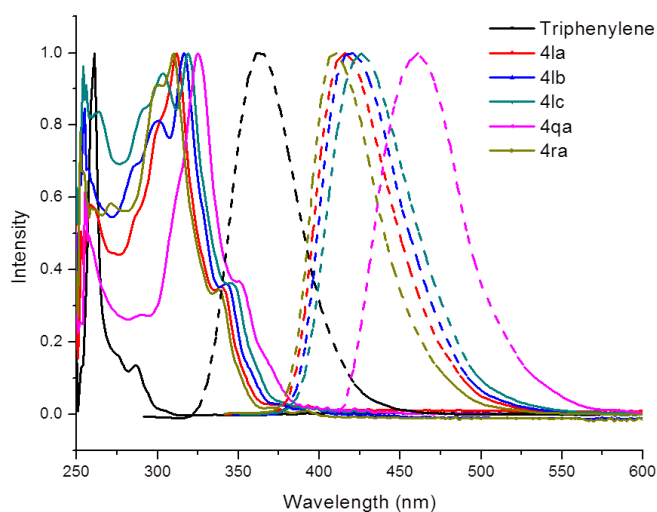


**Figure 4.5.** UV/Vis absorption spectra (solid lines, normalized data) and fluorescence emission spectra (dashed line, normalized data) obtained for compounds **4**.

Compound	$\lambda_{\text{abs}}$ [nm]	$E_{g(\text{opt})}$ [eV] <sup>b</sup>	$\lambda_{\text{em}}$ [nm]
Triphenylene	261	4.13	361
<b>4la</b>	312	3.40	415
<b>4lb</b>	316	3.35	420
<b>4lc</b>	319	3.33	425
<b>4qa</b>	325	3.22	461
<b>4ra</b>	310	3.43	410

[a] Compounds **4** were measured in dimethyl sulfoxide at room temperature. [b] Calculated based on the corresponding absorption onset.

**Table 4.4.** The photophysical properties of compounds **4**.<sup>a</sup>



## 5. References

- [1] Y. Segawa, H. Ito, K. Itami, *Nat. Rev. Mater.* **2016**, *1*, 15002.
- [2] A. Hirsch, *Nat. Mater.* **2010**, *9*, 868–871.
- [3] A. K. Geim, K. S. Novoselov, *Nat. Mater.* **2007**, *6*, 183–191.
- [4] K. S. Novoselov, A. K. Geim, S. V. Morozov, D. Jiang, Y. Zhang, S. V. Dubonos, I. V. Grigorieva, A. A. Firsov, *Science* **2004**, *306*, 666–669.
- [5] A. Narita, X.-Y. Wang, X. Feng, K. Mgllen, *Chem. Soc. Rev.* **2015**, *44*, 6616–6643.
- [6] L. Chen, Y. Hernandez, X. Feng, K. Mgllen, *Angew. Chem. Int. Ed.* **2012**, *51*, 7640–7654; *Angew. Chem.* **2012**, *124*, 7758–7773.
- [7] K. Ozaki, K. Kawasumi, M. Shibata, H. Ito, K. Itami, *Nat. Commun.* **2015**, *6*, 6251.
- [8] K. Kawasumi, Q. Zhang, Y. Segawa, L. T. Scott, K. Itami, *Nat. Chem.* **2013**, *5*, 739–744.
- [9] T. Dumslaff, B. Yang, A. Maghsoumi, G. Velpula, K. S. Mali, C. Castiglioni, S. De Feyter, M. Tommasini, A. Narita, X. Feng, K. Mgllen, *J. Am. Chem. Soc.* **2016**, *138*, 4726–4729.
- [10] M. Treier, C. A. Pignedoli, T. Laino, R. Rieger, K. Mgllen, D. Passerone, R. Fasel, *Nat. Chem.* **2011**, *3*, 61–67.
- [11] J. Cai, et al., *Nature* **2010**, *466*, 470–473.
- [12] T. Wassmann, A. P. Seitsonen, A. M. Saitta, M. Lazzeri, F. Mauri, *J. Am. Chem. Soc.* **2010**, *132*, 3440–3451.
- [13] D. P8rez, D. PeÇa, E. Guitian, *Eur. J. Org. Chem.* **2013**, 5981–6013.
- [14] T. Jin, J. Zhao, N. Asao, Y. Yamamoto, *Chem. Eur. J.* **2014**, *20*, 3554–3576.
- [15] D. P8rez, E. Guiti#n, *Chem. Soc. Rev.* **2004**, *33*, 274–283.
- [16] D. PeÇa, S. Escudero, D. Perez, E. Guitian, L. Castedo, *Angew. Chem. Int. Ed.* **1998**, *37*, 2659 – 2661; *Angew. Chem.* **1998**, *110*, 2804–2806.
- [17] Z. Liu, X. Zhang, R. C. Larock, *J. Am. Chem. Soc.* **2005**, *127*, 15716–15717.
- [18] M. Iwasaki, Y. Araki, S. Iino, Y. Nishihara, *J. Org. Chem.* **2015**, *80*, 9247–9263.
- [19] D. Vasu, H. Yorimitsu, A. Osuka, *Angew. Chem. Int. Ed.* **2015**, *54*, 7162–7166; *Angew. Chem.* **2015**, *127*, 7268–7272.
- [20] I. Nagao, M. Shimizu, T. Hiyama, *Angew. Chem. Int. Ed.* **2009**, *48*, 7573–7576; *Angew. Chem.* **2009**, *121*, 7709–7712.
- [21] E. A. Merritt, B. Olofsson, *Angew. Chem. Int. Ed.* **2009**, *48*, 9052–9070; *Angew. Chem.* **2009**, *121*, 9214–9234.
- [22] N. R. Deprez, M. S. Sanford, *Inorg. Chem.* **2007**, *46*, 1924–1935.
- [23] K. D. Collins, R. Honeker, S. Vasquez-Cespedes, D.-T. D. Tang, F. Glorius, *Chem. Sci.* **2015**, *6*, 1816–1824.
- [24] O. Daugulis, V. G. Zaitsev, *Angew. Chem. Int. Ed.* **2005**, *44*, 4046–4048; *Angew. Chem.* **2005**, *117*,

4114–4116.

[25] CCDC 1523986 (**4Ib**) contains the supplementary crystallographic data for this paper. These data can be obtained free of charge from The Cambridge Crystallographic Data Centre.

[26] J. Kim, M.-S. Lee, S. Jeon, M. Kim, S. Kim, K. Kim, F. Bien, S. Y. Hong, J.-U. Park, *Adv. Mater.* **2015**, *27*, 3292–3297.

[27] S. Y. Hong, et al., *Nat. Mater.* **2010**, *9*, 485–490.

[28] S. Y. Hong, G. Tobias, B. Ballesteros, F. El Oualid, J. C. Errey, K. J. Doores, A. I. Kirkland, P. D. Nellist, M. L. H. Green, B. G. Davis, *J. Am. Chem. Soc.* **2007**, *129*, 10966–10967.

[29] J. Park, et al., *Nanoscale* **2016**, *8*, 10591–10597.

[30] X. Li, et al., *Science* **2009**, *324*, 1312–1314.

[31] K. S. Novoselov, A. K. Geim, S. V. Morozov, D. Jiang, M. K. Katsnelson, I. V. Grigorieva, S. V. Dubonos, A. A. Firsov, *Nature* **2005**, *438*, 197–200.

[32] Y. Zhang, Y.-W. Than, H. L. Stormer, P. Kim, *Nature* **2005**, *438*, 201–204.

[33] M. Nagaraju, G. N. Sastry, *J. Mol. Model.* **2011**, *17*, 1801–1816.

[34] Y. Liu, X. Dong, P. Chen, *Chem. Soc. Rev.* **2012**, *41*, 2283–2307.

[35] R. J. Phipps, M. J. Gaunt, *Science* **2009**, *323*, 1593–1597.

[36] A. Albright, D. Eddings, R. Black, C. J. Welch, N. N. Gerasimchuk, R. E. Gawley, *J. Org. Chem.* **2011**, *76*, 7341–7351.

[37] L.-S. Zhang, K. Chen, G. Chen, B.-J. Li, S. Luo, Q.-Y. Guo, J.-B. Wei, Z.-J. Shi, *Org. Lett.* **2013**, *15*, 10–13.

[38] K. Aradi, Z. Novák, *Adv. Synth. Catal.* **2015**, *357*, 371–376.

[39] C. Wang, L. Liu, W. Wang, D.-S. Ma, H. Zhang, *Molecules* **2010**, *15*, 1154–1160.

[40] L. Jiang, *Molecules* **2014**, *19*, 13448–13460.

[41] T. Bathini, V. S. Rawat, B. Sreedhar, *Synlett* **2015**, *26*, 1348–1351.

[42] S. Sharma, E. Park, J. Park, I. S. Kim, *Org. Lett.* **2012**, *14*, 906–909.

[43] Z. Liu, D. Zhu, B. Luo, N. Zhang, Q. Liu, Y. Hu, R. Pi, P. Huang, S. Wen, *Org. Lett.* **2014**, *16*, 5600–5603.

[44] J. Kim, M.-S. Lee, S. Jeon, M. Kim, S. Kim, K. Kim, F. Bien, S. Y. Hong, J.-U. Park, *Adv. Mater.* **2015**, *27*, 3292–3297.

[45] J. Park, et al., *Nanoscale* **2016**, *8*, 10591–10597.

## Chapter V

### Acknowledgement (English version)

When I face finishing graduate school soon, I feel a long graduate school life seems to pass quickly. Because, the more I studied, the more I felt the scarceness and regret about my researches. However, I could feel a sense of accomplishment and pleasure due to many people who have supported me.

Firstly, I am most grateful for my *family* who always believes me. Thanks to my *mother*, I decided to go to graduate school and then I was able to learn a lot as well as meet good people. I really thank and love my *father* who gives a much bigger love than before, *sister* and *brother* who are indispensable friends for my life, and *grandmother* who is always worried about me.

I must be grateful to *Prof. Sung You Hong* as my supervisor. I did not know anything when I first came to the lab. However, I now know everything from experimental design to organizing the results, thanks to your sincere advice, praise, and encouragement. Furthermore, I also learned that researchers need to explore with independent and flexible thinking. I will do my best to be a better researcher even after becoming a worker of society.

As doctoral dissertation committees, I would like to thank *Prof. Ja Hun Kwak*, *Prof. Kwangjin An*, *Prof. Changduk Yang*, and *Prof. Chang Young Lee* for advising me about research presentation, in spite of their tight schedule. And I am much grateful to *Prof. Sebyung Kang* who helped me to do the protein cage research independently, *Prof. Joon Hak Oh* who trusted and led me to graduate school, lastly, all of coworkers, *Prof. Ja Hun Kwak* and their research member (*Dong Gun Oh*), *Prof. Sang Kyu Kwak* and their research member (*Jeong Hyeon Lee*), *Prof. Jang-Ung Park* and their research member (*Joohee Kim*) for cooperation and help.

Furthermore, I really want to thank synthetic organic chemistry lab members. I have been able to have a pleasant laboratory life thanks to past, current members and postdoctoral researchers (*Hyun Ho Lee*, *Woo Gyum Kim*, *Dong-Seon Shin*, *Jae Bin Lee*, *Min Ho Jeon*, *Mi Eun Kang*, *Jaeshin Kim*, *Dr. Mallesh*, *Dr. Bijoy* and *Sangbin Jeon*). Especially, I thank *Dr. Bijoy* who give a lot of help to publish the papers. And I was always fun with *So Ryung Lim*, *Eun Sun Jeong*, *Arah Cho* who were my greatest strength during graduate school life. I also thank my dear friends for supporting me.

I think I could complete my degree thanks to so many people who gave the interest and encouragement to me. Again, I would like to thank you. I will continuously try to be a researcher who is growing academically and personally.

## 감사의 글 (Korean version)

길게만 느껴졌던 대학원 생활이 졸업을 앞두고 보니 빠르게 지나간 것처럼 느껴집니다. 이것은 연구를 하면 할수록 느꼈던 부족함과 아쉬움 때문인 것 같습니다. 하지만 기쁨과 성취감 또한 느낄 수 있었던 것은 저를 응원해주시고 함께 해주신 분들 덕분이라고 생각합니다. 먼저, 항상 저를 믿어주는 우리 가족에게 가장 감사합니다. 엄마 덕분에 대학원에 와서 더 많은 것을 배울 수 있었고, 좋은 사람들도 만날 수 있었습니다. 그리고 엄마 빈자리 느껴지지 않도록 이전보다 훨씬 큰 사랑을 주시는 아빠, 미워 보일 때도 있지만 절대 없으면 안 되는 최고의 친구이자 동생인 현수와 원모, 처음에는 대학원 진학을 반대하셨지만 나중에는 건강 챙기면서 실험하라고 늘 걱정해주신 할머니 감사하고, 사랑합니다. 그리고 지도 교수님이신 홍성유 교수님, 감사합니다. 처음에 입학했을 때 아무것도 모르던 제가 교수님의 애정 어린 충고와 조언, 칭찬, 격려 덕분에 이제는 실험 설계부터 결과를 정리하는 법까지 익힐 수 있게 되었습니다. 또한 연구자란 주체적이고 유동적인 생각을 가지고 탐구해야 한다는 것을 배웠습니다. 앞으로 사회에 나가서도 이를 실천하여 더 나은 연구자가 될 수 있도록 하겠습니다. 논문 심사위원이셨던곽자훈 교수님, 안광진 교수님, 양창덕 교수님, 이창영 교수님 감사합니다. 교수님들의 질문과 조언 덕분에 제가 놓쳤던 부분에 대해서 한 번 더 생각할 수 있었고, 배울 수 있었습니다. 그리고 공동 연구를 할 때, 다른 실험실 학생이지만 개인미팅과 랩미팅까지 챙겨주시면서 protein cage 연구까지도 독립적으로 할 수 있도록 많이 신경 써주신 강세병 교수님. 대학원 입학을 포기하려고 할 때, 저를 믿어주시고 이끌어주신 오준학 교수님. 공동 연구를 하며 좋은 데이터와 조언을 주신 곽상규 교수님, 박장웅 교수님께도 감사 드립니다. 그 외 같이 논문을 냈던 강영지 언니, 김주희, 오동건, 이정현 학생에게도 감사 드립니다. 그리고 약 6년동안 동고동락했던 합성유기화학 실험실 동생들과 박사 후 연구원분들 덕분에 즐거운 실험실 생활을 할 수 있었습니다. 자장면 좋아하는 춘테레 호랑이 선생 홍랩 김경호 짱귀티티 현호, 식당이랑 편의점 제일 많이 같이 가주고, 멍청한 장난도 다 받아주는 홍랩 이소라 우겸, 홍랩 래퍼와 오락부장을 맡고 있는 분위기 메이커 명선 동선, 꽃힌 것 하나에 무섭게 집중하는 힘센 홍랩 트로트 가수 재빈, 앞으로 절대 아프지 않길 바라는 간식 잘 나눠주는 홍랩 버즈 민호, 남자만 있던 공간에 향기로운 꽃으로 와준 홍랩 미녀 미은, 실험실에서는 장난기를 많이 숨기고 있는 운동파트너, 카풀 재신, 실험실 안과 밖의 모습이 너무 달라서 놀라운 흥 많은 Dr. Mallesh, 카이스트에서 박사과정 중인 스포지밥의 다람이 님은 상빈. 특히, 실험 능률을 효과적으로 올릴 수 있는 법과 실험에

있어서 좋은 결과를 얻지 못했을 때, 스트레스 받지 않고 이를 받아들이는 자세를 알려준 Dr. Bijoy 고맙습니다. 그리고 대학원 생활의 모든 희로애락을 나눴던 룸메 은선이는 정말 고맙습니다. 이렇게 좋은 동생을 만난 것은 저의 행운이라고 생각할 정도로 대학원 기간, 세계 가장 큰 힘이 되어주었습니다. 또 울산에서도, 서울에서도 저를 잘 챙겨준 항상 웃는 모습의 소령언니, 아라와 함께 있으면 늘 재미있고 즐거웠습니다. 그 외에도 많은 좋은 친구, 언니, 오빠, 동생들 덕분에 삭막하지 않은 대학원 생활을 할 수 있었습니다. 홍랩에 대학원생으로 혼자 있을 때, 잘 챙겨준 재인이, 현규 오빠, 윤주 오빠, 재영 오빠. 8층에 힘찬 기운을 주던 호정 언니, 아름, 문정, 은광 오빠. 선배 없는 제가 혹시라도 놓치는 것이 있을까, 졸업까지도 신경 써주신 지원 언니, 미선 언니. 기쁜 일엔 축하를, 힘든 일엔 경청과 따뜻한 조언을 준 소민, 소연, 효진 언니. 언니~ 하면서 저를 잘 따라주었던 귀여운 베급. 부족한 저와 같이 살아준 룸메 민정, 서희, 솔미. 다들 고맙습니다. 그리고 오랜만에 만나도 어제 만났던 것 같은 느낌을 주는 친구들. 인생의 보물, 존경하는 수빈, 수진, 예슬, 지은. 안 맞을 것 같은데 정말 잘 맞는 예쁜 유나, 주연, 정빈. 자습실 인연 세훈, 우곤, 정윤, 석청, 경수, 병호. 가장 신나고 재미있게 놀았던 대학 생활을 함께 보낸 현영, 새롬, 태형이햄, 준오햄, 성진, 남우, 우현, 종현, 준환, 성은, 승훈, 민희, 동주, 원석. 잘 될 거라고 항상 응원해주셔서 감사합니다. 이렇게 많은 분들의 관심과 격려 덕분에 제가 무사히 학위를 마칠 수 있었다고 생각합니다. 다시 한 번 감사드리며, 앞으로도 학문적으로나 인성적으로 성장하는 연구자로서 노력하는 사람이 되도록 하겠습니다. 감사합니다.

2017년 6월 2일

양현지 올림

## Curriculum Vitae

### Hyun Ji Yang

Ulsan National Institute of Science and Technology (UNIST)  
Chemical Engineering Department  
50, UNIST-gil, Eonyang-eup, Ulju-gun, Ulsan, Republic of Korea  
Phone: +82-10-4567-7856 /E-Mail: [ccomo7856@unist.ac.kr](mailto:ccomo7856@unist.ac.kr)

### Education

- |           |                                                                                                                                                                                                                                                                       |              |
|-----------|-----------------------------------------------------------------------------------------------------------------------------------------------------------------------------------------------------------------------------------------------------------------------|--------------|
| 2012-2017 | <b>Ulsan National Institute of Science and Technology</b><br>Doctor of Philosophy<br>School of Energy and Chemical Engineering<br>Supervisor: Prof. Sung You Hong<br>Thesis: C–H Functionalization of Substituted Aromatic Compounds Using Transition-Metal Catalysts | Ulsan, Korea |
| 2007-2012 | <b>Pukyong National University</b><br>Bachelor of Science in Engineering<br>Department of Polymer Engineering                                                                                                                                                         | Busan, Korea |

### Publications

- [1] B. P. Mathew, ‡ **H. J. Yang**, ‡ J. Kim, J. B. Lee, Y.-T. Kim, S. Lee, C. Y. Lee, W. Choe, K. Myung, J.-U. Park, S. Y. Hong “An Annulative Synthetic Strategy for Building Triphenylene Frameworks by Multiple C–H Activations” (‡equal contribution)  
*Angew. Chem. Int. Ed.* **2017**, *56*, 5007–5011.
- [2] **H. J. Yang**, ‡ B. P. Mathew, ‡ D. G. Oh, K. Myung, J. H. Kwak, S. Y. Hong “Efficient Copper Catalysts for C–H Bond Arylation under Microwave Heating: Direct Access to Multi-Substituted Pivanilides” (‡equal contribution)  
*Catal. Commun.* **2017**, *90*, 83-86.
- [3] W. G. Kim, B. Choi, **H.-J. Yang**, J.-A. Han, H. Jung, H. Cho, S. Kang, S. Y. Hong “Covalent Conjugation of Small-Molecule Adjuvants to Nanoparticles Induces Robust Cytotoxic T Cell Responses via DC Activation”  
*Bioconjugate Chem.* **2016**, *27*, 2007-2013.
- [4] B. P. Mathew, **H. J. Yang**, H. Jeon, J. H. Lee, J. C. Kim, T. J. Shin, K. Myung, S. K. Kwak, J. H. Kwak, S. Y. Hong “C–H Bond Arylation of Anilines inside Copper-Exchanged Zeolites”  
*J. Mol. Catal. A: Chem.* **2016**, *417*, 64-70.
- [5] Y. J. Kang, **H. J. Yang**, S. Jeon, Y.-S. Kang, Y. K. Do, S. Y. Hong, S. Kang “Polyvalent Display of Monosaccharides on Ferritin Protein Cage Nanoparticles for the Recognition and Binding of Cell-Surface Lectins”  
*Macromol. Biosci.* **2014**, *14*, 619-625.

[6] J. Min, H. Moon, **H. J. Yang**, H.-H. Shin, S. Y. Hong, S. Kang “Development of P22 Viral Capsid Nanocomposite as Anti-Cancer Drug, Bortezomib (BTZ), Delivery Nanoplatforms” *Macromol. Biosci.* **2014**, *14*, 557-564.

### Poster Presentation

[1] **H. J. Yang**, S. Y. Hong, *Korean Chemical Society*, 19 April 2017, KINTEX, Korea, Title: Pd-catalyzed synthesis of substituted triphenylenes by aromatic annulation.

[2] **H. J. Yang**, S. Y. Hong, *Korean Chemical Society*, 14 October 2016, BEXCO, Korea, Title: Comparative Studies emphasizing the Microwave-assisted *Meta*-selective direct arylation using Homogeneous and Heterogeneous Cu catalysts.

[3] **H. J. Yang**, W. G. Kim, B. Choi, S. Kang, S. Y. Hong, *The Korean Association of Immunologists*, 17 April 2015, Salt Lake City, Korea, Title: Polyvalent Display of Toll-Like Receptor 7 Agonist on Ferritin Protein Cage Nanoparticles.

[4] **H. J. Yang**, S. Y. Hong, *Korean Chemical Society*, 16 October 2013, CECO, Korea, Title: Synthesis of Glyco-Ferritin Nanoparticles for the Development of Lectin Targeted Delivery.

### Collaborations

*Prof. Ja Hun Kwak*: The J. H. Kwak group prepared the Cu-exchanged zeolites (Cu- $\beta$ , Cu-Y, Cu-MOR) and carried out ICP and TEM analyses to examine the stability of the catalysts.

*Prof. Sang Kyu Kwak*: The S. K. Kwak group build zeolite framework models for the simulation studies. Cu-catalyzed C–H bond arylation within the zeolite frameworks was compared with homogeneous catalysis.

*Prof. Jang-Ung Park*: The Park group constructed graphene-based FET devices for application as a chemical gas sensor using *N*-substituted triphenylenes.

*Prof. Sebyung Kang*: The Kang group performed bioconjugation tests and related characterizations.

## Appendix

## Permission from all cited journal in this dissertation

Chapter II. *J. Mol. Catal. A: Chem.* 2016, 417, 64-70.

RightsLink®

Home

Account  
Info

Help



**Title:** CH bond arylation of anilides inside copper-exchanged zeolites

**Author:** Bijoy P. Mathew, Hyun Ji Yang, Himchan Jeon, Jeong Hyeon Lee, Jin Chul Kim, Tae Joo Shin, Kyungjae Myung, Sang Kyu Kwak, Ja Hun Kwak, Sung You Hong

**Publication:** Journal of Molecular Catalysis A: Chemical

**Publisher:** Elsevier

**Date:** June 2016

Copyright © 2016 Elsevier B.V. All rights reserved.

Logged in as:

Hyun Ji Yang

LOGOUT

## Order Completed

Thank you for your order.

This Agreement between Hyun Ji Yang ("You") and Elsevier ("Elsevier") consists of your license details and the terms and conditions provided by Elsevier and Copyright Clearance Center.

Your confirmation email will contain your order number for future reference.

[Printable details.](#)

License Number	4151251107989
License date	Jul 17, 2017
Licensed Content Publisher	Elsevier
Licensed Content Publication	Journal of Molecular Catalysis A: Chemical
Licensed Content Title	CH bond arylation of anilides inside copper-exchanged zeolites
Licensed Content Author	Bijoy P. Mathew, Hyun Ji Yang, Himchan Jeon, Jeong Hyeon Lee, Jin Chul Kim, Tae Joo Shin, Kyungjae Myung, Sang Kyu Kwak, Ja Hun Kwak, Sung You Hong
Licensed Content Date	Jun 1, 2016
Licensed Content Volume	417
Licensed Content Issue	n/a
Licensed Content Pages	7
Type of Use	reuse in a thesis/dissertation
Portion	full article
Format	electronic
Are you the author of this Elsevier article?	Yes
Will you be translating?	No
Order reference number	
Title of your thesis/dissertation	C-H Functionalization of Substituted Aromatic Compounds Using Transition-Metal Catalysts
Expected completion date	Aug 2017
Estimated size (number of pages)	1
Elsevier VAT number	GB 494 6272 12
Requestor Location	Miss. Hyun Ji Yang Busan SooJung2dong  Busan, 48776 Korea, Republic Of Attn: Miss. Hyun Ji Yang
Total	0.00 USD

ORDER MORE

CLOSE WINDOW

Copyright © 2017 Copyright Clearance Center, Inc. All Rights Reserved. [Privacy statement](#). [Terms and Conditions](#).  
Comments? We would like to hear from you. E-mail us at [customercare@copyright.com](mailto:customercare@copyright.com)



Chapter III. *Catal. Commun.* 2017, 90, 83-86.

RightsLink®

Home

Account  
Info

Help



**Title:** Efficient copper catalysts for CH bond arylation under microwave heating: Direct access to multi-substituted pivanilides

**Author:** Hyun Ji Yang, Bijoy P. Mathew, Dong Gun Oh, Kyungjae Myung, Ja Hun Kwak, Sung You Hong

**Publication:** Catalysis Communications

**Publisher:** Elsevier

**Date:** February 2017

© 2016 Elsevier B.V. All rights reserved.

Logged in as:

Hyun Ji Yang

Account #:

3001173490

**Order Completed**

Thank you for your order.

This Agreement between Hyun Ji Yang ("You") and Elsevier ("Elsevier") consists of your license details and the terms and conditions provided by Elsevier and Copyright Clearance Center.

Your confirmation email will contain your order number for future reference.

[Printable details.](#)

License Number	4151290267167
License date	Jul 17, 2017
Licensed Content Publisher	Elsevier
Licensed Content Publication	Catalysis Communications
Licensed Content Title	Efficient copper catalysts for CH bond arylation under microwave heating: Direct access to multi-substituted pivanilides
Licensed Content Author	Hyun Ji Yang, Bijoy P. Mathew, Dong Gun Oh, Kyungjae Myung, Ja Hun Kwak, Sung You Hong
Licensed Content Date	Feb 1, 2017
Licensed Content Volume	90
Licensed Content Issue	n/a
Licensed Content Pages	4
Type of Use	reuse in a thesis/dissertation
Portion	full article
Format	electronic
Are you the author of this Elsevier article?	Yes
Will you be translating?	No
Order reference number	
Title of your thesis/dissertation	C-H Functionalization of Substituted Aromatic Compounds Using Transition-Metal Catalysts
Expected completion date	Aug 2017
Estimated size (number of pages)	1
Elsevier VAT number	GB 494 6272 12
Requestor Location	Hyun Ji Yang Busan SeoJung2dong  Busan, 48776 Korea, Republic Of Attn: Miss. Hyun Ji Yang
Total	0.00 USD



Copyright © 2017 Copyright Clearance Center, Inc. All Rights Reserved. [Privacy statement](#). [Terms and Conditions](#).  
Comments? We would like to hear from you. E-mail us at [customercare@copyright.com](mailto:customercare@copyright.com)

Chapter IV. *Angew. Chem. Int. Ed.* 2017, 56, 5007–5011.

RightsLink®

Home

Account  
Info

Help



**Title:** An Annulative Synthetic Strategy for Building Triphenylene Frameworks by Multiple C–H Bond Activations

**Author:** Bijoy P. Mathew, Hyun Ji Yang, Joohee Kim, Jae Bin Lee, Yun-Tae Kim, Sungmin Lee, Chang Young Lee, Wonyoung Choe, Kyungjae Myung, Jang-Ung Park, Sung You Hong

**Publication:** Angewandte Chemie International Edition

**Publisher:** John Wiley and Sons

**Date:** Mar 30, 2017

Logged in as:

Hyun Ji Yang

Account #:

3001173490

LOGOUT

© 2017 Wiley-VCH Verlag GmbH &amp; Co. KGaA, Weinheim

## Order Completed

Thank you for your order.

This Agreement between Hyun Ji Yang ("You") and John Wiley and Sons ("John Wiley and Sons") consists of your license details and the terms and conditions provided by John Wiley and Sons and Copyright Clearance Center.

Your confirmation email will contain your order number for future reference.

[Printable details.](#)

License Number	4151290550336
License date	Jul 17, 2017
Licensed Content Publisher	John Wiley and Sons
Licensed Content Publication	Angewandte Chemie International Edition
Licensed Content Title	An Annulative Synthetic Strategy for Building Triphenylene Frameworks by Multiple C–H Bond Activations
Licensed Content Author	Bijoy P. Mathew, Hyun Ji Yang, Joohee Kim, Jae Bin Lee, Yun-Tae Kim, Sungmin Lee, Chang Young Lee, Wonyoung Choe, Kyungjae Myung, Jang-Ung Park, Sung You Hong
Licensed Content Date	Mar 30, 2017
Licensed Content Pages	5
Type of use	Dissertation/Thesis
Requestor type	Author of this Wiley article
Format	Electronic
Portion	Full article
Will you be translating?	No
Title of your thesis / dissertation	C–H Functionalization of Substituted Aromatic Compounds Using Transition-Metal Catalysts
Expected completion date	Aug 2017
Expected size (number of pages)	1
Requestor Location	Hyun Ji Yang Busan SooJung2dong  Busan, 48776 Korea, Republic Of Attn: Miss. Hyun Ji Yang
Publisher Tax ID	EU826007151
Billing Type	Invoice
Billing address	Miss. Hyun Ji Yang Busan SooJung2dong  Busan, Korea, Republic Of 48776 Attn: Miss. Hyun Ji Yang
Total	0.00 USD

Would you like to purchase the full text of this article? If so, please continue on to the content ordering system located here: [Purchase PDF](#)

If you click on the buttons below or close this window, you will not be able to return to the content ordering system.

ORDER MORE

CLOSE WINDOW

Copyright © 2017 Copyright Clearance Center, Inc. All Rights Reserved. [Privacy statement](#). [Terms and Conditions](#).  
Comments? We would like to hear from you. E-mail us at [customer@copyright.com](mailto:customer@copyright.com)